Published for SISSA by Springer

Received: March 30, 2017
Accepted: April 29, 2017
Published: May 16, 2017

Right-handed charged currents in the era of the Large Hadron Collider

S. Alioli,[a] V. Cirigliano,[b] W. Dekens,[b,c] J. de Vries[d] and E. Mereghetti[b]

[a] *CERN Theory Division, CH-1211, Geneva 23, Switzerland*
[b] *Theoretical Division, Los Alamos National Laboratory, Los Alamos, NM 87545, U.S.A.*
[c] *New Mexico Consortium, Los Alamos Research Park, Los Alamos, NM 87544, U.S.A.*
[d] *Nikhef, Theory Group, Science Park 105, 1098 XG, Amsterdam, The Netherlands*

E-mail: simone.alioli@cern.ch, cirigliano@lanl.gov, wdekens@newmexicoconsortium.org, jordy.de.vries@nikhef.nl, emereghetti@lanl.gov

Abstract: We discuss the phenomenology of right-handed charged currents in the framework of the Standard Model Effective Field Theory, in which they arise due to a single gauge-invariant dimension-six operator. We study the manifestations of the nine complex couplings of the W to right-handed quarks in collider physics, flavor physics, and low-energy precision measurements. We first obtain constraints on the couplings under the assumption that the right-handed operator is the dominant correction to the Standard Model at observable energies. We subsequently study the impact of degeneracies with other Beyond-the-Standard-Model effective interactions and identify observables, both at colliders and low-energy experiments, that would uniquely point to right-handed charged currents.

Keywords: Beyond Standard Model, CP violation, Higgs Physics

ArXiv ePrint: 1703.04751

doi:10.1007/JHEP05(2017)086

JHEP05(2017)086

Contents

1 Introduction

The existence of right-handed charged currents (RHCC) is a distinctive signature of left-right symmetric extensions of the Standard Model (SM) [1–3]. This class of models is quite attractive as it allows parity to be restored at high energies by extending the SM gauge symmetries to $SU(3)_c \times SU(2)_R \times SU(2)_L \times U(1)_{B-L}$. An explanation for parity violation is then provided by the spontaneous symmetry breaking of this extended gauge group. Moreover, TeV scale left-right theories provide an appealing realization of the seesaw mechanism for neutrino masses [4]. In light of the ongoing efforts to search for new physics at the Large Hadron Collider (LHC) and in low-energy precision measurements, it is timely to assess the status and prospects of detecting signals of right-handed charged currents over a broad spectrum of probes.

In this paper, we consider a setup in which RHCC interactions manifest themselves at observable energies, including the scales probed at colliders, through a single $SU(3)_c \times SU(2)_L \times U(1)_Y$-invariant dimension-six operator [5, 6], namely

$$\mathcal{L}_{6,qq\varphi\varphi} = \frac{2}{v^2} i\tilde{\varphi}^\dagger D_\mu \varphi\, \bar{u}^i_R \gamma^\mu\, \xi_{ij} d^j_R + \text{h.c.}\,, \tag{1.1}$$

where D_μ is the covariant derivative, φ is the Higgs doublet, $\tilde{\varphi} = i\sigma_2\varphi^*$, $v = 246\,\text{GeV}$ is the Higgs vacuum expectation value, i and j are generation indices, and we work in the quark mass eigenbasis. After electroweak symmetry breaking this operator gives rise to a coupling of the $W^\pm$ boson to a right-handed charged current. In the unitary gauge we have

$$\mathcal{L}_{6,qq\varphi\varphi} = \frac{g}{\sqrt{2}} \left[\xi_{ij}\, \bar{u}^i_R \gamma^\mu d^j_R\, W^+_\mu\right] \left(1 + \frac{h}{v}\right)^2 + \text{h.c.}, \tag{1.2}$$

where g is the $SU(2)_L$ gauge coupling. The operator in eq. (1.1) arises in left-right symmetric models from the mixing between the charged gauge bosons of the $SU(2)_R$ and $SU(2)_L$ gauge groups. In this case ξ_{ij} is proportional to a unitary 3×3 matrix, the right-handed analog of the Cabibbo-Kobayashi-Maskawa (CKM) matrix. Here we do not commit to a specific model, so that ξ is a generic 3×3 matrix, with 9 independent complex parameters. The elements ξ_{ij} scale as $\xi_{ij} \sim \mathcal{O}(v^2/\Lambda^2)$, where Λ is the scale of new physics. We work within the framework of the SM effective field theory (SMEFT), in which it is a valid approximation to only consider dimension-six operators as long as there is a gap between the scale of new physics and the largest energy scale in the problem. For low-energy observables the largest energy scale will be the electroweak scale, such that we have the requirement

$\Lambda > v$. Instead, due to the larger energies available at colliders, the effects of eq. (1.1) can be investigated in pp collisions at the LHC if one assumes that $\Lambda >$ few TeV.

Although we do not restrict ourselves to a specific model it is worthwhile to mention how eq. (1.2) can be induced in UV-complete models. For example, in the minimal left-right symmetric model (see e.g. ref. [7]) the effective operator arises due to the mixing between left- and right-handed W bosons. In this set-up, after integrating out the heavy right-handed W boson, we can identify $\xi_{ij} \sim (\kappa\kappa'/v_R^2)(V_R)_{ij}e^{i\alpha}$ where κ and κ' are vacuum expectation values of the order of the electroweak scale, $v_R \gg v$ is the right-handed scale, α is a CP-violating phase arising from the extended Higgs sector of the model, and V_R the right-handed analogue of the CKM matrix. With further assumptions, such as explicit P and/or C symmetry at high energies, V_R can even be calculated in terms of SM quantities, such as quark masses and CKM elements, and the new model parameters κ, κ', and α [8–10]. In this way, our results can be used in phenomenological analyses of UV-complete scenarios, although care must be taken as other effective operators might be induced at the matching scale.

The operator (1.1) has several interesting manifestations, both at high- and low-energy. At colliders, it affects the production and polarization of W bosons. Furthermore, the operator (1.1) affects the production cross section of the Higgs boson, both in associated production with a W boson and in the vector boson fusion (VBF) channel. As we will discuss, invariance under the SM gauge group causes eq. (1.2) to modify not only the Wqq' vertex, but also the $HWqq'$ interaction. This latter interaction produces a very different dependence of the Higgs production cross section on kinematic variables such as the partonic center of mass energy or the Higgs transverse momentum. This in turn results in a large enhancement of the ξ-mediated cross section compared to the SM, especially for WH associated production. As a consequence, we will see that, for the first two rows of the ξ matrix, processes involving the Higgs are already more constraining than single W production. The third row of the ξ matrix is directly constrained by single-top production, and top decay. In particular, the measurement of the W polarization in top decay allows for a direct access to the Lorentz structure of the Wtb vertex, and to test its left-handed nature.

The operator (1.1) leaves a distinctive trace at low energy as well. Indeed, it is the only dimension-six operator in the SMEFT that induces a tree-level charged-current coupling of left-handed leptons to right-handed quarks, thus affecting baryon β decays, and meson leptonic and semileptonic charged-current decays. We will see that, under the assumption that the SM is modified predominantly by a RHCC at the high energy scale Λ, low-energy probes provide very stringent constraints on the first two rows of the ξ matrix. However, the most constraining observables are degenerate enough that, by introducing new physics beyond the ξ_{ij}, the bounds can be weakened to levels that are comparable to collider sensitivities. Less degenerate observables, such as decay correlations in the neutron β decays, suffer from comparatively large theoretical uncertainties, so that, once again, they probe the ξ_{ij} at levels comparable to collider experiments. One of our main findings is that once one tries to remove degeneracies by identifying observables that are sensitive primarily to ξ_{ij}, collider searches and low-energy probes have comparable sensitivity, and it is of great value to pursue both.

JHEP05(2017)086

In addition to observables that are at least in principle directly sensitive to RHCC, we also consider indirect bounds, both at high- and low-energy. Some of the most stringent indirect limits arise through top-quark loops which induce large corrections, enhanced by m_t/m_{d_j}, to the bottom-Yukawa coupling and dipole operators. In turn, the bottom Yukawa induces $h \to b\bar{b}$, while the dipole operators contribute to $B \to X_{s,d}\gamma$, the rare decay $K_L \to \pi^0 e^+ e^-$, and hadronic electric dipole moments (EDMs). We will see that the constraints from these loop processes are several orders of magnitude stronger than direct constraints from top production and decay. Furthermore, RHCC of light quarks induce tree-level contributions to EDMs and direct CP-violation (CPV) in kaon decays [11]. The stringent bounds on hadronic EDMs and the experimental value of ϵ'/ϵ can therefore be used to rule out couplings larger that $\mathrm{Im}\, \xi_{ud,us} \sim 10^{-6} - 10^{-7}$, suggesting a very high right-handed scale. While these indirect probes are certainly more "degenerate" than direct observables (i.e. they receive contributions from several other dimension-six operators in the SMEFT), the bounds that they imply are nonetheless very significant. Within the SMEFT these limits put stringent bounds on certain directions in the space of dimension-six Wilson coefficients, thereby imposing non-trivial constraints on new physics scenarios.

This paper is organized as follows. We start by investigating the constraints coming from colliders in section 2. We discuss direct W production in section 2.1, associated production of a Higgs and a W boson in section 2.2, and Higgs production via VBF in section 2.3. We then consider constraints on the ξ_{tj} elements coming from top production and decay in section 2.4, and from the decays of the Higgs in section 2.5. To connect to low-energy observables, in section 3, we integrate out the heavy SM particles and match onto a low-energy effective Lagrangian. In section 4 we consider the constraints coming from β decay, and from leptonic and semileptonic meson decays. We then discuss observables sensitive to non-leptonic operators induced by the operator (1.1), organizing the discussion in $\Delta F = 0$ observables (section 5), which consists of hadronic EDMs, $\Delta S = 1$ observables, including ϵ'/ϵ and $K_L \to \pi^0 e^+ e^-$ (section 6), and $\Delta B = 1$ observables, mainly related to inclusive and exclusive $b \to s, d\gamma$ transitions (section 7). In section 8, we obtain limits on the real and imaginary part of ξ_{ij} by taking into account all the observables discussed above, in a scenario in which only one of the elements is turned on at the high scale. In section 9 we discuss strategies to unambiguously identify the signal of a RHCC, both at low energies, and in associated production of a Higgs and a W. Finally, in section 9.3 we consider more in detail the Wtb vertex. We conclude in section 10.

2 Right-handed charged currents at colliders

In this section we study the effects of the RHCC operator ξ on several processes of interest at the LHC. We focus on W production, associated production of a W and a Higgs boson, Higgs production via vector boson fusion, and single-top production, as we expect these processes to be the most sensitive to RHCC. For all these processes, we include NLO QCD corrections to both the SM and BSM contributions, and, with the exception of single-top production, we implement the processes in the `POWHEG BOX V2` [12–14]. We also consider the effect of the ξ operator on the decays of the top-quark and the Higgs boson.

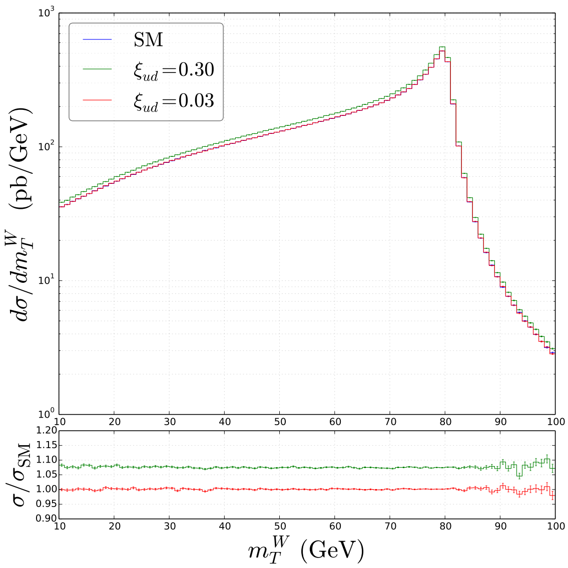

Figure 1. Transverse mass distribution m_T^W in $pp \to W^+ \to e^+\nu$ at $\sqrt{S} = 13\,\text{TeV}$ in the presence of right-handed charged currents.

Throughout this section we always consider $n_f = 5$ massless quarks and we include the exact top-quark mass dependence when necessary. For processes involving light quarks only, this is justified by the fact that the interference of the right-handed currents with the SM is suppressed by two insertions of the light quark masses. The interference is negligible for values of the couplings $\xi_{ij} \gg y_{u_i} y_{d_j}$, where y_{u_i,d_j} are the SM Yukawa couplings. Even in the most favorable case, ξ_{cb}, neglecting the charm and bottom masses is reasonable for $\xi_{cb} > 10^{-3}$, a level that, as we will see, is far from the sensitivity that can be reached by present collider experiments. In the case of single-top production and top decays, interference terms are important for $\xi_{tb} \sim y_b y_t$. While in this case the corrections are more relevant, they are still subleading with respect to terms quadratic in ξ_{tb} for the values of the coupling accessible at colliders.

2.1 *W* production

The first process we analyze to look for manifestations of RHCC is $W^\pm$ production. This process is accurately measured at the LHC, both at the level of the inclusive cross section as well as for differential distributions [15–25]. Precise high-order calculations of the SM background are available up to fixed NNLO QCD corrections [26–28] and also include the resummation of the vector-boson transverse momentum [29, 30]. More recently, the interface of the NNLO predictions with the parton shower has been presented in ref. [31]. A careful quantitative assessment of the size of the corrections at different orders, both in QCD and EW, has been presented in ref. [32]. For this study, we have calculated the NLO QCD corrections to the partonic processes mediated by RHCC and interfaced with the parton shower according to the POWHEG method, extending the original work of ref. [33].

The contribution of the RHCC operator to $W^\pm$-production observables that are symmetric under the exchange of the charged lepton and the neutrino momenta, is identical to

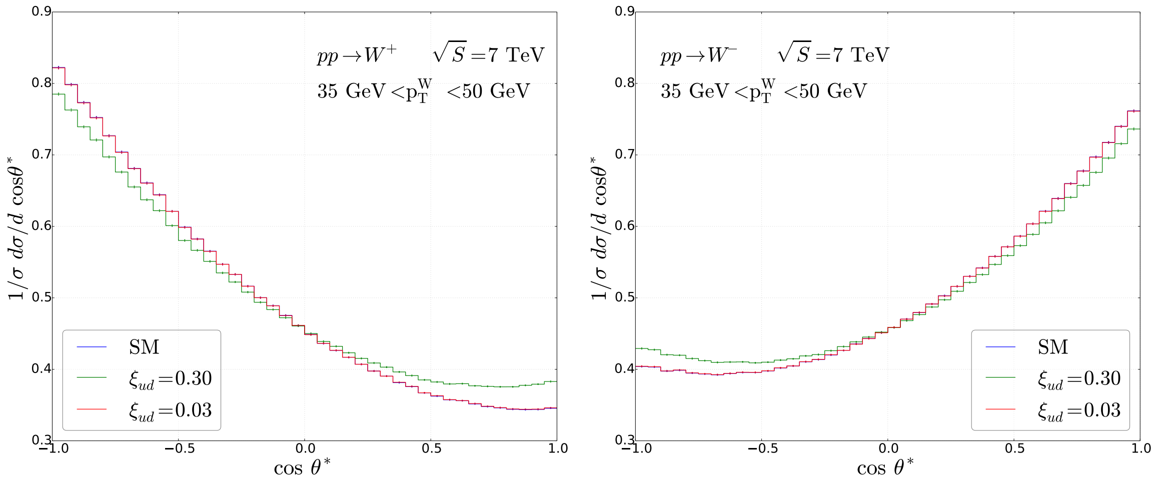

Figure 2. Polar angle $\cos\theta^*$ distribution in $pp \to W^+ \to e^+\nu$ and $pp \to W^- \to e^-\bar{\nu}$ at $\sqrt{S} = 7\,\text{TeV}$, in the SM and in the presence of ξ_{ud}. θ^* is the polar angle of the charged lepton, measured in the W boson rest frame, with the z-axis chosen to be oriented along the W direction in the lab frame.

the SM contribution after the replacement of the CKM elements V_{ij} by ξ_{ij}. For example, in figure 1 we show the differential distribution with respect to the W transverse mass which is defined as [34]

$$m_T^W = \sqrt{2|p_{T\,l}||p_{T\,\nu}|(1-\cos\Delta\phi_{l\nu})}\,. \tag{2.1}$$

Here $p_{T\,l}$ and $p_{T\,\nu}$ are the charged-lepton and the neutrino transverse momenta, respectively, and $\Delta\phi_{l\nu}$ is their azimuthal separation. We evaluate the cross section at $\sqrt{S} = 13\,\text{TeV}$ for the SM (blue curve), $\xi_{ud} = 0.3$ (green curve), and $\xi_{ud} = 0.03$ (red curve). The effect of the RHCC amounts to a rescaling of the cross section. Since the correction is quadratic in ξ_{ij}, choosing $\xi_{ud} = 0.3$ gives approximately a 10% correction to the SM prediction, while $\xi_{ud} = 0.03$ gives sub-permille corrections. Presently, the $W^\pm$ cross section at 13 TeV is known with roughly 3% experimental uncertainty and a similar theoretical uncertainty [16], implying that the bound on ξ_{ud} that can be extracted from the $W^\pm$ cross section is at best around $|\xi_{ud}| \lesssim 0.2$. Due to PDF suppression, the bounds on the other elements of the ξ_{ij} matrix are even weaker. As we discuss in section 2.2, with current sensitivity, the associated production of a Higgs and a W boson is already more constraining than W production. For this reason, we do not list the bounds coming from W production on the various ξ_{ij} elements.

The angular distribution of the charged leptons in $W^\pm$ decay is sensitive to the left-handed nature of the W boson in the SM [35]. One might therefore expect that angular distributions can provide stronger constraints. In figure 2 we plot the differential distribution with respect to $\cos\theta^*$, where θ^* is the polar angle of the charged lepton in the W-boson rest frame, with the z-axis chosen to be in the direction of the W-boson momentum in the laboratory frame. The differential $\cos\theta^*$ distribution is related to the W boson polarization

JHEP05(2017)086

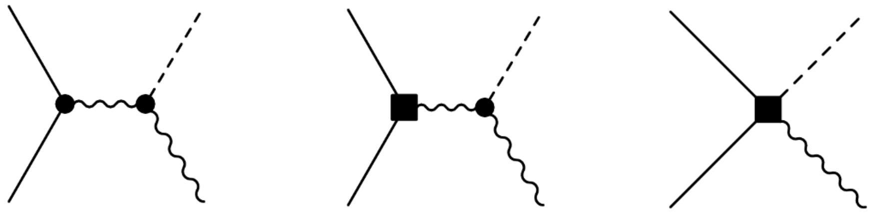

Figure 3. Leading-order contribution to the associated production of a Higgs and a vector boson. Dots denote SM vertices, while squares denote an insertion of ξ.

fractions, F_0, F_L, and F_R by the relations [35]

$$F_0 = \int d\cos\theta^*(2-5\cos^2\theta^*)\frac{1}{\sigma}\frac{d\sigma}{d\cos\theta^*}\,, \tag{2.2}$$

$$F_L = \int d\cos\theta^*\left(-\frac{1}{2}\mp\cos\theta^*+\frac{5}{2}\cos^2\theta^*\right)\frac{1}{\sigma}\frac{d\sigma}{d\cos\theta^*}\,, \tag{2.3}$$

$$F_R = \int d\cos\theta^*\left(-\frac{1}{2}\pm\cos\theta^*+\frac{5}{2}\cos^2\theta^*\right)\frac{1}{\sigma}\frac{d\sigma}{d\cos\theta^*}\,, \tag{2.4}$$

where the upper (lower) sign is for $W^{+(-)}$.

Figure 2 depicts the $\cos\theta^*$ distribution for the SM (blue curve), for $\xi_{ud} = 0.3$, and for $\xi_{ud} = 0.03$. These predictions were evaluated at $\sqrt{S} = 7\,\text{TeV}$ and we applied the same p_T^W cuts as used in the analysis of ref. [18]. We observe that ξ_{ud} does not affect the longitudinal fraction F_0, while it increases the fraction of right-handed polarized W's, and decreases $F_L - F_R$. We find the helicity fractions to be given by

$$F_0 = 0.21, \qquad F_L = 0.54\frac{1+0.3\,\xi_{ud}^2}{1+0.8\,\xi_{ud}^2} \qquad F_R = 0.25\frac{1+1.9\,\xi_{ud}^2}{1+0.8\,\xi_{ud}^2}\,, \tag{2.5}$$

for $35\,\text{GeV} < p_T^W < 50\,\text{GeV}$, and

$$F_0 = 0.19, \qquad F_L = 0.55\frac{1+0.4\,|\xi_{ud}|^2}{1+0.8\,|\xi_{ud}|^2} \qquad F_R = 0.26\frac{1+1.8\,|\xi_{ud}|^2}{1+0.8\,|\xi_{ud}|^2}, \tag{2.6}$$

for $p_T^W > 50\,\text{GeV}$. These helicity fractions were measured in ref. [18] with uncertainties of roughly 20% on $F_L - F_R$ and larger uncertainties on F_0. The significant uncertainties allow for rather large values of ξ_{ud}, up to $\xi_{ud} \sim 0.4$. The contributions to the W helicity fractions involving other elements of the ξ_{ij} matrix are further suppressed by the respective PDF's resulting in even weaker bounds. We conclude that at the moment the W polarization fractions do not provide strong constraints on the effects of RHCC.

2.2 Associated production of a Higgs and a $W^\pm$ boson

As for single W-boson production, WH associated production is available at NNLO in QCD [36–38] and is matched to the parton shower up to the NNLO+PS level [39].

A representative set of tree-level diagrams contributing to associated WH production at LO in presence of RHCC is shown in figure 3. The first diagram denotes the SM

		$\lvert\xi_{ud}\rvert^2$	$\lvert\xi_{us}\rvert^2$	$\lvert\xi_{ub}\rvert^2$	$\lvert\xi_{cd}\rvert^2$	$\lvert\xi_{cs}\rvert^2$	$\lvert\xi_{cb}\rvert^2$
σ_{W^+H} (pb)	central	230	158	66.4	12.7	7.48	2.84
σ_{W^+H} (pb)	scale	± 4	± 3	$^{+0.8}_{-0.4}$	$^{+0.2}_{-0.1}$	$^{+0.08}_{-0.04}$	$^{+0.08}_{-0.04}$
σ_{W^+H} (pb)	PDF	20	36.0	3.2	1.8	2.32	0.48
σ_{W^-H} (pb)	central	100	17.4	6.64	50.4	7.72	2.84
σ_{W^-H} (pb)	scale	± 2	$^{+2.8}_{-2.4}$	$^{+0.08}_{-0.04}$	$^{+0.8}_{-0.4}$	$^{+0.08}_{-0.04}$	$^{+0.08}_{-0.04}$
σ_{W^-H} (pb)	PDF	10.4	4.00	1.12	3.2	2.08	0.48

Table 1. Corrections to the $W^\pm H$ cross section induced by the RHCC ξ_{ij} at $\sqrt{S} = 8\,\text{TeV}$. The total cross section is $\sigma_{W^\pm H} = \sigma^{SM}_{W^\pm H} + \sum a_{ij}|\xi_{ij}|^2$, where the sum is over all light quarks. The values and theoretical uncertainties of a_{ij} are given in the table.

contribution. The remaining two diagrams involve an insertion of ξ, which is denoted by a square. In addition to a contribution similar to the SM (the second diagram), the ξ operator induces a local $(\bar{q}'q)_R hW$ interaction (the third diagram), which leads to a large enhancement of the RHCC contribution. The interference of the right-handed currents with the SM is suppressed by two insertions of the light quark masses and is negligible for values of the couplings that can be probed at the LHC. We therefore focus on the contributions quadratic in ξ.

We computed the NLO QCD corrections to the RHCC contributions to the WH cross section, also considering the decay of the W into leptons. This implementation builds upon the original NLO+PS `POWHEG BOX` code in [40]. The SM NLO cross section at $\sqrt{S} = 8\,\text{TeV}$ is

$$\sigma_{W^+H} = (0.461 \pm 0.021)\,\text{pb}, \quad \sigma_{W^-H} = (0.264 \pm 0.017)\,\text{pb}\,, \tag{2.7}$$

where we used the NLO PDF sets `CT10`, `MSTW08`, and `NNPDF2.3`. The error is dominated by PDF uncertainties while scale variations are about (2-3)%. In table 1 we give the cross sections induced by ξ at $\sqrt{S} = 8\,\text{TeV}$. The central value is evaluated at the scale $\mu = m_H + m_W$. As for the SM results, the errors are dominated by PDF variations that are roughly 10%. As expected, PDF errors are larger for processes involving the strange PDF, which is not known at the same level as the PDFs of the lighter quarks. The cross sections at 13 and 14 TeV have similar theoretical uncertainties.

Using the total cross sections in table 1, we construct the production signal strength in the presence of the RHCC,

$$\mu^{\xi}_{WH} = 1 + \frac{\sigma^{\xi}_{W^+H} + \sigma^{\xi}_{W^-H}}{\sigma^{SM}_{W^+H} + \sigma^{SM}_{W^-H}}\,. \tag{2.8}$$

Our results for the production signal strengths at $\sqrt{S} = 8$, 13 and 14 TeV are summarized in the upper half of table 2. As discussed in section 2.5, the first two rows of the ξ_{ij} matrix do not significantly affect the Higgs branching ratios. We can thus safely assume that Higgs

JHEP05(2017)086

	$\sqrt{S}$	$\lvert\xi_{ud}\rvert^2$	$\lvert\xi_{us}\rvert^2$	$\lvert\xi_{ub}\rvert^2$	$\lvert\xi_{cd}\rvert^2$	$\lvert\xi_{cs}\rvert^2$	$\lvert\xi_{cb}\rvert^2$
μ_{WH} -1	8 TeV	451 ± 29	250 ± 57	101 ± 7	87 ± 7	22 ± 6	8 ± 2
	13 TeV	663 ± 42	381 ± 80	164 ± 11	142 ± 10	42 ± 10	16 ± 3
	14 TeV	703 ± 45	406 ± 84	177 ± 12	153 ± 11	46 ± 11	18 ± 3
		$\lvert\xi_{ud}\rvert$	$\lvert\xi_{us}\rvert$	$\lvert\xi_{ub}\rvert$	$\lvert\xi_{cd}\rvert$	$\lvert\xi_{cs}\rvert$	$\lvert\xi_{cb}\rvert$
ATLAS, CMS [41]	8 TeV	0.04	0.05	0.08	0.08	0.19	0.30
ATLAS [44]	13 TeV	0.04	0.06	0.08	0.09	0.18	0.28
future	14 TeV	0.02	0.03	0.04	0.05	0.09	0.13

Table 2. Signal strength for the WH production channel at $\sqrt{S} = 8\,\text{TeV}$, 13 TeV, and 14 TeV, and 90% CL bounds on ξ_{ij}. The projected bounds at 14 TeV assume 20% uncertainties on μ_{WH}.

decays are SM-like and we simply use the production signal strength in the WH channel in our analysis. The combined result from the ATLAS and CMS collaborations is [41]

$$\mu_{WH}(8\,\text{TeV}) = 0.89^{+0.40}_{-0.38}\,. \tag{2.9}$$

In the lower half of table 2 we list the 90% CL bounds on $|\xi_{ij}|$, with the assumption that the SM is modified only by a RHCC at the high-energy scale $\Lambda \gg v$.[1] The constraints are much stronger than those extracted from $W^{\pm}$ production. The ATLAS collaboration also published preliminary results obtained at 13 TeV [44]

$$\mu_{WH}(13\,\text{TeV}) = 0.33^{+0.95}_{-0.92}\,. \tag{2.10}$$

The larger contribution of the RHCC operators to the cross section is compensated by the larger experimental errors, resulting in similar constraints as obtained from the 8 TeV data.

In table 2 we also show the signal strength and projected bounds at $\sqrt{S} = 14\,\text{TeV}$. The RHCC contributions to the cross section grow faster than the SM contributions, resulting in a greater sensitivity at the LHC Run 2. The projected bounds in table 2 assume a 20% uncertainty on the μ_{WH} signal strength. For all coefficients the improvement is roughly a factor of 2.

The pattern of the constraints in table 2 can be simply understood in terms of the parton distributions. WH production is most sensitive to ξ_{ud}, which involves two valence quarks in the proton, followed by the couplings with one valence quark, ξ_{us}, ξ_{ub}, and ξ_{cd}. The bounds become weaker for ξ_{cs} and ξ_{cb} as the PDFs involve two sea quarks in these cases. While the current and projected bounds on ξ_{ud}, ξ_{us}, ξ_{cd}, and ξ_{cs} are at least a factor of 10 smaller than the corresponding CKM matrix element, the WH cross section allows for values of ξ_{ub} and ξ_{cb} that are much larger than V_{ub} and V_{cb}. As we will discuss, this possibility is excluded by inclusive and exclusive B decays.

[1] Since the coefficients ξ_{ij} depend very mildly on the initial scale Λ [42, 43], we do not specify its precise value.

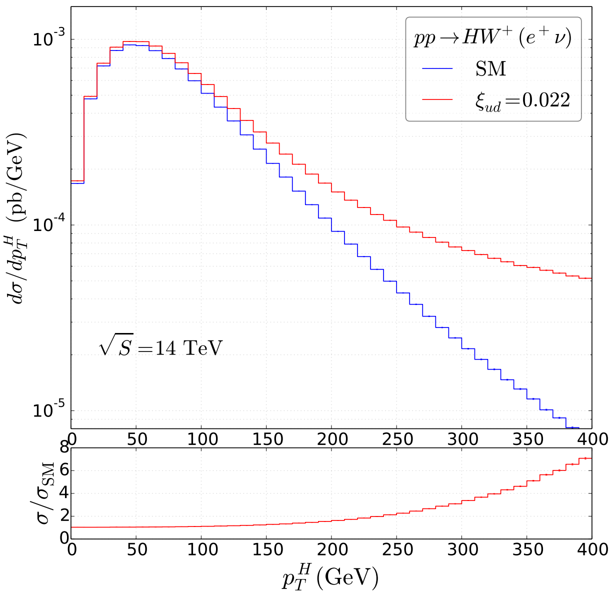

Figure 4. Cross section for the production of HW^+, with $W^+ \to \nu e^+$, at $\sqrt{S} = 14\,\text{TeV}$, differential with respect to the Higgs p_T.

We have focused so far on the signal strengths alone. Differential distributions can provide additional valuable information. In particular, as shown in figure 4, the RHCC contribution is enhanced for large values of the Higgs transverse momentum, or of the WH invariant mass, so that the study of differential distributions at the current and future LHC runs could further improve the collider bounds on ξ. In section 9 we will explore in more detail how to construct observables that can discriminate between RHCC and corrections to the WH cross section from other dimension-six operators in the SMEFT.

2.3 Vector boson fusion

The production rate for an Higgs boson via vector boson fusion (VBF) is also sensitive to the RHCC. The tree-level diagrams contributing to VBF Higgs production are shown in figure 5. As for WH associated production, one topology is identical to the SM with the CKM matrix replaced by ξ_{ij}. In addition, the ξ operator induces a $\bar{q}'qhW$ vertex depicted in the last diagram of figure 5. This topology again leads to an enhancement with respect to the SM, albeit not as numerically significant as for WH associated production.

The total cross section for Higgs production through VBF has been recently computed in the SM at N^{3}LO in QCD [45]. Fully-differential distributions are available up to NNLO [46] and the interface with parton showering is available at NLO+PS accuracy [47]. For this study, we computed the NLO QCD corrections to both the SM and the RHCC VBF cross sections, building upon the `POWHEG` implementation presented in ref. [47]. We find that the total VBF cross section is

$$\frac{\sigma_{\rm VBF}(8\,\text{TeV})}{\text{pb}} = 1.6\left(1+16.4|\xi_{ud}|^2+9.1|\xi_{us}|^2+8.5|\xi_{ub}|^2+6.2|\xi_{cd}|^2+2.6|\xi_{cs}|^2+1.1|\xi_{cb}|^2\right), \tag{2.11}$$

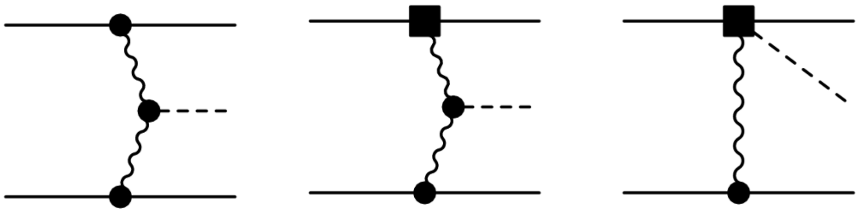

Figure 5. Leading order contribution to Higgs production via vector boson fusion. Dots denote SM vertices, while squares denotes an insertion of ξ.

where we used $\mu = m_W$ as the renormalization and factorization scale, and we computed the cross section with the `CT10nlo` PDF set. PDF and scale variations indicate that the theory uncertainties are below the 10% level.

In order to disentangle VBF from gluon-fusion contributions, the final state is required to have at least two well-separated jets. The invariant mass of the two jets has to be $m_{jj} > 600\,\mathrm{GeV}$, while the rapidity separation has to be $|y_{j_1} - y_{j_2}| > 4.2$. Furthermore, all jets are required to have $p_{Tj} > 20\,\mathrm{GeV}$ and $|y_j| < 5$. Within these cuts, the NLO cross section becomes

$$\frac{\sigma_{\mathrm{VBF}}(8\,\mathrm{TeV})}{\mathrm{pb}} = 0.30\left(1+12.0|\xi_{ud}|^2+7.3|\xi_{us}|^2+6.7|\xi_{ub}|^2+5.7|\xi_{cd}|^2+1.3|\xi_{cs}|^2+0.3|\xi_{cb}|^2\right). \tag{2.12}$$

From eqs. (2.11) and (2.12) we see that the VBF channel is sensitive to RHCC, but the modifications to the signal strength are much smaller than for WH associated production. The combined ATLAS and CMS signal strength from Run I is [41]

$$\mu_{VBF} = 1.18 \pm 0.25\,. \tag{2.13}$$

This implies that from the signal strength alone we get constraints on, for example, $|\xi_{ud}| < 0.2$, $|\xi_{ub}| < 0.3$, and $|\xi_{cb}| \sim 1$. These bounds are considerably weaker than those given in table 2 arising from associated production.

At 14 TeV, the cross section within the aforementioned VBF cuts is

$$\frac{\sigma_{\mathrm{VBF}}(14\,\mathrm{TeV})}{\mathrm{pb}} = 1.1\left(1+23.2|\xi_{ud}|^2+12.4|\xi_{us}|^2+11.8|\xi_{ub}|^2+8.7|\xi_{cd}|^2+2.4|\xi_{cs}|^2+1.0|\xi_{cb}|^2\right), \tag{2.14}$$

which again signals a smaller sensitivity to ξ_{ij} compared to WH associated production.

One advantage of using VBF is the presence of jets in the final state, which gives an additional handle on the flavor structure of the RHCC. For example, by requiring that at least one of the jets in the final state is b tagged, we can enhance the contributions of the couplings ξ_{ub} and ξ_{cb} at the price of a reduced cross section,

$$\left.\frac{\sigma_{\mathrm{VBF}}(14\,\mathrm{TeV})}{\mathrm{pb}}\right|_{\mathrm{btag}} = 0.05\left(1+235|\xi_{ub}|^2+19.3|\xi_{cb}|^2\right). \tag{2.15}$$

$\sqrt{S}$ (TeV)	σ_t (pb)	$\sigma_{\bar{t}}$ (pb)	$\sigma_{t+\bar{t}}$ (pb)	Experiment
7	46 ± 6	23 ± 3	68 ± 8	ATLAS [48]
	—	—	67 ± 7	CMS [49]
8	57 ± 4	33 ± 3	90 ± 5	ATLAS [50]
	54 ± 5	28 ± 4	84 ± 8	CMS [51]
13	156 ± 28	91 ± 18	247 ± 46	ATLAS [52]
	150 ± 22	82 ± 16	232 ± 31	CMS [53]

Table 3. t-channel single-top total cross sections measured by ATLAS and CMS.

After b tagging, the enhancement of the ξ_{ub} and ξ_{cb} contributions to VBF is slightly better than the one quoted in table 2 for WH. Since the flavor tag allows for more direct access to specific elements of the ξ matrix, it can be interesting to pursue such observables at the Run II.

2.4 Single-top production and W-boson helicity fractions in top decays

The processes considered so far (W production, WH production, and Higgs production via VBF) do not constrain the ξ_{tj} elements of the right-handed current matrix. In this section, we consider single-top production, which is sensitive to Wtq couplings, and the W-boson helicity fractions in top decay, which probe the Wtb coupling, and are sensitive to its left-handed nature.

The largest SM contribution to single-top production at the LHC is via the t-channel exchange of a W boson. Smaller contributions arise from the associated production of a top and a W boson and by s-channel W exchange. ATLAS published the measurement of the inclusive and differential cross sections at $\sqrt{S} = 7$, 8, and 13 TeV, with luminosities of, respectively, $5\,\text{fb}^{-1}$, $20.2\,\text{fb}^{-1}$ and $3.2\,\text{fb}^{-1}$ [48, 50, 52]. CMS published results at $\sqrt{S} = 7$, 8, and 13 TeV, with luminosities of 1.56, 20, and $2.3\,\text{fb}^{-1}$, respectively [49, 51, 53]. The observed cross sections are summarized in table 3. The associated production of a top and a W boson, and s-channel single-top production have also been observed [54–56]. In our analysis, however, we include only t-channel production as this gives the most stringent constraints.

The production of a top-quark in the t-channel can be described both in the 5-flavor scheme, in which the b quark is considered massless and appears in the initial state, and in the 4-flavor scheme, which keeps into account m_b effects. The total and differential SM cross sections are known at NNLO in QCD [57] only in the 5-flavor scheme. Top-quark decay is also available at NNLO [58, 59]. A combination of production and decay in the top-quark narrow-width approximation has been presented in ref. [60]. The calculation in the 4-flavor scheme has been presented at NLO in QCD in ref. [61] and the interface to the parton shower is discussed in ref. [62]. More recently, this process was interfaced with the parton shower at the NLO+PS level, including off-shell and interference effects [63–65].

$\sqrt{S}$ (TeV)		SM	$\lvert\xi_{td}\rvert^2$	$\lvert\xi_{ts}\rvert^2$	$\lvert\xi_{tb}\rvert^2$
7	σ_t (pb)	$41.9^{+1.8}_{-0.9}$	309 ± 3	85.6 ± 6.4	36.0 ± 1.2
	$\sigma_{\bar{t}}$ (pb)	$22.7^{+0.9}_{-1.0}$	89.2 ± 2.4	58.0 ± 4.8	24.0 ± 0.8
8	σ_t (pb)	$56.4^{+2.4}_{-1.1}$	375 ± 4	110 ± 8	48 ± 1.6
	$\sigma_{\bar{t}}$ (pb)	$30.7^{+1.1}_{-1.3}$	115 ± 3	76 ± 6.4	32 ± 1.0
13	σ_t (pb)	136 ± 5	720 ± 12	259 ± 18	126 ± 12
	$\sigma_{\bar{t}}$ (pb)	$81.0^{+4.1}_{-3.6}$	265 ± 11	200 ± 14	88 ± 2.4

Table 4. t-channel single-top cross section in the presence of ξ_{tj}.

We computed the corrections of the operators ξ_{tj} to the t-channel single top cross section in the 5-flavor scheme, including NLO QCD effects building upon the POWHEG implementation in ref. [66]. The right-handed current operators interfere with the SM through terms proportional to the mass of the light down-type quark. For ξ_{td} and ξ_{ts} operators it is safe to neglect these terms considering the current collider sensitivity. For ξ_{tb}, the interference is more important but can also be neglected at present.

In table 4 we give the SM cross section at $\sqrt{S} = 7$, 8, and 13 TeV, and the corrections induced by the RHCC operators. The cross sections are evaluated at the factorization and renormalization scale $\mu = m_t$. The scale uncertainty was estimated by varying the factorization and renormalization scales between $\mu = m_t/2$ and $\mu = 2m_t$. The PDF and α_s uncertainties were conservatively estimated following the original PDF4LHC recipe [67] using the three PDF sets CT10 [68], MSTW08 [69], and NNPDF2.3 [70]. PDF uncertainties turn out to dominate the theoretical uncertainty.

In addition to the single-top production cross section, modifications of the Wtq vertex strongly affect the decay of the top quark. An observable particularly sensitive to RHCC is the ratio of the top decay width into a W and a b quark and the width into all down-type quarks. This ratio is measured to be [71]

$$\frac{\Gamma(t \to Wb)}{\sum_{q=d,s,b} \Gamma(t \to Wq)} = 0.957 \pm 0.034\,. \tag{2.16}$$

In the presence of ξ_{tj}, neglecting terms proportional to m_b, this becomes

$$\frac{\Gamma(t \to Wb)}{\sum_{q=d,s,b} \Gamma(t \to Wq)} = \frac{|V_{tb}|^2 + |\xi_{tb}|^2}{\sum_{q=d,s,b} \left(|V_{tq}|^2 + |\xi_{tq}|^2\right)}\,. \tag{2.17}$$

Additional information is carried by the helicity fractions of W bosons produced from top quark decays, which are mostly sensitive to ξ_{tb}. The helicity fractions have been measured at the Tevatron [72] and at the LHC [73–77]. In table 5 we summarize the results used in our analysis. The experimental uncertainty is obtained by combining in quadrature the statistical and systematic errors reported by the experimental collaborations, and considering the correlations between F_0 and $F_{L,R}$ in the determination of the χ^2 function.

JHEP05(2017)086

F_0	F_L	F_R	experiment	
0.72 ± 0.08	0.31 ± 0.09	-0.03 ± 0.04	CDF & D0	[72]
0.67 ± 0.07	0.32 ± 0.04	0.01 ± 0.04	ATLAS	[73]
0.68 ± 0.04	0.31 ± 0.03	0.01 ± 0.01	CMS	[74]
0.72 ± 0.06	0.30 ± 0.04	-0.02 ± 0.02	CMS	[76]
0.709 ± 0.019	0.299 ± 0.015	0.008 ± 0.014	ATLAS	[77]

Table 5. W helicity fractions measured at CDF, D0, ATLAS, and CMS.

The SM helicity fractions have been computed at NNLO in QCD [78]. They can be expressed as functions of the ratio $x = m_W/m_t$. Choosing the top pole mass $m_t = 173\,\text{GeV}$ and $m_W = 80.4\,\text{GeV}$, the SM helicity fractions at NNLO are $F_0 = 0.687$, $F_L = 0.311$, and $F_R = 0.0017$. The theoretical uncertainty is very small, only at the permille level, and is negligible compared to the experimental uncertainty. The corrections to the helicity fractions induced by a right-handed Wtb vertex have been computed at NLO in QCD in ref. [79], and they can be obtained from the SM by exchanging F_R and F_L.

Combining the information from single-top production, top decay, and W boson helicity fractions, we obtain the following 90% C.L. bounds

$$|\xi_{td}| < 0.13, \qquad |\xi_{ts}| < 0.22, \qquad |\xi_{tb}| < 0.16\,, \tag{2.18}$$

where, as in the previous sections, we assumed that the SM is modified only by a RHCC.

2.5 Higgs branching ratios

RHCC affect Higgs decays at tree level, by modifying the $h \to WW^*$ channel, and, more importantly, contributing at one loop to the Yukawa couplings of the Higgs boson to fermions. In particular, ξ_{tb} induces large corrections to the bottom Yukawa coupling y_b. The corrections are proportional to the top Yukawa coupling y_t and alter the $h \to b\bar{b}$ width and thereby the total Higgs width as well. Defining the quark Yukawa couplings as

$$\mathcal{L} \supset -y_q\, \bar{q}_L q_R\, h + \text{h.c.}\ , \tag{2.19}$$

the running of the bottom Yukawa and mass are modified by ξ_{tb} as follows [42, 43, 80],

$$\begin{aligned} \frac{dm_b}{d\ln\mu} &= \gamma_m \frac{\alpha_s}{4\pi} m_b + \frac{g^2}{(4\pi)^2} m_t (x_t - 3) V_{tb}^* \xi_{tb}\,, \\ \frac{dy_b}{d\ln\mu} &= \gamma_m \frac{\alpha_s}{4\pi} y_b + \frac{g^2}{(4\pi)^2} \frac{m_t}{v} (x_h + 3x_t - 9) V_{tb}^* \xi_{tb}\,, \end{aligned} \tag{2.20}$$

where $x_i = m_i^2/m_W^2$. The anomalous dimension $\gamma_m = -6C_F$ determines the usual one-loop evolution from QCD effects, while the ξ_{tb} terms alter the evolution between the scale of new physics, Λ, and $\mu = M_W$. We use the boundary condition $y_b(\Lambda) = m_b(\Lambda)/v$, which

JHEP05(2017)086

follows from our assumption that the ξ operators are the only dimension-six terms present at $\mu = \Lambda$. In this case the SM Yukawa couplings are not modified at this scale.

Apart from these RG effects, the right-handed current operators affect the $h \to b\bar{b}$ process through finite loop contributions. The effective coupling that is probed in Higgs decays, is then given by

$$
\begin{aligned}
y_b^{(\text{eff})} = y_b(\mu) - \frac{g^2}{(4\pi)^2}\frac{m_t}{v}\frac{\xi_{tb}V_{tb}^*}{2}\Bigg[&(x_h + 3x_t - 9)\log\frac{\mu^2}{m_W^2} \\
&-3\frac{x_t(x_t-3)}{x_t-1}\log x_t + x_t\beta_t \log\left(\frac{\beta_t - 1}{\beta_t+1}\right) \\
&+(x_h-2)\beta_w \log\left(\frac{\beta_W-1}{\beta_W+1}\right) + (2x_h + x_t(x_t-7))f_1(x_h,x_t) \\
&-(4+(2-x_h)x_t)f_2(x_h,x_t) + (-5+2x_h+4x_t)\Bigg], \quad (2.21)
\end{aligned}
$$

where $y_b(\mu)$ is given by the solution of eq. (2.20), $\beta_i = \sqrt{1 - 4m_i^2/m_h^2}$, and the two functions $f_{1,2}$ are given by

$$
\begin{aligned}
f_1(x_h,x_t) &= \int_0^1 dz \frac{1}{1-x_t+x_h z}\log\left(\frac{x_t - x_h(1-z)z}{1+(x_t-1)z}\right), \\
f_2(x_h,x_t) &= \int_0^1 dz \frac{1}{-1+x_t+x_h z}\log\left(\frac{1 - x_h(1-z)z}{x_t+z(1-x_t)}\right). \qquad (2.22)
\end{aligned}
$$

Setting $\mu = m_H$ and $\Lambda = 1\,\text{TeV}$, we find numerically $y_b^{(\text{eff})} \simeq 0.012 - 0.019\,\xi_{tb}V_{tb}^*$. We then compute the $h \to b\bar{b}$ decay rate using expressions in ref. [81]. Using the ATLAS and CMS combination [41] for the $\gamma\gamma$, WW, ZZ, $\tau\tau$, $b\bar{b}$, and $\mu\mu$ signal strengths, we obtain,

$$
\text{Re}\,\xi_{tb} \in [-0.01,\, 0.13]\,, \qquad \text{Im}\,\xi_{tb} \in [-0.22,\, 0.22]\,, \qquad (2.23)
$$

where we turned on only one parameter, the real or imaginary part, at the time, and the bounds assume $\Lambda = 1\,\text{TeV}$. The limits are only mildly sensitive to the choice of initial scale Λ. Setting, for example, $\Lambda = 10\,\text{TeV}$ results in $\text{Re}\,\xi_{tb} \in [-0.005, 0.10]$, and $\text{Im}\,\xi_{tb} \in [-0.15, 0.15]$. Notice that the bounds from $h \to b\bar{b}$ are already competitive with the direct bounds from single-top production and top decay.

Analogously to ξ_{tb}, the ξ_{td} and ξ_{ts} elements give contributions to the down- and strange-quark Yukawas that are enhanced by y_t, with, in this case, some suppression from the small CKM elements V_{td} and V_{ts}. Since, at the moment, y_d and y_s are constrained at the same level as y_b [82, 83], the bounds on ξ_{td} and ξ_{ts} are weaker than eq. (2.23) and not competitive with single top production and top decay. The contributions of the first two rows of the ξ_{ij} matrix to the quark Yukawa couplings are not enhanced by the top Yukawa. In this case, tree level corrections to $h \to WW^*$ are more important. Neglecting quark and lepton masses, the decay rate at LO in QCD is equal to

$$
\Gamma(h \to WW^*) = \frac{3m_H m_W^4}{32\pi^3 v^4}\left(R(x_W) + \sum_{i,j}\left(|V_{ij}|^2 R(x_W) + |\xi_{ij}|^2 R_\xi(x_W)\right)\right), \qquad (2.24)
$$

where $x_W = m_W^2/m_H^2$, the sum over i and j extends over all light quarks, and the functions R and R_ξ are [81]

$$
\begin{aligned}
R(x) &= -\frac{1-x}{6x}(2-13x+47x^2)-\frac{1}{2}(1-6x+4x^2)\log x+\frac{(1-8x+20x^2)}{\sqrt{4x-1}}\arccos\left(\frac{3x-1}{2x^{3/2}}\right) \\
R_\xi(x) &= -\frac{1-x}{36x^2}(-3+53x-541x^2+407x^3)+\frac{1}{6x}(2+3x+114x^2-12x^3)\log x \\
&\quad +\frac{-2+19x-80x^2+156x^3}{3x\sqrt{4x-1}}\arccos\left(\frac{3x-1}{2x^{3/2}}\right). \qquad (2.25)
\end{aligned}
$$

For $m_H = 125\,\text{GeV}$, $R_\xi(x_W)/R(x_W) = 0.03$, such that

$$
\Gamma(h \to WW^*) = \Gamma_{\rm SM}(h \to WW^*)\left(1 + 0.01\sum_{ij}|\xi_{ij}|^2\right), \qquad (2.26)
$$

and very large couplings, $\xi_{ij} > 1$, are needed to significantly affect the Higgs branching ratios.

2.6 Summary of collider bounds

To summarize, the 90% C.L. bounds on the ξ_{ij} matrix are

$$
\begin{pmatrix} |\xi_{ud}| & |\xi_{us}| & |\xi_{ub}| \\ |\xi_{cd}| & |\xi_{cs}| & |\xi_{cb}| \\ |\xi_{td}| & |\xi_{ts}| & |\xi_{tb}| \end{pmatrix} \le \begin{pmatrix} 0.04 & 0.05 & 0.08 \\ 0.08 & 0.19 & 0.30 \\ 0.13 & 0.22 & 0.16 \end{pmatrix}. \qquad (2.27)
$$

The bounds on the first two rows are dominated by WH production, while the bounds on ξ_{tj} are determined by single-top production and top decay. Including the constraint from $h \to b\bar{b}$ changes the bounds on ξ_{tb} into $\mathrm{Re}\,\xi_{tb} \in [-0.01, 0.13]$ and $\mathrm{Im}\,\xi_{tb} \in [-0.15, 0.15]$. The above collider constraints still leave room for BSM physics around, or even slightly below, the TeV scale.

3 Low-energy effective Lagrangian

The effects of the RHCC operator ξ at low energies are obtained by integrating out the W boson and the other heavy SM degrees of freedom. We start by analyzing the tree-level contributions to semileptonic and four-quark operators and then discuss the loop-level operators that are relevant for EDMs ($\Delta F = 0$) and rare flavor-changing neutral-current (FCNC) processes such as $B \to X_q\gamma$ and $K_L \to \pi^0 e^+ e^-$ ($\Delta F = 1$). The matching onto $\Delta F = 1$ penguin operators and $\Delta F = 2$ operators relevant for meson-antimeson mixing, which involve two insertions of ξ, are discussed in appendix A. A similar analysis for SM-EFT operators involving the Z boson was recently reported in ref. [84].

JHEP05(2017)086

3.1 Tree-level effective Lagrangian

The combination of the SM left-handed charged current and the RHCC generates at low-energy one semileptonic four-fermion and two four-quark operators. Including the four-fermion operators induced by the SM at tree level, we have

$$\mathcal{L} = -\frac{4G_F}{\sqrt{2}} \left(V_{ij}^* \, \bar{d}^j \gamma^\mu P_L u^i \, \bar{\nu} \gamma_\mu P_L l + \xi_{ij}^* \, \bar{d}^j \gamma^\mu P_R u^i \, \bar{\nu} \gamma_\mu P_L l + \text{h.c.} \right) \\ - \sum_{a=1}^{2} \left(C_{a\,LL}^{ij\,lm} \mathcal{O}_{a\,LL}^{ij\,lm} + C_{a\,LR}^{ij\,lm} \mathcal{O}_{a\,LR}^{ij\,lm} + C_{a\,LR}^{ij\,lm\,*} (\mathcal{O}_{a\,LR}^{ij\,lm})^\dagger \right) , \tag{3.1}$$

where $P_{L,R} = (1 \mp \gamma_5)/2$, i-m are flavor indices, and the four-quark operators are defined as

$$\mathcal{O}_{1\,LL}^{ij\,lm} = \bar{d}^m \gamma^\mu P_L u^l \, \bar{u}^i \gamma_\mu P_L d^j , \qquad \mathcal{O}_{2\,LL}^{ij\,lm} = \bar{d}^m_\alpha \gamma^\mu P_L u^l_\beta \, \bar{u}^i_\beta \gamma_\mu P_L d^j_\alpha , \\ \mathcal{O}_{1\,LR}^{ij\,lm} = \bar{d}^m \gamma^\mu P_L u^l \, \bar{u}^i \gamma_\mu P_R d^j , \qquad \mathcal{O}_{2\,LR}^{ij\,lm} = \bar{d}^m_\alpha \gamma^\mu P_L u^l_\beta \, \bar{u}^i_\beta \gamma_\mu P_R d^j_\alpha , \tag{3.2}$$

where α, β are color indices. The tree-level matching coefficients at the scale m_W are given by

$$C_{1\,LL}^{ij\,lm}(m_W) = \frac{4G_F}{\sqrt{2}} V_{lm}^* V_{ij} , \qquad C_{1\,LR}^{ij\,lm}(m_W) = \frac{4G_F}{\sqrt{2}} V_{lm}^* \xi_{ij} , \qquad C_{2\,AB}^{ij\,lm}(m_W) = 0 , \tag{3.3}$$

where $A, B \in \{L, R\}$ and hermiticity implies $C_{1\,LL}^{lm\,ij\,*} = C_{1\,LL}^{ij\,lm}$. As usual, the SM couplings scale as two inverse powers of the electroweak scale, $C_{i\,LL} \sim 1/v^2$, while the 'left-right' operators induced by the RHCC scale as two inverse powers of the scale of new physics, $C_{i\,LR} \sim \xi/v^2 \sim 1/\Lambda^2$. We neglect four-quark operators that are quadratic in ξ and are suppressed by v^2/Λ^2 with respect to the linear terms.

The operators in eq. (3.1) need to be evolved to lower energies. While the semileptonic operators are not affected by QCD RG evolution, the anomalous dimensions of the four-quark operators are defined by [85, 86]

$$\frac{d}{d \log \mu} \left(C_{1\,AB}, C_{2\,AB} \right)^T = \frac{\alpha_s}{4\pi} \sum_{n=0} \left(\frac{\alpha_s}{4\pi} \right)^n \gamma_{AB}^{(n)} \left(C_{1\,AB}, C_{2\,AB} \right)^T , \tag{3.4}$$

and, at lowest order, we have

$$\gamma_{LL}^{(0)} = \begin{pmatrix} -\frac{6}{N_c} & 6 \\ 6 & -\frac{6}{N_c} \end{pmatrix} , \qquad \gamma_{LR}^{(0)} = \begin{pmatrix} \frac{6}{N_c} & 0 \\ -6 & -6\frac{N_c^2-1}{N_c} \end{pmatrix} . \tag{3.5}$$

The solution of the RGE for the operators of interest is given in table 7.

The semileptonic operators in eq. (3.1) affect leptonic and semileptonic decays of mesons and the β decay of baryons. In particular, ξ is the only dimension-six operator in the SMEFT that induces a tree-level charged-current coupling of right-handed quarks to left-handed leptons, allowing for clean low-energy tests. The coefficients of the four-quark operators $\mathcal{O}_{i\,LR}$ have an imaginary part which leads to CP violation even if all generation indices are the same. They therefore induce large tree-level contributions to observables such as EDMs and ϵ'/ϵ.

3.2 One-loop contributions to $\Delta F = 0$ and $\Delta F = 1$ operators

Next we consider loop diagrams, which can induce important contributions to processes such as $B \to X_q \gamma$, $K_L \to \pi^0 e^+ e^-$ and to EDMs. At linear order in ξ, the most important operators that are generated are dipole operators and the Weinberg three-gluon operator, described by

$$\mathcal{L}=\Bigg(-\frac{g_s}{2} \sum_{ij\in\{u,c\}} m_{u_j} C_{gu}^{ij} \bar{u}_L^i \sigma^{\mu\nu} G_{\mu\nu}^a t^a u_R^j - \frac{g_s}{2} \sum_{ij\in\{d,s,b\}} m_{d_j} C_{gd}^{ij} \bar{d}_L^i \sigma^{\mu\nu} G_{\mu\nu}^a t^a d_R^j \\ -\frac{eQ_u}{2} \sum_{ij\in\{u,c\}} m_{u_j} C_{\gamma u}^{ij} \bar{u}_L^i \sigma^{\mu\nu} F_{\mu\nu} u_R^j - \frac{eQ_d}{2} \sum_{ij\in\{d,s,b\}} m_{d_j} C_{\gamma d}^{ij} \bar{d}_L^i \sigma^{\mu\nu} F_{\mu\nu} d_R^j \\ -\frac{eQ_e}{2} \sum_{ij\in\{e,\mu,\tau\}} m_{e_j} C_{\gamma l}^{ij} \bar{e}_L^i \sigma^{\mu\nu} F_{\mu\nu} e_R^j + \text{h.c.}\Bigg) + \frac{g_s}{3} f^{abc} \Big(C_G G^{a\,\mu\nu} + \frac{C_{\tilde{G}}}{2} \varepsilon^{\mu\nu\alpha\beta} G_{\alpha\beta}^a \Big) G_{\mu\rho}^b G_\nu^{c\,\rho} \,, \tag{3.6}$$

where we chose to factor the mass of the right-handed quark or lepton out of the definition of the dipole operators. The lepton dipoles receive a contribution from ξ_{tb} at two loops, which, neglecting neutrino mass effects, is diagonal in lepton flavor. We discuss this contribution in appendix B. The operators in eq. (3.6) satisfy the RGEs

$$\frac{d}{d\log\mu} (C_{\gamma u}^{ij}, C_{gu}^{ij}, C_G + iC_{\tilde{G}})^T = \frac{\alpha_s}{4\pi} \sum_n \left(\frac{\alpha_s}{4\pi}\right)^n \gamma_{\text{dipole}}^{(n)} (C_{\gamma u}^{ij}, C_{gu}^{ij}, C_G + iC_{\tilde{G}})^T \\ + \frac{\alpha_s}{4\pi} \frac{m_{d_m}}{m_{u_j}} \sum_n \left(\frac{\alpha_s}{4\pi}\right)^n \gamma_{\text{dipole, uLR}}^{(n)} \Big(C_{1\,LR}^{jm\,im\,*}, C_{2\,LR}^{jm\,im\,*} \Big)^T \tag{3.7}$$

$$\frac{d}{d\log\mu} \Big(C_{\gamma d}^{ij}, C_{gd}^{ij}, C_G + iC_{\tilde{G}}\Big)^T = \frac{\alpha_s}{4\pi} \sum_n \left(\frac{\alpha_s}{4\pi}\right)^n \gamma_{\text{dipole}}^{(n)} \Big(C_{\gamma d}^{ij}, C_{gd}^{ij}, C_G + iC_{\tilde{G}}\Big)^T \\ + \frac{\alpha_s}{4\pi} \frac{m_{u_m}}{m_{d_j}} \sum_n \left(\frac{\alpha_s}{4\pi}\right)^n \gamma_{\text{dipole, dLR}}^{(n)} \Big(C_{1\,LR}^{mj\,mi}, C_{2\,LR}^{mj\,mi} \Big)^T . \tag{3.8}$$

At lowest order γ_{dipole} is given by [86–89]

$$\gamma_{\text{dipole}}^{(0)} = \begin{pmatrix} 8C_F & -8C_F & 0 \\ 0 & (16C_F - 4N_c) & 2N_c\delta_{ij} \\ 0 & 0 & N_c + 2n_f + \beta_0 \end{pmatrix} . \tag{3.9}$$

The mixing between the tree-level operators $C_{1,2\,LR}$ and the dipole operators was computed in ref. [90] for down-type dipoles, and it is given by [90, 91][2]

$$\gamma_{\text{dipole,dLR}}^{(0)} = \frac{1}{(4\pi)^2} \begin{pmatrix} 32\frac{Q_u}{Q_d}\left(1 + \frac{2}{3}\frac{Q_d}{Q_u}\right) & 160\frac{Q_u}{Q_d} \\ \frac{16}{3} & -8 \\ 0 & 0 \end{pmatrix} . \tag{3.10}$$

$\gamma_{\text{dipole, uLR}}^{(0)}$ is obtained by replacing Q_d with Q_u in eq. (3.10).

[2]We thank M. Misiak for providing us the expression of $\gamma_{\text{dipole,dLR}}^{(0)}$ for general charges Q_d and Q_u [91].

$q' \to q\gamma$	$\xi_{uq'}V^*_{uq}$	$\xi_{cq'}V^*_{cq}$	$\xi_{tq'}V^*_{tq}$
$\frac{m_{q'}}{m_b}v^2 C^{qq'}_{\gamma d}(m_W)$	$-3.6\cdot 10^{-5}$	-0.019	-3.2
$\frac{m_{q'}}{m_b}v^2 C^{qq'}_{gd}(m_W)$	$-$	$-$	-0.48
$\frac{m_{q'}}{m_b}v^2 C^{qq'}_{\gamma d}(\mu_b^+)$	$-4.7\cdot 10^{-5}$	-0.025	-2.0
$\frac{m_{q'}}{m_b}v^2 C^{qq'}_{gd}(\mu_b^+)$	$-8.0\cdot 10^{-7}$	$-4.3\cdot 10^{-4}$	-0.30
$\frac{m_{q'}}{m_b}v^2 C^{qq'}_{\gamma d}(\mu_b^-)$	$-4.7\cdot 10^{-5}$	-0.054	-2.0
$\frac{m_{q'}}{m_b}v^2 C^{qq'}_{gd}(\mu_b^-)$	$-8.0\cdot 10^{-7}$	$-6.2\cdot 10^{-3}$	-0.30

Table 6. Contributions of the right-handed W-current to the $q' \to q\gamma$ dipole operators at $\mu = m_W$ and $\mu = \mu_b^\pm = 2\,\text{GeV}$. Here μ_b^- and μ_b^+ differentiate between cases in which the charm quark has been integrated out at $\mu = \mu_b$, or is still present within the EFT, respectively. A "$-$" denotes the contribution is negligible for our purposes.

The one-loop matching coefficients at the scale m_W are

$$\begin{aligned}
C^{il}_{\gamma u}(m_W) &= \frac{4G_F}{\sqrt{2}}\frac{2}{(4\pi)^2}\sum_{j\in\{d,s,b\}}\frac{m_{d_j}}{m_{u_l}Q_u}\xi^*_{lj}V_{ij}\,,\\
C^{il}_{gu}(m_W) &= 0\,,\\
C^{il}_{\gamma d}(m_W) &= \frac{4G_F}{\sqrt{2}}\frac{2}{(4\pi)^2}\sum_{j\in\{u,c\}}\frac{m_{u_j}}{m_{d_l}Q_d}\xi_{jl}V^*_{ji}+\frac{4G_F}{\sqrt{2}}\frac{1}{(4\pi)^2}\frac{m_tQ_u}{m_{d_l}Q_d}\xi_{tl}V^*_{ti}\left[f_W(x_t)+\frac{1}{Q_u}g_W(x_t)\right],\\
C^{il}_{gd}(m_W) &= -\frac{4G_F}{\sqrt{2}}\frac{1}{(4\pi)^2}\frac{m_t}{m_{d_l}}\xi_{tl}V^*_{ti}f_W(x_t)\,,\\
C_{\tilde{G}}(m_W) &= 0\,,
\end{aligned} \tag{3.11}$$

where $x_t = m_t^2/m_W^2$, and we neglected powers of x_{u_j} and x_{d_j} except for the top quark. The loop functions are given by

$$f_W(x) = \frac{x^3+3x-4-6x\ln x}{2(x-1)^3}\,, \qquad g_W(x) = \frac{4+x(x-11)}{2(x-1)^2}+3\frac{x^2\ln x}{(x-1)^3}\,. \tag{3.12}$$

Notice that at the scale m_W there is no matching contribution to the Weinberg operator. Two-loop diagrams with internal top and bottom quarks, and a W exchange within the loop, as the ones computed in ref. [92], are exactly canceled by a diagram in the EFT below m_W, with an insertion of a bottom chromo-EDM (CEDM), the C^{bb}_{gd} operator in eq. (3.11), such that $C_{\tilde{G}}(m_W) = 0$.

The operators $C^{bq}_{\gamma(g)d}$ and $C^{qb}_{\gamma(g)d}$ contribute to $B \to X_q\gamma$, and their value at the scales $\mu = m_W$ and $\mu = \mu_b = 2\,\text{GeV}$ are given in table 6. The contributions from diagrams with internal top quarks are enhanced by m_t/m_b with respect to the SM, which, as we will see, leads to stringent bounds on the ξ_{tq} elements of the right-handed matrix. In order to match onto the relevant operators for EDMs and $K_L \to \pi^0 e^+ e^-$ one has to consider the contributions arising at the bottom and charm thresholds. At the scale m_b, four-quark operators such as $C_{1\,LR}^{ub\,ub}$ generate threshold corrections to the up and charm EDM and CEDMs, while the bottom CEDM contributes to the Weinberg operator. Thus, at the b threshold

$$\begin{aligned}
C_{\gamma u}^{il}(m_b^-) &= C_{\gamma u}^{il}(m_b^+) + \frac{2}{(4\pi)^2}\frac{m_b Q_d}{m_{u_l} Q_u}\left(C_{1LR}^{lb\,ib\,*}(m_b) + N_c\, C_{2\,LR}^{lb\,ib\,*}(m_b)\right)\,, \\
C_{gu}^{il}(m_b^-) &= -\frac{2}{(4\pi)^2}\frac{m_b}{m_{u_l}}\, C_{1LR}^{lb\,ib\,*}(m_b)\,, \\
C_{\tilde G}(m_b^-) &= -\frac{\alpha_s}{8\pi}\mathrm{Im}\, C_{gd}^{bb}(m_b)\,,
\end{aligned} \tag{3.13}$$

where we took into account that, with the initial condition of eq. (3.11), the running from m_W to m_b does not induce an up-type CEDM, or a Weinberg operator. There is no b-threshold contribution to C_{gd}^{il} and $C_{\gamma d}^{il}$.

At a scale $\mu_c \sim m_c$, one similarly integrates out the charm quark, and obtains additional threshold corrections to the d and s dipoles, and to the Weinberg operator

$$\begin{aligned}
C_{\gamma d}^{il}(\mu_c^-) &= C_{\gamma d}^{il}(\mu_c^+) + \frac{2}{(4\pi)^2}\frac{m_c Q_u}{m_{d_l} Q_d}\left(C_{1LR}^{cl\,ci}(\mu_c) + N_c\, C_{2\,LR}^{cl\,ci}(\mu_c)\right)\,, \\
C_{gd}^{il}(\mu_c^-) &= C_{gd}^{il}(\mu_c^+) - \frac{2}{(4\pi)^2}\frac{m_c}{m_{d_l}} C_{1LR}^{cl\,ci}(\mu_c)\,, \\
C_{\tilde G}(\mu_c^-) &= C_{\tilde G}(\mu_c^+) - \frac{\alpha_s}{8\pi}\mathrm{Im}\, C_{gu}^{cc}(\mu_c)\,.
\end{aligned} \tag{3.14}$$

In order to avoid large perturbative corrections, we run to the scale $\mu_c = 2\,\mathrm{GeV}$.

The numerical solution of the RGEs is shown in table 7, where, for convenience, we introduced the short-hand notation $\tilde c_i = v^2\,\mathrm{Im}\, C_i$. As the RHCC operator does not undergo QCD renormalization, the results in table 7, as those in table 6, are independent of Λ to good approximation. Some of these results, especially the contributions of $\xi_{ub,cb,tb}$ to the light quark EDMs, are rather sensitive to the choice of renormalization scale. This effect is due to a partial cancellation between matching contributions and contributions from the CEDMs. In these cases, however, the largest contributions to hadronic EDMs come from other operators ($\tilde c_{gu}^{uu}$ for ξ_{ub} and $C_{\tilde G}$ for $\xi_{cb,tb}$) that are less sensitive to the details of the running such that the impact of perturbative uncertainties is still minor. We expect the large hadronic uncertainties related to these operators, which we discuss in section 5, to dominate the theoretical uncertainties on hadronic EDMs.

4 Leptonic and semileptonic charged-current decays

The right-handed current matrix ξ_{ij} is strongly constrained by leptonic and semileptonic meson decays, and semileptonic decays of baryons. Leptonic decays of pseudoscalar mesons, such as $\pi^+ \to \mu^+\nu_\mu$ or $D^+ \to \mu^+\nu_\mu$, are sensitive to the axial component of the weak current, while semileptonic decays of pseudoscalar mesons into pseudoscalar mesons and leptons, such as $K \to \pi l \nu_l$, probe the vector component. For the B system, one can in addition study semileptonic decays of pseudoscalar to vector mesons, such as $B \to D^* l \nu_l$,

	$V_{ud}^*\xi_{ud}$	$V_{us}^*\xi_{us}$	$V_{ub}^*\xi_{ub}$	$V_{cd}^*\xi_{cd}$	$V_{cs}^*\xi_{cs}$	$V_{cb}^*\xi_{cb}$	$V_{td}^*\xi_{td}$	$V_{ts}^*\xi_{ts}$	$V_{tb}^*\xi_{tb}$
$\tilde{c}_{\gamma l}^{ee}$	–	–	–	–	–	–	–	–	6.8×10^{-6}
$\tilde{c}_{\gamma u}^{uu}$	-0.033	-0.65	7.1	–	–	$-1.7 \cdot 10^{-8}$	–	–	$-1.5 \cdot 10^{-5}$
$\tilde{c}_{gu}^{uu}$	$3.6 \cdot 10^{-3}$	0.073	47	–	–	$-2.3 \cdot 10^{-7}$	–	–	$-2.0 \cdot 10^{-4}$
$\tilde{c}_{\gamma d}^{dd}$	-0.047	–	–	-54	–	$-1.7 \cdot 10^{-8}$	-2029	–	$-1.5 \cdot 10^{-5}$
$\tilde{c}_{gd}^{dd}$	$-8.0 \cdot 10^{-4}$	–	–	-6.2	–	$-2.3 \cdot 10^{-7}$	-298	–	$-2.0 \cdot 10^{-4}$
$\tilde{c}_{\gamma d}^{ss}$	–	$-2.3 \cdot 10^{-3}$	–	–	-2.7	$-1.7 \cdot 10^{-8}$	–	-102	$-1.5 \cdot 10^{-5}$
$\tilde{c}_{gd}^{ss}$	–	$-4.0 \cdot 10^{-5}$	–	–	-0.31	$-2.3 \cdot 10^{-7}$	–	-15	$-2.0 \cdot 10^{-4}$
$v^2 C_{\tilde{G}}$	–	–	–	–	–	$-1.2 \cdot 10^{-3}$	–	–	$2.2 \cdot 10^{-3}$
$\tilde{C}_{1\,LR}^{ud\,ud}$	1.8	–	–	–	–	–	–	–	–
$\tilde{C}_{2\,LR}^{ud\,ud}$	0.91	–	–	–	–	–	–	–	–
$\tilde{C}_{1\,LR}^{us\,us}$	–	1.8	–	–	–	–	–	–	–
$\tilde{C}_{2\,LR}^{us\,us}$	–	0.91	–	–	–	–	–	–	–

Table 7. Contributions of the CP-odd combinations, $\mathrm{Im}\,(V_{ij}^*\xi_{ij})$, to the operators at $\mu = 2\,\mathrm{GeV}$. Here $\tilde{c}_i \equiv v^2\,\mathrm{Im}\,C_i$ and a " – " denotes that the contribution is negligible for our purposes.

	Decay constant		Form Factor
f_π	$130.2 \pm 1.4\,\mathrm{MeV}$	$f_+^{K\pi}(0)$	0.9677 ± 0.0027
f_K/f_π	1.192 ± 0.005		
f_D	$209.2 \pm 3.3\,\mathrm{MeV}$	$f_+^{D\pi}(0)$	0.666 ± 0.029
f_{D_s}	$249.8 \pm 2.3\,\mathrm{MeV}$	$f_+^{DK}(0)$	0.747 ± 0.019
f_B	$192.0 \pm 4.3\,\mathrm{MeV}$	$\mathcal{F}_D(1)$	1.035 ± 0.040
f_{B_s}	$228.4 \pm 3.7\,\mathrm{MeV}$	$\mathcal{F}_{D^*}(1)$	$0.906 \pm 0.004 \pm 0.012$

Table 8. Lattice input on pseudoscalar meson decay constants and form factors. We use the FLAG lattice averages with $n_f = 2 + 1$ [93].

and further orthogonal information is provided by inclusive B decays, $B \to X_{u,c} l \nu_l$. β decays of heavy and light baryons, such as $n \to p e^- \bar{\nu}$ or $\Lambda_b \to \Lambda_c \mu^- \bar{\nu}$, give, in principle, a direct handle on the chiral structure of the interactions, and allow one to construct observables that are sensitive to CP violation in the matrix ξ. An example is the triple correlation, D_n, measured in neutron β decay.

From the theoretical point of view, leptonic and semileptonic decays are very clean observables. Leptonic decays are characterized by a single nonperturbative parameter, the meson decay constant, whose values are nowadays precisely computed with lattice QCD

JHEP05(2017)086

(LQCD) [93]. Semileptonic transitions have also been the subject of intense lattice study, and the required form factors are known to high accuracy. In table 8 we list the values of the pseudoscalar meson decay constants and form factors that we use in our analysis. The LQCD input has been taken from the FLAG review [93].

We now list the experimental information we use to constrain the elements of the matrix ξ.

$u \to d$ and $u \to s$ transitions. V_{ud} is extracted from superallowed nuclear β decay, which is only sensitive to the vector component of the weak current, and from leptonic decays of the pion, which probe the axial component of the current. We use the following experimental input [71, 94]

$$\begin{aligned} |V_{ud}(0^+ \to 0^+)|_{\rm exp} &= 0.97425 \pm 0.00022\,, \\ |V_{ud}(\pi \to \mu\nu) f_\pi|_{\rm exp} &= (127.13 \pm 0.02 \pm 0.13)\,\text{MeV}\,, \end{aligned} \tag{4.1}$$

where $f_\pi \sim 130\,\text{MeV}$ is the pion decay constant. The first uncertainty in the second line of eq. (4.1) is experimental, while the second is due to radiative corrections.

For the determination of V_{us}, we use two quantities that are experimentally very well determined [95, 96]. From semileptonic kaon decays, one can extract

$$(|V_{us}| f_+^{K\pi}(0))_{\rm exp} = 0.2163 \pm 0.0005\,, \tag{4.2}$$

where $f_+^{K\pi}(0)$ is the form factor entering the $K^0 \to \pi^- l \nu_l$ decay at zero momentum transfer. The ratio of the pion and kaon leptonic decays gives

$$\left(\left| \frac{V_{us}}{V_{ud}} \right| \frac{f_K}{f_\pi} \right)_{\rm exp} = 0.2758 \pm 0.0005\,. \tag{4.3}$$

Because leptonic and semileptonic decays are sensitive to either the axial or the vector components of the current, we can easily modify the relevant expressions in the presence of a RHCC to obtain

$$\begin{aligned} |V_{ud} + \xi_{ud}| &= 0.97425 \pm 0.00022\,, \quad & |V_{ud} - \xi_{ud}| f_\pi &= (127.13 \pm 0.02 \pm 0.13)\,\text{MeV}\,, \\ |V_{us} + \xi_{us}| f_+^{K\pi}(0) &= 0.2163 \pm 0.0005\,, \quad & \frac{|V_{us} - \xi_{us}| f_K}{|V_{ud} - \xi_{ud}| f_\pi} &= 0.2758 \pm 0.0005\,. \end{aligned} \tag{4.4}$$

Using the LQCD input in table 8, eq. (4.4) provides four constraints on V_{ud}, V_{us}, ξ_{ud}, and ξ_{us}. Two additional constraints on the imaginary part of ξ_{ud} and ξ_{us} can be obtained from neutron and hyperon β decays. Time-reversal violation can be measured in neutron β decay by reconstructing the triple correlation $\langle \vec{J} \rangle \cdot (\vec{p}_e \times \vec{p}_\nu)$, where $\vec{J}$ is the neutron polarization. Current measurements give $D_n = (-1 \pm 2.1) \cdot 10^{-4}$ [97]. This observable is contaminated by fake T-odd signals from final-state interactions, which, with current experimental accuracy, can still be neglected (see ref. [98] for a more detailed discussion). The same correlation was measured in the decay of the Σ baryon, $\Sigma^- \to n e^- \bar{\nu}$, with a much weaker bound, $D_\Sigma = 0.11 \pm 0.10$. Following ref. [99], the D_n and D_Σ coefficients can be calculated as

$$D_n = \frac{4 g_A}{1 + 3 g_A^2} \,\text{Im}\, \frac{\xi_{ud}}{V_{ud}} \simeq 0.87\, \text{Im}\, \frac{\xi_{ud}}{V_{ud}}\,, \quad D_\Sigma = \frac{4 g_{A\,\Sigma n}}{1 + 3 g_{A\,\Sigma n}^2} \,\text{Im}\, \frac{\xi_{us}}{V_{us}} \simeq 1.01\, \text{Im}\, \frac{\xi_{us}}{V_{us}}\,, \tag{4.5}$$

where g_A is the nucleon axial coupling, $g_A = 1.27$, and $g_{A\,\Sigma n}$ is the axial coupling of a Σ to a neutron, measured to be 0.340 ± 0.017 [71]. D_n gives a strong bound on $\mathrm{Im}\,\xi_{ud}/V_{ud}$, at the 10^{-4} level. The constraint on $\mathrm{Im}\,\xi_{us}$ is at the few-percent level. As we will see, both bounds are significantly weaker than bounds from EDMs and direct CPV in kaon decays.

$c \to d$ and $c \to s$ transitions. Analogously to the ud and us case, we can use the leptonic and semileptonic decays of the D and D_s mesons, $D^+ \to \mu^+\nu_\mu$, $D_s^+ \to \mu^+\nu_\mu$, $D \to \pi l \nu_l$, and $D \to K l \nu_l$, to constrain the vector and axial couplings of a charm quark to s and d quarks. The leptonic decays of the pseudoscalar D and D_s mesons probe the axial current, while the semileptonic decays probe the vector current. The experimental input is [71]

$$f_D|V_{cd} - \xi_{cd}| = 45.91 \pm 1.05\,\mathrm{MeV}\,, \qquad f_{D_s}|V_{cs} - \xi_{cs}| = 250.9 \pm 4.0\,\mathrm{MeV}\,, \tag{4.6}$$

$$f_+^{D\pi}(0)|V_{cd} + \xi_{cd}| = 0.1425 \pm 0.0019\,, \qquad f_+^{DK}(0)|V_{cs} + \xi_{cs}| = 0.728 \pm 0.005\,, \tag{4.7}$$

and the LQCD input for the D and D_s decay constants and form factors is given in table 8.

$b \to u$ and $b \to c$ transitions. In the case of $b \to c$ transitions, the vector component of the charged current is constrained by the semileptonic decay $B \to D l \nu_l$. For the axial component, the purely leptonic decay of the B_c meson has not yet been observed. The decay $B \to D^* l \nu_l$ depends on both the vector and axial current. In the zero-recoil limit, when $w = v \cdot v' = 1$, where v and v' are the B and D mesons four-velocities, only the axial contribution survives [100]. Using the HFAG averages [101], we can write

$$\begin{aligned} \eta_{EW}\mathcal{F}_D(1)|V_{cb} + \xi_{cb}| &= (42.65 \pm 0.72 \pm 1.35)\cdot 10^{-3}\,, \\ \eta'_{EW}\mathcal{F}_{D^*}(1)|V_{cb} - \xi_{cb}| &= (35.81 \pm 0.11 \pm 0.44)\cdot 10^{-3}\,, \end{aligned} \tag{4.8}$$

where $\eta_{EW} = 1.012 \pm 0.005$ and $\eta'_{EW} = 1.015 \pm 0.005$ [71] are electroweak corrections. $\mathcal{F}_D(1)$ and $\mathcal{F}_{D^*}(1)$ denote the form factors, evaluated at $w = 1$, for which we used the FLAG averages in table 8. Angular distributions in $B \to D^* l \nu_l$ could provide additional information on the Lorentz structure of the Wbc vertex [102].

The inclusive decays $\bar{B} \to X_c l \bar{\nu}_l$ also constrain ξ_{cb}. Neglecting power corrections of order $\mathcal{O}(\Lambda_{\mathrm{QCD}}/m_b)$, the inclusive semileptonic width into charmed final states is given by

$$\begin{aligned} \Gamma(B \to X_c l \nu) = \frac{G_F^2 m_b^5 |V_{cb}|^2}{192\pi^3} \Bigg[&\left(1 + \left|\frac{\xi_{cb}}{V_{cb}}\right|^2\right)\left(1 - 8\rho + 8\rho^3 - \rho^4 - 12\rho^2 \log\rho\right) \\ &- 4\frac{m_c}{m_b}\mathrm{Re}\left(\frac{\xi_{cb}}{V_{cb}}\right)\left(1 + 9\rho - 9\rho^2 - \rho^3 + 6\rho(1+\rho)\log\rho\right)\Bigg]\,, \end{aligned} \tag{4.9}$$

where $\rho = m_c^2/m_b^2$. We then set constraints by using the PDG average [71],

$$|V_{cb}^{\mathrm{eff}}| = (42.2 \pm 0.8)\cdot 10^{-3} \qquad (B \to X_c l \nu)\,, \tag{4.10}$$

where $|V_{cb}^{\mathrm{eff}}|^2 = |V_{cb}|^2\,\Gamma(B \to X_c l \nu)/\Gamma^{\mathrm{SM}}(B \to X_c l \nu)$.

The constraints from the inclusive decays we obtain in this way should only be viewed as order-of-magnitude constraints for a number of reasons. First of all, we should take into account power corrections, which are not included in eq. (4.9), in order to obtain V_{cb}

from inclusive decays [103–106]. Furthermore, eq. (4.10) relies on fits to the leptonic and hadronic moments of the decay distribution. As the dependence on the lepton-energy is not the same for ξ_{cb} and V_{cb} after applying cuts, the SM fit will be altered in the presence of right-handed currents. We should therefore refit the leptonic moments, while taking into account contributions from right-handed currents. Such an analysis is beyond the scope of the current work. We will use eq. (4.10) to estimate the limits from the inclusive measurements, and refer to refs. [107–109] for a more detailed discussion.

In the case of $b \to u$ transitions, the leptonic channel $B^+ \to \tau^+ \nu_\tau$ allows us to determine the axial current $|V_{ub} - \xi_{ub}|$, while the vector current is probed by $B \to \pi l \nu_l$. Additional exclusive decays, such as $B \to \rho l \nu_l$, can be used to further improve the sensitivity to RHCC [109, 110]. For the leptonic decays, we use the HFAG average of the BaBar and Belle results, $\mathrm{Br}(B^+ \to \tau\nu) = (1.06 \pm 0.19) \cdot 10^{-4}$, and we employ the FLAG extraction for the semileptonic case,

$$\begin{aligned} |V_{ub} - \xi_{ub}| f_B &= 0.77 \pm 0.07\,, \\ |V_{ub} + \xi_{ub}| &= (3.62 \pm 0.14) \cdot 10^{-3}\,, \end{aligned} \tag{4.11}$$

where the decay constant, f_B, is given in table 8.

The inclusive determination from $B \to X_u l \nu_l$ decays suffers from the same problems as the charm-bottom transition. In principle, power corrections should be included [111, 112] and the leptonic spectrum should be refitted taking into account a right-handed current. Since such an analysis is beyond the scope of our work, we take a similar approach as in the case of V_{cb}. We thus estimate constraints from inclusive decays by [71],

$$\sqrt{|V_{ub}|^2 + |\xi_{ub}|^2} = (4.49 \pm 0.18^{+0.16}_{-0.18}) \cdot 10^{-3} \qquad (B \to X_u l \nu)\,. \tag{4.12}$$

Another exclusive determination of V_{cb} and V_{ub} is provided by measurements of $\mathrm{Br}(\Lambda_b^0 \to p\mu^-\bar{\nu})_{q^2>15\,\mathrm{GeV}} / \mathrm{Br}(\Lambda_b^0 \to \Lambda_c^+ \mu^- \bar{\nu})_{q^2>7\,\mathrm{GeV}}$. This ratio of branching fractions can be calculated using lattice determinations of the relevant form factors [113]. Following the procedure outlined in ref. [113] we obtain for the partially integrated decay widths,

$$\begin{aligned} \Gamma(\Lambda_b^0 \to p\mu^-\bar{\nu})_{q^2>15\,\mathrm{GeV}} &= 4.17\,\mathrm{ps}^{-1}|V_{ub}+\xi_{ub}|^2 + 8.17\,\mathrm{ps}^{-1}|V_{ub}-\xi_{ub}|^2 \pm \sigma^{(p)}_{\mathrm{stat}} \pm \sigma^{(p)}_{\mathrm{syst}}\,, \\ \Gamma(\Lambda_b^0 \to \Lambda_c^+\mu^-\bar{\nu})_{q^2>7\,\mathrm{GeV}} &= 1.41\,\mathrm{ps}^{-1}|V_{cb}+\xi_{cb}|^2 + 6.99\,\mathrm{ps}^{-1}|V_{cb}-\xi_{cb}|^2 \pm \sigma^{(\Lambda_c^+)}_{\mathrm{stat}} \pm \sigma^{(\Lambda_c^+)}_{\mathrm{syst}}\,, \end{aligned} \tag{4.13}$$

where the lattice uncertainties are given by

$$\begin{aligned} (\sigma^{(p)}_{\mathrm{stat}})^2 &= \left(0.10\,|V_{ub}+\xi_{ub}|^4 + 0.33\,|V_{ub}-\xi_{ub}|^4 + 0.16\,|V_{ub}^2 - \xi_{ub}^2|^2\right)\,\mathrm{ps}^{-2}\,, \\ (\sigma^{(p)}_{\mathrm{syst}})^2 &= \left(0.10\,|V_{ub}+\xi_{ub}|^4 + 0.44\,|V_{ub}-\xi_{ub}|^4 + 0.050\,|V_{ub}^2 - \xi_{ub}^2|^2\right)\,\mathrm{ps}^{-2}\,, \\ (\sigma^{(\Lambda_c^+)}_{\mathrm{stat}})^2 &= \left(0.0023\,|V_{cb}+\xi_{cb}|^4 + 0.017\,|V_{cb}-\xi_{cb}|^4 + 0.0052\,|V_{cb}^2 - \xi_{cb}^2|^2\right)\,\mathrm{ps}^{-2}\,, \\ (\sigma^{(\Lambda_c^+)}_{\mathrm{syst}})^2 &= \left(0.0053\,|V_{cb}+\xi_{cb}|^4 + 0.11\,|V_{cb}-\xi_{cb}|^4 + 0.0027\,|V_{cb}^2 - \xi_{cb}^2|^2\right)\,\mathrm{ps}^{-2}\,. \end{aligned} \tag{4.14}$$

The ratio of these decay widths is experimentally determined to be [114]

$$\frac{\mathrm{Br}(\Lambda_b^0 \to p\mu^-\bar{\nu})_{q^2>15\,\mathrm{GeV}}}{\mathrm{Br}(\Lambda_b^0 \to \Lambda_c^+\mu^-\bar{\nu})_{q^2>7\,\mathrm{GeV}}} = (1.00 \pm 0.04 \pm 0.08) \cdot 10^{-2}\,. \tag{4.15}$$

In principle, measurements of angular distributions and correlations in semileptonic Λ_b decays could provide more detailed probes of the Lorentz structure of the Wbc vertex [115].

JHEP05(2017)086

	d_e	d_n	$d_{\rm Hg}$	$d_{\rm Xe}$	$d_{\rm Ra}$	$d_{p,D}$
current limit	$8.7 \cdot 10^{-16}$	$3.0 \cdot 10^{-13}$	$6.2 \cdot 10^{-17}$	$5.5 \cdot 10^{-14}$	$1.2 \cdot 10^{-10}$	x
expected limit	$5.0 \cdot 10^{-17}$	$1.0 \cdot 10^{-15}$	$6.2 \cdot 10^{-17}$	$5.0 \cdot 10^{-16}$	$1.0 \cdot 10^{-14}$	$1.0 \cdot 10^{-16}$

Table 9. Current limits on the electron [116], neutron [117, 118], mercury [119, 120], xenon [121] and radium [122, 123] EDMs in units of $e\,$fm (90% confidence level). We also show future sensitivities [124, 125].

5 $\Delta F = 0$ processes: electric dipole moments

Permanent EDMs of leptons, nucleons, nuclei, atoms, and molecules provide stringent bounds on flavor-diagonal CPV interactions. The right-handed charged-current couplings ξ_{ij} contribute mostly to hadronic and nuclear EDMs. Right-handed couplings of the light quarks, such as ξ_{ud} and ξ_{us}, induce EDMs through the tree-level operators $C^{ud\,ud}_{1,2\,LR}$ and $C^{us\,us}_{1,2\,LR}$, while the couplings to heavier quarks, such as ξ_{ub} or ξ_{tb}, induce loop corrections to the light quark EDMs, CEDMs, and the Weinberg operator.

In table 9 we summarize the current limits on the EDMs of the electron, nucleons, ^{199}Hg, ^{225}Ra, and ^{129}Xe that we used in our analysis, as well as projected sensitivities for these systems, and for the EDMs of the proton and deuteron that are targets for storage-ring experiments.

The calculation of nucleon and nuclear EDMs in terms of the operators in eqs. (3.1) and (3.6) involves two steps. The operators are first matched to an extension of chiral perturbation theory (ChPT) that contains CPV hadronic interactions [126, 127]. The most important interactions are short-range contributions to the nucleon EDM and CPV pion-nucleon couplings. The latter give rise to long-range contributions to the nucleon EDM (from pion loops) and, for chiral-symmetry-breaking operators like the quark CEDMs and four-quark operators, dominate the CPV nucleon-nucleon potential. This CPV potential provides the dominant contribution to the EDMs of nuclei and diamagnetic atoms.

The chiral power counting predicts that the four-quark operators $C^{ud\,ud}_{1,2\,LR}$ and $C^{us\,us}_{1,2\,LR}$ contribute mainly to the isospin-breaking pion-nucleon coupling $\bar g_1$ [11, 126]. $C^{ud\,ud}_{1,2\,LR}$ do not induce the isoscalar coupling $\bar g_0$, while $C^{us\,us}_{1,2\,LR}$ give corrections that, while formally LO, are small with respect to $\bar g_1$. As discussed in ref. [11], it is possible to calculate the sizes of $\bar g_{0,1}$ by noticing that these couplings receive large contributions from tadpole diagrams, which involve the coupling of the neutral pion to the vacuum. The tadpole coupling can be related, at leading order in ChPT, to the $K \to \pi\pi$ matrix element of the SM electroweak penguin operators $\mathcal{Q}_{7,8}$. Using recent LQCD of these matrix elements [128, 129], it then becomes possible to give a solid estimate of the sizes of $\bar g_{0,1}$ [11]. The error on $\bar g_{0,1}$ is at the moment dominated by ChPT uncertainties, which we conservatively estimate at the 50% level.

$\bar g_{0,1}$ also receive contributions from the dipole operators C^{uu}_{gu}, C^{dd}_{gd} and C^{ss}_{gd}. These contributions can be in principle computed in LQCD [130], but, at the moment, the best estimate comes from QCD sum rules. The sum rules estimates have roughly (50-100)% uncertainties [131–134]. We thus find that the pion-nucleon couplings induced by the

JHEP05(2017)086

operators in eqs. (3.1) and (3.6) are

$$\frac{\bar{g}_1}{2F_\pi} = -\Big((4.5\pm 2.2)\left(\tilde{C}^{us\,us}_{1\,LR} + 2\tilde{C}^{ud\,ud}_{1\,LR}\right) + (22.0\pm 11.0)\left(\tilde{C}^{us\,us}_{2\,LR} + 2\tilde{C}^{ud\,ud}_{2\,LR}\right) + (0.2^{+0.4}_{-0.1})(0.7\,\tilde{c}^{uu}_{gu} - 1.5\,\tilde{c}^{dd}_{gd})\Big)\times 10^{-6}\,, \tag{5.1}$$

$$\frac{\bar{g}_0}{2F_\pi} = -\Big((0.3\pm 0.1)\tilde{C}^{us\,us}_{1\,LR} + (1.3\pm 0.6)\tilde{C}^{us\,us}_{2\,LR} + (0.05\pm 0.10)(0.7\tilde{c}^{uu}_{gu} + 1.5\tilde{c}^{dd}_{gd})\Big) \times 10^{-6}\,, \tag{5.2}$$

where $F_\pi = f_\pi/\sqrt{2}$, all the couplings are evaluated at $\mu = 2\,\mathrm{GeV}$, and their values in terms of ξ_{ij} can be read off from table 7. As in table 7, we have defined $\tilde{c}_i = v^2\,\mathrm{Im}\,C_i$. Eqs. (5.1) and (5.2) assume that the strong CP problem is solved by the Peccei-Quinn mechanism [135] which somewhat affects the values of the matrix elements.

A variety of techniques are available for the calculation of the nucleon EDM induced by four-quark and dipole operators in eqs. (3.1) and (3.6). In refs. [11, 136], we estimated the nucleon EDM induced by the four-quark operators in eq. (3.1) by considering long-range contributions induced by the pion-nucleon couplings $\bar{g}_{0,1}$ (see also ref. [137]). This estimate has intrinsically large uncertainties mainly due to uncertainties on $\bar{g}_{0,1}$ and our ignorance of the size of short-range contributions that appear at the same chiral order. Here we use the uncertainty estimate of ref. [11].

The contributions of $\tilde{c}^{uu}_{\gamma u}$ and $\tilde{c}^{dd}_{\gamma d}$, the up- and down-quark EDMs, are known with $\mathcal{O}(15\%)$ uncertainties [138–140], while the strange contribution is still highly uncertain. While considerable effort is underway for the calculation of the qCEDM contribution to the nucleon EDM [141–143], the best estimate at the moment comes from QCD sum rules, and has an estimated 50% uncertainty [131–134]. Finally, the Weinberg operator appears with the largest uncertainty, $\mathcal{O}(100\%)$, based on a combination of QCD sum-rules [144] and naive dimensional analysis estimates [87]. Combining these results, we find

$$\begin{aligned} d_n =& \Big((43\pm 27)\tilde{C}^{us\,us}_{1\,LR} + (210\pm 130)\,\tilde{C}^{us\,us}_{2\,LR} + (22\pm 14)\,\tilde{C}^{ud\,ud}_{1\,LR} + (110\pm 70)\,\tilde{C}^{ud\,ud}_{2\,LR} \\ & -(0.93\pm 0.05)\,\tilde{c}^{uu}_{\gamma u} - (4.0\pm 0.2)\,\tilde{c}^{dd}_{\gamma d} - (0.8\pm 0.9)\,\tilde{c}^{ss}_{\gamma d} \\ & -(3.9\pm 2.0)\,\tilde{c}^{uu}_{gu} - (16.8\pm 8.4)\,\tilde{c}^{dd}_{gd} \pm (320\pm 260)v^2 C_{\tilde{G}}\Big) \times 10^{-9}\,e\,\mathrm{fm}\,, \\ d_p =& \Big(-(56\pm 30)\,\tilde{C}^{us\,us}_{1\,LR} - (280\pm 150)\,\tilde{C}^{us\,us}_{2\,LR} - (42\pm 26)\,\tilde{C}^{ud\,ud}_{1\,LR} - (210\pm 130)\,\tilde{C}^{ud\,ud}_{2\,LR} \\ & +(3.8\pm 0.2)\,\tilde{c}^{uu}_{\gamma u} + (1.0\pm 0.1)\,\tilde{c}^{dd}_{\gamma d} - (0.8\pm 0.9)\,\tilde{c}^{ss)}_{\gamma d} \\ & +(9.3\pm 4.6)\,\tilde{c}^{uu}_{gu} + (9.2\pm 4.2)\,\tilde{c}^{dd}_{gd} \mp (320\pm 260)v^2 C_{\tilde{G}}\Big) \times 10^{-9}\,e\,\mathrm{fm}. \end{aligned} \tag{5.3}$$

Finally, using the nuclear calculations of refs. [127, 145–155] we can predict nuclear EDMs in terms of $\bar{g}_{0,1}$ and $d_{n,p}$

$$\begin{aligned} d_D =& (0.94\pm 0.01)(d_n + d_p) - (0.18\pm 0.02)\frac{\bar{g}_1}{2F_\pi}\,e\ \mathrm{fm}\,, \\ d_{\mathrm{Hg}} =& -(2.8\pm 0.6)\cdot 10^{-4}\cdot\Bigg[(1.9\pm 0.1)d_n + (0.20\pm 0.06)d_p \\ & - \left(0.13^{+0.5}_{-0.07}\,\frac{\bar{g}_0}{2F_\pi} + 0.25^{+0.89}_{-0.63}\,\frac{\bar{g}_1}{2F_\pi}\right) e\ \mathrm{fm}\Bigg]\,, \end{aligned}$$

JHEP05(2017)086

Re A_0	$33.201 \cdot 10^{-8}$ GeV	Re A_2	$1.479 \cdot 10^{-8}$ GeV
$\|\epsilon\|$	$(2.228 \pm 0.011) \cdot 10^{-3}$	Arg ϵ	0.75957 rad
Re (ϵ'/ϵ)	$(16.6 \pm 2.3) \cdot 10^{-4}$	$\mathrm{Br}(K^+ \to \pi^0 e^+ \nu)$	$(5.07 \pm 0.04) \cdot 10^{-2}$
$\tau(K_L)$	$(5.116 \pm 0.021) \cdot 10^{-8}$ s	$\tau(K^+)$	$(1.2380 \pm 0.0020) \cdot 10^{-8}$ s

Table 10. Experimental input for the $\Delta S = 1$ processes ϵ'/ϵ and $K_L \to \pi^0 e^+ e^-$ [71].

$$
\begin{aligned}
d_{\mathrm{Xe}} &= (0.33 \pm 0.05) \cdot 10^{-4} \cdot \Bigg[(-0.32 \pm 0.02) d_n + (0.0061 \pm 0.001) d_p \\
&\qquad + \left(0.10^{+0.53}_{-0.037} \frac{\bar{g}_0}{2F_\pi} + 0.076^{+0.55}_{-0.038} \frac{\bar{g}_1}{2F_\pi}\right)\Bigg] e \text{ fm}\,, \\
d_{\mathrm{Ra}} &= (7.7 \pm 0.8) \cdot 10^{-4} \cdot \left(-19^{+6.4}_{-57} \frac{\bar{g}_0}{2F_\pi} + 76^{+227}_{-25} \frac{\bar{g}_1}{2F_\pi}\right) e \text{ fm} \quad .
\end{aligned} \tag{5.4}
$$

The nucleon EDM contributions to d_{Ra} have, as far as we know, not been calculated but are expected to be small compared to the large pion-exchange contributions.

The estimates of the nucleon and nuclear EDMs in eqs. (5.3) and (5.4) are affected by large hadronic and nuclear uncertainties. Several matrix elements are consistent with zero and the large uncertainties allow for cancellations between different contributions, which can significantly affect the constraints on the ξ_{ij} couplings. Therefore, when setting constraints, we vary the hadronic and nuclear matrix elements within their allowed ranges in order to minimize the total χ^2. This corresponds to the Rfit approach for treating theoretical errors as defined in ref. [156].

6 $\Delta S = 1$ processes

In this section we discuss the contribution of RHCC to direct CP violation in kaon decays and to the FCNC decay $K_L \to \pi^0 e^+ e^-$. While the real parts of the ξ_{ij} elements are well constrained by the leptonic and semileptonic charged-current decays discussed in section 4, ϵ'/ϵ and $K_L \to \pi^0 e^+ e^-$ provide additional information on the imaginary parts of the ξ_{is} and ξ_{id} elements. ϵ'/ϵ is dominated by tree-level contributions from the four-quark operators $C^{ud\,us}_{1,2\,LR}$ and $C^{us\,ud}_{1,2\,LR}$, while $K_L \to \pi^0 e^+ e^-$ receives correction at one loop. The latter arise from matching the RHCC to the flavor-changing dipole operators $C^{ds}_{\gamma d}$ and $C^{sd}_{\gamma d}$, which are particularly important for internal charm and top quarks. Other $\Delta S = 1$ FCNC decays, such as $K_L \to \pi^0 \nu \bar{\nu}$, receive contributions from RHCC that are only quadratic in ξ and therefore play a less important role. We discuss them briefly in appendix A.2. In table 10 we list the experimental input needed in sections 6.1 and 6.2.

6.1 ϵ'/ϵ

ξ_{ud} and ξ_{us} give large contributions to direct CP violation in $K_L \to \pi\pi$ decays, while indirect CP violation in kaon mixing is not significantly affected [11]. Direct CP violation

JHEP05(2017)086

is quantified by ϵ', which can be expressed as

$$\mathrm{Re}\left(\frac{\epsilon'}{\epsilon}\right) = \mathrm{Re}\left(\frac{i\omega e^{i(\delta_2-\delta_0)}}{\sqrt{2}\epsilon}\right)\left[\frac{\mathrm{Im}\,A_2}{\mathrm{Re}\,A_2} - \frac{\mathrm{Im}\,A_0}{\mathrm{Re}\,A_0}\right]. \tag{6.1}$$

Here $A_{0,2}e^{i\delta_{0,2}} = \frac{1}{\sqrt{2}}\langle(\pi\pi)_{I=0,2}|\mathcal{H}|K\rangle$ are the amplitudes for final-state pions with total isospin $I = 0, 2$, the corresponding strong phases are denoted by $\delta_{0,2}$, $\mathcal{H}$ is the weak Hamiltonian, and $\omega \equiv \mathrm{Re}\,A_2/\mathrm{Re}\,A_0 = 0.04454$.

In the SM, A_0 and A_2 are sensitive to contributions from charged-current operators, $\mathcal{Q}_{1-2}$, strong penguin operators, $\mathcal{Q}_{3-6}$, and electroweak penguin operators, $\mathcal{Q}_{7-10}$. The values of their NLO Wilson coefficients have been calculated in refs. [85, 157–159], while lattice determinations of the necessary matrix elements are given in refs. [128, 129, 160]. Combining these results with the experimental values in table 10 and lattice determinations of the strong phases, $\delta_0 = (23.8 \pm 4.9 \pm 1.2)^\circ$, $\delta_2 = -(11.6 \pm 2.5 \pm 1.2)^\circ$, leads to the SM prediction [160]

$$\mathrm{Re}\left(\frac{\epsilon'}{\epsilon}\right)_{\mathrm{SM}} = (1.38 \pm 5.15 \pm 4.59)\cdot 10^{-4} \simeq (1.4 \pm 6.9)\cdot 10^{-4}\,, \tag{6.2}$$

where we combined the statistical and systematical errors in quadrature.

As noticed in ref. [11], chiral symmetry relates the contributions to ϵ'/ϵ of the four-quark tree-level operators induced by ξ_{ud} and ξ_{us}, given in eq. (3.1), to those of the electroweak penguin operators $\mathcal{Q}_7$ and $\mathcal{Q}_8$. Such a determination in principle still suffers from higher-order, $\mathcal{O}(m_K^2)$, corrections. Fortunately, the $I = 3/2$ parts of the LR operators, $O_{1\,LR}^{ud\,us}$ and $O_{2\,LR}^{ud\,us}$, coincide after an isospin decomposition with those of $\mathcal{Q}_7$ and $\mathcal{Q}_8$, respectively. Isospin symmetry therefore implies a stronger relation between the contributions of the left-right operators to the $I = 2$ amplitude and the matrix elements of $\mathcal{Q}_{7,8}$ [161, 162]. As this relation depends on isospin arguments, it is only subject to $\mathcal{O}((m_d - m_u)/\Lambda_\chi)$ and $\mathcal{O}(\alpha/\pi)$ corrections, expected at the few-percent level. The resulting expression for the $I = 2$ amplitude is [11]

$$\begin{aligned}\mathrm{Im}\,A_2(\xi) = \frac{1}{6\sqrt{2}}\mathrm{Im}\Big[&\left(C_{1LR}^{ud\,us} - C_{1LR}^{us\,ud^*}\right)\langle(\pi\pi)_{I=2}|\mathcal{Q}_7|K^0\rangle \\ &+\left(C_{2LR}^{ud\,us} - C_{2LR}^{us\,ud^*}\right)\langle(\pi\pi)_{I=2}|\mathcal{Q}_8|K^0\rangle\Big]\,,\end{aligned} \tag{6.3}$$

where [128, 129]

$$\langle(\pi\pi)_{I=2}|\mathcal{Q}_7|K^0\rangle = (0.36\pm0.02)\,\mathrm{GeV}^2\,, \qquad \langle(\pi\pi)_{I=2}|\mathcal{Q}_8|K^0\rangle = (1.6\pm0.094)\,\mathrm{GeV}^2\,. \tag{6.4}$$

Such a relation does not exist for the $I = 0$ amplitude, however, at leading order in ChPT we obtain $A_0(\xi) = -2\sqrt{2}A_2(\xi)$. We thus find

$$\mathrm{Re}\left(\frac{\epsilon'}{\epsilon}\right) = \mathrm{Re}\left(\frac{\epsilon'}{\epsilon}\right)_{\mathrm{SM}} + \mathrm{Re}\left(\frac{i\omega e^{i(\delta_2-\delta_0)}}{\sqrt{2}\epsilon}\right)\left[\frac{\mathrm{Im}\,A_2(\xi)}{\mathrm{Re}\,A_2} - \frac{\mathrm{Im}\,A_0(\xi)}{\mathrm{Re}\,A_0}\right], \tag{6.5}$$

where we use the experimental values for $\mathrm{Re}\,A_{0,2}$. The expression for $A_0(\xi)$ might suffer from relatively large SU(3) corrections. However, it is the $A_2(\xi)$ term that constitutes the dominant ξ contribution to ϵ', while the $A_0(\xi)$ term is suppressed by $2\sqrt{2}\omega \simeq 0.1$. We therefore expect eq. (6.5) to be accurate up to the lattice uncertainties in eq. (6.4).

6.2 $K_L \to \pi^0 e^+ e^-$

In the SM, the decay $K_L \to \pi^0 e^+ e^-$ has a large direct CPV component dominated by the penguin operators $C_{7V} \bar{s}\gamma^\mu d\, \bar{e}\gamma_\mu e$ and $C_{7A} \bar{s}\gamma^\mu d\, \bar{e}\gamma_\mu \gamma_5 e$ [85]. In addition, there is a CP-even long-distance component dominated by two-photon exchange and an indirect CPV contribution proportional to the mixing parameter ϵ_K. Finally, in the presence of right-handed currents, this decay gets contributions from the dipole operators $C^{ds}_{\gamma d}$ and $C^{sd}_{\gamma d}$. Due to the large factors of $m_t/m_{s,d}$ and $m_c/m_{s,d}$ that appear in the matching coefficients (3.11), this K_L decay is particularly sensitive to the imaginary part of the couplings ξ_{td}, ξ_{ts} and, to a lesser extent, ξ_{cd} and ξ_{cs}.

The decay rate can be expressed in terms of the vector and tensor form factors

$$\begin{aligned}
\langle \pi^0 | \bar{s}\gamma^\mu d | K_L \rangle &= \frac{1}{\sqrt{2}} f_+^{K^0\pi^+}(q^2)(p_K^\mu + p_\pi^\mu)\,, \\
\langle \pi^0 | \bar{s}\sigma^{\mu\nu} d | K_L \rangle &= i f_T^{K\pi}(q^2) \frac{\sqrt{2}}{m_K + m_\pi}(p_\pi^\mu p_K^\nu - p_K^\mu p_\pi^\nu)\,,
\end{aligned} \tag{6.6}$$

where $f_+^{K\pi}$ (see table 8) is related to the vector form factor in $K^+ \to \pi^0 e^+ \nu$, while $f_T^{K\pi}$ has been computed on the lattice. We will use the evaluation of ref. [163], $f_T^{K\pi} = 0.417 \pm 0.015$, at a renormalization scale $\mu = 2\,\text{GeV}$.

The RHCC contribution to the branching ratio is determined by the coupling C_T

$$C_T(\mu) = -\frac{Q_d}{4}\left(m_s C^{ds*}_{\gamma d}(\mu) + m_d C^{sd}_{\gamma d}(\mu) \right)\,, \tag{6.7}$$

where the values of the coefficients at $\mu = 2\,\text{GeV}$ are given in table 6. The SM contribution is expressed by the functions $\tilde{y}_{7V}$ and $\tilde{y}_{7A}$ [85] given in appendix A.2. The ξ operators also contribute to the penguin operators C_{7V} and C_{7A}, as discussed in appendix A.2, but these contributions are quadratic in ξ and not enhanced by $m_{t,c}/m_s$. We therefore do not include them in our analysis.

In terms of $\tilde{y}_{7V}$, $\tilde{y}_{7A}$, and C_T, the branching ratio becomes

$$\text{Br}(K_L \to \pi^0 e^+ e^-) = \kappa_e \left[\left(\text{Im}\lambda_t\, \tilde{y}_{7V} + \frac{2}{m_K + m_\pi} \frac{f_T^{K\pi}(0)}{f_+^{K\pi}(0)} 16\pi^2 \text{Im}(v^2 C_T) \right)^2 + \text{Im}\lambda_t^2\, \tilde{y}_{7A}^2 \right]\,, \tag{6.8}$$

where $\lambda_t = V_{ts}^* V_{td}$. The factor κ_e is introduced to cancel the SM dependence on the vector form factor $f_+^{K\pi}$ by normalizing to the $K^+ \to \pi^0 e^+ \nu$ decay rate. κ_e is defined as

$$\kappa_e = \frac{1}{|V_{us} + \xi_{us}|^2} \frac{\tau(K_L)}{\tau(K^+)} \left(\frac{\alpha_{\text{em}}}{2\pi}\right)^2 \text{Br}(K^+ \to \pi^0 e^+ \nu) \sim \left(\frac{0.225}{|V_{us} + \xi_{us}|}\right)^2 6 \cdot 10^{-6}\,, \tag{6.9}$$

where we used the experimental values in table 10. The expression in eq. (6.8) involves only the direct CPV contributions from the SM. However, since the experimental limit is currently only sensitive to branching ratios that are roughly two orders of magnitude larger than the SM prediction [71],

$$\text{BR}(K_L \to \pi^0 e^+ e^-) < 2.8 \cdot 10^{-10} \quad (90\%\,\text{C.L.})\,, \tag{6.10}$$

we simply use eq. (6.8) to estimate the branching ratio.

$\mathrm{BR}\,(B \to X_d\gamma)$	$(14.1 \pm 5.7) \cdot 10^{-6}$	$\mathrm{BR}\,(B \to X_s\gamma)$	$(3.32 \pm 0.15) \times 10^{-4}$
$A_{CP}(B \to X_{d+s}\gamma)$	0.032 ± 0.034	$A_{CP}(B \to s\gamma)$	0.015 ± 0.02
		$S_{K^*\gamma}$	-0.16 ± 0.22
Δm_d	(0.5064 ± 0.0019) ps^{-1}	Δm_s	(17.757 ± 0.021) ps^{-1}
$\Delta\Gamma^{(d)}$	$(-1.3 \pm 6.7) \cdot 10^{-3}$ ps^{-1}	$\Delta\Gamma^{(s)}$	(0.086 ± 0.006) ps^{-1}
a^d_{fs}	-0.0020 ± 0.0016	a^s_{fs}	-0.0006 ± 0.0028

Table 11. Experimental input for the processes discussed in section 7 [71, 101]. The branching ratios $\mathrm{BR}\,(B \to X_{d,s}\gamma)$ have a cut on the photon energy, $E_\gamma > 1.6\,\mathrm{GeV}$.

7 $\Delta B = 1$ and $\Delta B = 2$ processes

$\Delta B = 1$ FCNC processes such as $B \to X_{s,d}\,\gamma$ lead to very strong constraints on RHCC in the top sector. These processes are described by the effective Hamiltonian

$$\mathcal{H}_{\text{eff}} = -\frac{4G_F}{\sqrt{2}} V_{tb}V^*_{tq}\left[C_7\mathcal{O}_7 + C'_7\mathcal{O}'_7 + C_8\mathcal{O}_8 + C'_8\mathcal{O}'_8\right] , \tag{7.1}$$

with

$$\mathcal{O}_7 = \frac{e}{(4\pi)^2} m_b \bar{q}_L \sigma^{\mu\nu} b_R\, F_{\mu\nu}\,, \qquad \mathcal{O}_8 = -\frac{g_s}{(4\pi)^2} m_b \bar{q}_L \sigma^{\mu\nu} G^a_{\mu\nu} t^a b_R\,. \tag{7.2}$$

$\mathcal{O}'_{7,8}$ have analogous definitions with $L \leftrightarrow R$. Relations between the coefficients in eq. (7.1) and the coefficients of the dipole operators in eq. (3.6) are given by

$$C_7(m_W) = -\frac{4\pi^2 Q_d}{V_{tb}V^*_{tq}}\, v^2 C^{qb}_{\gamma d} \qquad C'_7(m_W) = -\frac{4\pi^2 Q_d}{V_{tb}V^*_{tq}}\frac{m_q}{m_b}\left(v^2 C^{bq}_{\gamma d}\right)^* ,$$
$$C_8(m_W) = \frac{4\pi^2}{V_{tb}V^*_{tq}}\, v^2 C^{qb}_{gd} \qquad C'_8(m_W) = \frac{4\pi^2}{V_{tb}V^*_{tq}}\frac{m_q}{m_b}\left(v^2 C^{bq}_{gd}\right)^* . \tag{7.3}$$

The coefficients at the scales $\mu = \mu_b = 2\,\mathrm{GeV}$ are given in table 6. From eq. (3.11) we see that the contribution of ξ_{tb} to $C_{7,8}$ and of ξ_{ts} and ξ_{td} to $C'_{7,8}$ are enhanced by m_t/m_b with respect to the SM, and therefore give rise to large effects in the $B \to X_{s,d}\gamma$ branching ratios. Information on the phases of the ξ_{tb} and ξ_{ts} elements can be gained by studying the CP asymmetries in inclusive $B \to X_{d,s}\gamma$ decays, and in the exclusive channel $B \to K^{*0}\gamma$. We discuss the $B \to X_{d,s}\gamma$ branching ratios in section 7.1, and the inclusive and exclusive CP asymmetries in sections 7.2 and 7.3, respectively.

$B \to X_{d,s}\gamma$ is not very sensitive to RHCC in the Wbc vertex. In section 7.4, we therefore study the corrections from RHCC to $B_q - \bar{B}_q$ mixing with $q = d, s$. While the contributions to the mass differences Δm_d and Δm_s are either quadratic in ξ, or suppressed by m_b/m_t with respect to the SM, corrections to the real and imaginary part of the width are more important and lead to constraints on $\mathrm{Im}\,\xi_{cb}$ that are comparable to those obtained from the tree-level processes discussed in section 4.

The experimental input used in this section is taken from refs. [71, 101] and is summarized in table 11.

7.1 The $B \to X_{d,s}\gamma$ branching ratio

For the $B \to X_{d,s}\gamma$ branching ratios, we employ the expressions derived in ref. [164] rescaled by the SM predictions of refs. [165–167],

$$\begin{aligned} \mathrm{BR}\,(B \to X_q\gamma) = r_q \frac{\mathcal{N}}{100} \frac{\left|V_{tq}^* V_{tb}\right|^2}{|V_{cb}|^2 + |\xi_{cb}|^2} \Big[& a + a_{77}(|R_7|^2 + |R_7'|^2) + a_7^r \,\mathrm{Re}\, R_7 + a_7^i \,\mathrm{Im}\, R_7 \\ & + a_{88}(|R_8|^2 + |R_8'|^2) + a_8^r \,\mathrm{Re}\, R_8 + a_8^i \,\mathrm{Im}\, R_8 + a_{\epsilon\epsilon}|\epsilon_q|^2 + a_\epsilon^r \,\mathrm{Re}\, \epsilon_q \\ & + a_\epsilon^i \,\mathrm{Im}\, \epsilon_q + a_{87}^r \,\mathrm{Re}\,(R_8 R_7^* + R_8' R_7'^*) + a_{87}^i \,\mathrm{Im}\,(R_8 R_7^* + R_8' R_7'^*) \\ & + a_{7\epsilon}^r \,\mathrm{Re}\,(R_7 \epsilon_q^*) + a_{7\epsilon}^i \,\mathrm{Im}\,(R_7 \epsilon_q^*) + a_{8\epsilon}^r \,\mathrm{Re}\,(R_8 \epsilon_q^*) + a_{8\epsilon}^i \,\mathrm{Im}\,(R_8 \epsilon_q^*) \Big] , \end{aligned} \tag{7.4}$$

where $R_{7,8} = \frac{C_{7,8}(m_t)}{C_{7,8}^{\rm SM}(m_t)}$, $R'_{7,8} = \frac{C'_{7,8}(m_t)}{C_{7,8}^{\rm SM}(m_t)}$, $C_7^{\rm SM}(m_t) = -0.189$, and $C_8^{\rm SM}(m_t) = -0.095$. Furthermore, $\mathcal{N} = 2.567(1 \pm 0.064) \cdot 10^{-3}$. r_q is a factor that rescales the above expression to the SM predictions of refs. [165–167]. It is given by $r_s = \frac{3.36}{3.61}$ and $r_d = \frac{1.73}{1.38}$. Finally, $\epsilon_q = \frac{V_{uq}^* V_{ub}}{V_{tq}^* V_{tb}}$ and the numerical values of a_{ij} can be found in ref. [164]. In our analysis, we applied the expressions relevant for the following cut on the photon energy $E_\gamma > 1.6\,\mathrm{GeV}$. For $B \to X_d\,\gamma$ this requires extrapolating the branching ratio quoted in ref. [101], as discussed in ref. [166],

The branching ratios in eq. (7.4) should be compared with the current experimental world averages [71, 101], which we give in table 11. To derive constraints we follow refs. [168, 169] and apply the relative uncertainties on the SM predictions $\sigma_d = \frac{0.22}{1.73}\mathrm{BR}(B \to X_d\gamma)$ $\sigma_s = \frac{0.23}{3.36}\mathrm{BR}(B \to X_s\gamma)$. These theoretical uncertainties are then added in quadrature to the experimental ones.

7.2 The $B \to X_{d,s}\gamma$ CP asymmetry

The phase of ξ_{tb} can be probed by the $B \to X_s\gamma$ CP asymmetry. We employ the expression derived in ref. [170],

$$\begin{aligned} \frac{A_{CP}(B \to s\gamma)}{\pi} &\equiv \frac{1}{\pi} \frac{\Gamma(\bar{B} \to X_s\gamma) - \Gamma(B \to X_{\bar{s}}\gamma)}{\Gamma(\bar{B} \to X_s\gamma) + \Gamma(B \to X_{\bar{s}}\gamma)} \\ &\approx \left[\left(\frac{40}{81} - \frac{40}{9}\frac{\Lambda_c}{m_b} \right) \frac{\alpha_s}{\pi} + \frac{\Lambda_{17}^c}{m_b} \right] \mathrm{Im}\, \frac{C_2}{C_7} - \left(\frac{4\alpha_s}{9\pi} + 4\pi\alpha_s \frac{\Lambda_{78}}{3m_b} \right) \mathrm{Im}\, \frac{C_8}{C_7} \\ &\quad - \left(\frac{\Lambda_{17}^u - \Lambda_{17}^c}{m_b} + \frac{40}{9}\frac{\Lambda_c}{m_b}\frac{\alpha_s}{\pi} \right) \mathrm{Im}\left(\epsilon_s \frac{C_2}{C_7} \right) , \end{aligned} \tag{7.5}$$

where C_2 is the coefficient of the charged-current operator $\mathcal{O}_{1\,LL}^{cb\,cs}$, $C_2 = C_{1\,LL}^{cb\,cs}/(V_{cb}V_{cs}^*)$, which, along with $C_{7,8}$, should be evaluated at the factorization scale $\mu_b \simeq 2\,\mathrm{GeV}$. We employ the following SM values for these coefficients [170],

$$C_2^{\rm SM}(2\,\mathrm{GeV}) = 1.204\,, \qquad C_7^{\rm SM}(2\,\mathrm{GeV}) = -0.381\,, \qquad C_8^{\rm SM}(2\,\mathrm{GeV}) = -0.175\,. \tag{7.6}$$

In addition, the CP asymmetry depends on the scale, $\Lambda_c \simeq 0.38\,\mathrm{GeV}$, and on three hadronic parameters that are estimated to lie in the following ranges [170],

$$\Lambda_{17}^u \in [-0.33,\, 0.525]\,\mathrm{GeV}, \quad \Lambda_{17}^c \in [-0.009,\, 0.011]\,\mathrm{GeV}, \quad \Lambda_{78} \in [-0.017,\, 0.19]\,\mathrm{GeV}. \tag{7.7}$$

We use the Rfit procedure to deal with these uncertainties [156].

In the case of $B \to X_d\gamma$ decays, instead of the CP asymmetry $A_{CP}(B \to X_d\gamma)$, the combined asymmetry $A_{CP}(B \to X_{d+s}\gamma)$ is measured. This combination can be expressed as [164],

$$A_{CP}(B \to X_{d+s}\gamma) = \frac{A_{CP}(B \to X_s\gamma) + R_{ds}A_{CP}(B \to X_d\gamma)}{1 + R_{ds}}\,, \tag{7.8}$$

with $R_{ds} = (\Gamma(B \to X_d\gamma) + \Gamma(\bar{B} \to X_d\gamma))/(\Gamma(B \to X_s\gamma) + \Gamma(\bar{B} \to X_s\gamma))$. Since the branching ratio of $B \to X_s\gamma$ is significantly larger than that of $B \to X_d\gamma$, R_{ds} is expected to be at the percent level and $A_{CP}(B \to X_{d+s}\gamma)$ is therefore mainly sensitive to $A_{CP}(B \to s\gamma)$. In addition, the experimental precision on the determination of $A_{CP}(B \to X_{d+s}\gamma)$ is of the same order as $A_{CP}(B \to X_s\gamma)$, such that the latter does not provide any additional constraints.

7.3 The $B \to K^{*0}\gamma$ CP asymmetry

The time-dependent CP asymmetry in the exclusive decay $B \to K^{*0}\gamma$ can be described by

$$\frac{\Gamma(\bar{B} \to \bar{K}^{*0}\gamma) - \Gamma(B \to K^{*0}\gamma)}{\Gamma(\bar{B} \to \bar{K}^{*0}\gamma) + \Gamma(B \to K^{*0}\gamma)} = S_{K^*\gamma}\cos(\Delta m_d t) + C_{K^*\gamma}\sin(\Delta m_d t)\,. \tag{7.9}$$

Here we are interested in the parameter $S_{K^*\gamma}$, which is given by

$$S_{K^*\gamma} = 2\frac{\operatorname{Im}\lambda_{K^*\gamma}}{1 + |\lambda_{K^*\gamma}|^2}, \qquad \lambda_{K^*\gamma} = \frac{q}{p}\frac{A(\bar{B} \to \bar{K}^{*0}\gamma)}{A(B \to K^{*0}\gamma)}\,, \tag{7.10}$$

where the ratio $\frac{q}{p} = \frac{V_{tb}V_{td}^*}{V_{tb}^*V_{td}}$ arises from $B_d - \bar{B}_d$ mixing. At leading order the coefficient $S_{K^*\gamma}$ is generated by the electromagnetic dipole operators, C_7 and C_7'. The dependence on C_7' is particularly interesting as this Wilson coefficient is induced by right-handed currents, while being suppressed by m_s/m_b in the SM. In fact, the leading-order expression is [169, 171],

$$S_{K^*\gamma} = \frac{2\operatorname{Im}\left(\frac{V_{tb}V_{td}^*}{V_{tb}^*V_{td}}\frac{V_{tb}V_{ts}^*}{V_{tb}^*V_{ts}}C_7C_7'\right)}{|C_7|^2 + |C_7'|^2}\,, \tag{7.11}$$

such that $S_{K^*\gamma}$ vanishes unless C_7' is nonzero. As mentioned above, the SM prediction is rather small [172, 173]

$$S_{K^*\gamma}^{\rm SM} = (-2.3 \pm 1.6)\cdot 10^{-2}\,. \tag{7.12}$$

The experimental value for $S_{K^*\gamma}$ is given in table 11.

7.4 $B_q - \bar{B}_q$ mixing

Right-handed currents can affect $B_q - \bar{B}_q$ oscillations through insertions of ξ in $\Delta B = 2$ box diagrams that govern this mixing. The contributions to the dispersive part of these amplitudes, M_{12}, are either quadratic in ξ_{ij} or suppressed with respect to the SM by a factor of the external quark mass, which is at most m_b^2/m_t^2. We will therefore neglect the contributions to M_{12} which are linear in ξ, as well as the dimension-eight effects discussed in appendix A.3. In contrast, the ξ_{ij} contributions to the absorptive part of the mixing amplitude are not suppressed with respect to the SM, as both are proportional to m_b^2. The largest contributions come from ξ_{cb} and ξ_{cq}, for which we find

$$\begin{aligned}\Gamma_{12}^{(q)}(\xi) = &-\frac{G_F^2 m_b^2 m_{B_q} f_{B_q}^2}{\pi}\sqrt{z}\left(\lambda_c^{(q)\,2}\left(\sqrt{1-4z}-(1-z)^2\right)-\lambda_c^{(q)}\lambda_t^{(q)}(1-z)^2\right)\times \\ &\times\Bigg[\left(\left[\frac{2}{3}B_1-\frac{5}{6}B_2R\right]\frac{\xi_{cb}}{V_{cb}}+\frac{1}{3}B_5R\frac{\xi_{cq}^*}{V_{cq}^*}\right)\eta_{11LL}\eta_{11LR} \\ &+\left(\left[\frac{2}{3}B_1+\frac{1}{6}B_3R\right]\frac{\xi_{cb}}{V_{cb}}+B_4R\frac{\xi_{cq}^*}{V_{cq}^*}\right)\left(\eta_{11LL}\eta_{21LR}+\eta_{21LL}\eta_{11LR}+3\,\eta_{21LL}\eta_{21LR}\right)\Bigg],\end{aligned} \tag{7.13}$$

where $z \equiv m_c^2/m_b^2$, $\lambda_i^{(q)} = V_{ib}V_{iq}^*$, and $R = m_{B_q}^2/(m_b+m_q)^2$. The B_i are given in appendix A.3 and represent the bag factors of the $\Delta B = 2$ operators in eq. (A.13). Finally, the η factors originate from the RG evolution, between m_W and m_b, of the four-fermion operators in eq. (3.1). These factors relate the four-fermion operators at different scales through $C_{i\,LL(LR)}(m_b) = \eta_{ij\,LL(LR)}C_{j\,LL(LR)}(m_W)$, and are determined by eq. (3.4). Explicitly we have

$$\begin{aligned}\eta_{11\,LL} &= \frac{1}{2}\left(\eta^{6/23}+\eta^{-12/23}\right), &\qquad \eta_{11\,LR} &= \eta^{3/23}, \\ \eta_{21\,LL} &= \frac{1}{2}\left(\eta^{6/23}-\eta^{-12/23}\right), &\qquad \eta_{21\,LR} &= \frac{1}{3}\left(\eta^{-24/23}-\eta^{3/23}\right),\end{aligned} \tag{7.14}$$

where $\eta = \alpha_s(m_W)/\alpha_s(m_b)$.

The real part of the right-handed contribution to Γ_{12} can be constrained by the width difference between the mass eigenstates, whereas the imaginary parts are probed by the measure of CP violation, $a_{\rm fs}^q$ [174],

$$\Delta\Gamma^{(q)} = 4\frac{\mathrm{Re}\left(\Gamma_{12}^{(q)*}M_{12}^{(q)}\right)}{\Delta m_{B_q}}, \qquad a_{\rm fs}^q = 1-\left|\frac{q}{p}\right|^2 = \mathrm{Im}\left(\frac{\Gamma_{12}^{(q)}}{M_{12}^{(q)}}\right). \tag{7.15}$$

As mentioned above, the right-handed corrections to M_{12} are small and we neglect them here, while the SM expression for M_{12} can be found in appendix A.3. The SM values for these quantities are given by [175],

$$\begin{aligned}\Delta\Gamma_{\rm SM}^{(d)} &= (2.61\pm0.59)\cdot10^{-3}\,\mathrm{ps}^{-1}, &\qquad \Delta\Gamma_{\rm SM}^{(d)} &= (0.085\pm0.015)\,\mathrm{ps}^{-1}, \\ a_{\rm fs}^d\big|_{\rm SM} &= (-4.7\pm0.6)\cdot10^{-4}, &\qquad a_{\rm fs}^s\big|_{\rm SM} &= (2.22\pm0.27)\cdot10^{-5},\end{aligned} \tag{7.16}$$

while the current experimental determinations are given in table 11.

8 Single-coupling constraints

In this section we discuss the constraints on the various right-handed couplings in the case that a single ξ_{ij} element dominates at the scale of new physics. To obtain bounds we construct a χ^2 involving the observables described in sections 4–7. Furthermore, we assume that the CKM matrix is SM-like and apply the Wolfenstein parametrization to write the

CKM matrix in terms of A, λ, $\bar{\rho}$, and $\bar{\eta}$, up to $\mathcal{O}(\lambda^6)$ corrections [176].[3] Since the standard extraction of the CKM elements can be modified by the inclusion of right-handed currents, we determine the SM CKM parameters along with the ξ_{ij} from the χ^2. Thus, for each ξ_{ij} we simultaneously fit for A, λ, $\bar{\rho}$, and $\bar{\eta}$ as well as the real and imaginary parts of ξ_{ij}.

Apart from the observables discussed in the sections above, we include $B \to J/\psi K$, $B_q^0 \to \mu^+\mu^-$ and the $\Delta F = 2$ processes ϵ_K, Δm_d, and Δm_s. As discussed in appendix A.1, A.2 and A.3, these processes do not get large corrections from the RHCC operators. However, we include these observables in our analysis as they provide an important role in determining the SM CKM parameters.

We do not include other non-leptonic B decays, such as $B \to \pi\pi$. These processes are affected by right-handed currents at tree level, and a reliable estimate of the corrections requires non-perturbative information on the matrix elements of the four-quark operators $C_{1\,LR}$ and $C_{2\,LR}$, which, at the moment, is not available. As a result, even without taking into account ξ contributions, we find wider ranges for $\bar{\rho}$ and $\bar{\eta}$ compared to ref. [71], but we expect these differences to have small impact on the bounds on ξ.

Finally, most of the observables in sections 4–7 involve theory uncertainties, which we treat by adding them in quadrature to the experimental errors. However, there are several cases in which these uncertainties are large and allow for cancellations, notably in ϵ'/ϵ, ϵ_K, d_n, $d_{\rm Hg}$, and $A_{CP}(b \to s\gamma)$. In these specific cases, where cancellations between different contributions can significantly affect the constraints, we treat the theoretical errors using the Rfit approach as defined in [156]. We vary the matrix elements within their allowed ranges and apply those values of the matrix elements that minimize the χ^2. This procedure leads to conservative constraints as it allows for cancellations between different contributions.

Using the approach described above, we find the following 90% C.L. constraints on the real and imaginary part of ξ_{ij}

$$\mathrm{Re}\,\xi_{ij} \in \begin{pmatrix} [-7.0,\, 1.6]\cdot 10^{-4} & [-2.1,\, 0.05]\cdot 10^{-3} & [-1.4,\, 1.3]\cdot 10^{-3} \\ [-1.0,\, 0.8]\cdot 10^{-2} & [-4.2,\, 0.55]\cdot 10^{-2} & [0.1,\, 3.5]\cdot 10^{-3} \\ [-1.0,\, 1.0]\cdot 10^{-4} & [-2.1,\, 2.5]\cdot 10^{-4} & [-1.4,\, 1.2]\cdot 10^{-3} \end{pmatrix}, \tag{8.1}$$

$$\mathrm{Im}\,\xi_{ij} \in \begin{pmatrix} [0.15,\, 3.4]\cdot 10^{-6} & [0.5,\, 7.9]\cdot 10^{-7} & [-0.4,\, 0.7]\cdot 10^{-3} \\ [-8.5,\, 7.2]\cdot 10^{-6} & [-5.7,\, 7.0]\cdot 10^{-3} & [-1.5,\, 0.6]\cdot 10^{-2} \\ [-4.2,\, 4.2]\cdot 10^{-5} & [-2.5,\, 1.9]\cdot 10^{-4} & [-2.4,\, 2.3]\cdot 10^{-3} \end{pmatrix}, \tag{8.2}$$

where we stress that the bounds are obtained turning on one complex ξ_{ij} element at a time.

For the CKM parameters we obtain the 90% C.L. allowed ranges in case of the ξ_{ud} fit

$$\lambda \in [0.2232,\, 0.2255], \quad A \in [0.787,\, 0.827], \quad \bar{\rho} \in [0.060,\, 0.20], \quad \bar{\eta} \in [0.33,\, 0.40]. \tag{8.3}$$

These values are in agreement with those found in ref. [71], although the constraints found here are generally weaker. As mentioned above, this is to be expected as the fit of ref. [71]

[3] The higher-order terms are mainly important for ϵ_K, which we employ to constrain the CKM parameters. The imaginary part of the $V_{cs}^* V_{cd}$ term only appears after expanding V to $\mathcal{O}(\lambda^5)$.

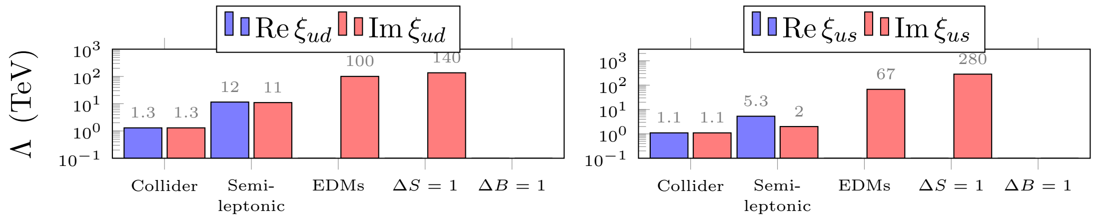

Figure 6. The figure shows naive constraints on the real (in blue) and imaginary (in red) parts of ξ_{ud} and ξ_{us} converted to an effective scale Λ by using $\xi_{ij} \equiv v^2/\Lambda^2$. These limits are obtained by setting the CKM parameters to the values of ref. [71], and turning on only one real or imaginary part of ξ_{ij} at a time. In the cases where the bounds are asymmetrical, we show the limit that results in the lowest value of Λ. The different bars represent the limits from the collider, semileptonic, EDM ($\Delta F = 0$), $\Delta S = 1$, and $\Delta B = 1$ observables, discussed in sections 2, 4, 5, 6, and 7, respectively.

includes several more observables than we take into account here. This affects $\bar{\rho}$ the most, which is reflected by the observation that our allowed ranges are roughly twice as wide. In addition, at 68% C.L. our upper limit for $\bar{\eta}$ extends roughly one standard deviation upwards compared to ref. [71], while our lower limit for λ extends one standard deviation downwards. For most of the ξ_{ij} couplings, the ranges in eq. (8.3) are rather stable and do not vary significantly between the different ξ_{ij}. The upper and lower ranges of both λ and A vary by less than 1% between the different fits, while $\bar{\rho}$ and $\bar{\eta}$ exhibit variations of up to a few percent. The exception occurs in the case of ξ_{cb}, where the upper ranges of A and $\bar{\rho}$ widen by about 5%, while the allowed lower range for $\bar{\eta}$ is widened by roughly 5%.

While the χ^2 function used to obtain eqs. (8.1) and (8.2) includes all the observables described in sections 4–7, the bounds on most entries of the ξ_{ij} elements are dominated by a smaller set of processes. Below we briefly describe which observables drive the constraints for each ξ element.

ξ_{ud} and ξ_{us}. An overview of the constraints on $\mathrm{Re}\,\xi_{ud}$ is shown in blue in the left panel of figure 6. These constraints are obtained by setting the CKM parameters to the values of ref. [71] and assuming that only $\mathrm{Re}\,\xi_{ud}$ is turned on. As these limits indicate, in the single coupling analysis, the best constraints on $\mathrm{Re}\,\xi_{ud}$ come from semileptonic decays, in particular, superallowed β decay. Indeed, the unitarity of the CKM matrix V and the absence of modifications of the us element allow one to use leptonic and semileptonic kaon decays to accurately determine λ, and then extract ξ_{ud} from superallowed β decays without relying on leptonic pion decays, which suffer $\sim 1\%$ percent theoretical uncertainty from the LQCD determination of the pion decay constant. As is shown in red in the left panel of figure 6, $\mathrm{Im}\,\xi_{ud}$ is constrained by the D coefficient, ϵ'/ϵ and EDMs. The stronger constraint comes from ϵ'/ϵ, followed closely by the neutron EDM. The limit from the D coefficient is two orders of magnitude weaker, $\mathrm{Im}\,\xi_{ud} \in [-2.9, 5.1] \cdot 10^{-4}$. This translates into a difference of one order of magnitude between the semileptonic and EDM constraints on Λ in figure 6.

The situation is very similar for ξ_{us} as shown the right panel of figure 6. Here the real part is constrained by leptonic and semileptonic kaon decays, while the imaginary part is constrained by EDMs and ϵ'/ϵ, with the latter giving again the stronger bound. In

JHEP05(2017)086

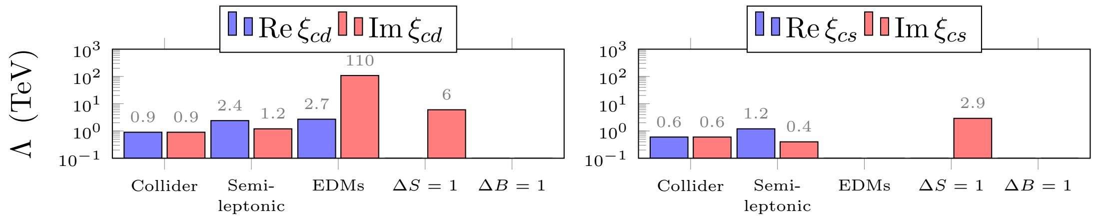

Figure 7. The figure shows naive constraints on ξ_{cd} and ξ_{cs}. Notation is the same as in figure 6.

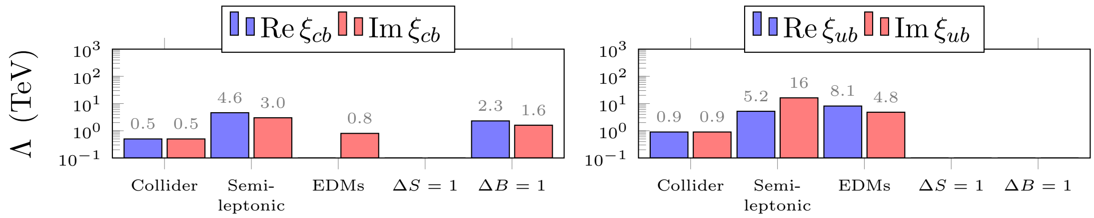

Figure 8. The figure shows naive constraints on ξ_{cb} and ξ_{ub}. Notation is the same as in figure 6.

this case, the semileptonic constraint on the imaginary part is weaker due to the fact that the experimental limit on D_Σ is significantly less stringent than that on D_n. As noticed in ref. [11], an imaginary part of ξ_{ud} or ξ_{us} can solve the 2σ discrepancy between the measured value of ϵ'/ϵ and the SM predictions of refs. [160, 177–180], without conflict with EDM and other low- and high-energy constraints. This manifests in the non-zero values for $\mathrm{Im}\,\xi_{ud}$ and $\mathrm{Im}\,\xi_{us}$ in eq. (8.2).

ξ_{cd} and ξ_{cs}. As shown in the left (right) panel of figure 7, the real part of ξ_{cd} (ξ_{cs}) is mainly constrained by leptonic and semileptonic D (D_s) decays, while the collider limits are weaker by a factor of a few. The larger theoretical and experimental errors cause the bounds from semileptonic decays to be less stringent than for ξ_{ud} and ξ_{us}. The bound on $\mathrm{Im}\,\xi_{cd}$ is dominated by the neutron EDM, while the small imaginary part of V_{cd} gives rise to a (much weaker) EDM bound on $\mathrm{Re}\,\xi_{cd}$ as well. $\mathrm{Im}\,\xi_{cd}$ also contributes to $K_L \to \pi^0 e^+ e^-$, but the bound is three orders of magnitude weaker, $|\mathrm{Im}\,\xi_{cd}| < 2 \cdot 10^{-3}$. $\mathrm{Im}\,\xi_{cs}$ mainly contributes to the nucleon EDM by generating a strange quark EDM. As shown in eq. (5.3), the matrix element linking the neutron EDM to the strange EDM is consistent with zero [138, 139], which, in the Rfit approach, leads to no constraint on $\mathrm{Im}\,\xi_{cs}$. The bound in eq. (8.2) therefore comes from $K_L \to \pi^0 e^+ e^-$.

ξ_{cb} and ξ_{ub}. As can be seen in figure 8, ξ_{cb} and ξ_{ub} are both constrained by the inclusive and exclusive semileptonic B decays. Furthermore, the $B_q - \bar{B}_q$ oscillation observables, $\Delta\Gamma_q$ and $a^q_{\rm fs}$, constrain the real and imaginary parts of ξ_{cb}, while EDMs only constrain the imaginary part. Instead, for ξ_{ub} both the real part and imaginary parts are constrained by d_n (due to the sizable imaginary part of the relevant CKM element, V_{ub}), while the contributions to $B_q - \bar{B}_q$ mixing are negligible.

For both ub and cb elements there is some tension between the determination via inclusive and exclusive decays. We find that adding a right-handed current improves the χ^2.

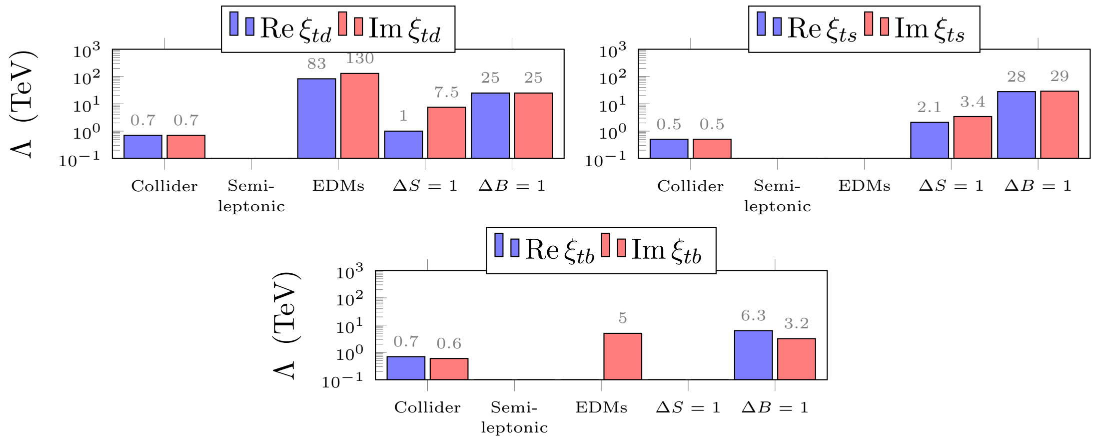

Figure 9. The figure shows naive constraints on ξ_{td}, ξ_{ts} and ξ_{tb}. Notation is the same as in figure 6.

As shown in eq. (8.1), in the case of cb, our fit prefers a non-zero value of $\mathrm{Re}\,\xi_{cb}$, while for the ub element, both real and imaginary part are compatible with zero. The reason being that the nonzero values of ξ_{ub} that are preferred by the semileptonic decays are disfavored by the neutron EDM. We caution though that our analysis of the inclusive decays is incomplete, and, in particular, we did not repeat the fits to the lepton spectrum, which receive different contributions from left- and right-handed currents. We notice that the bounds on ξ_{ub} and $\mathrm{Im}\,\xi_{cb}$ are rather weak when compared to the magnitudes of V_{ub} and V_{cb}, and sizable right-handed corrections (up to 50% for V_{ub} and 30% for V_{cb}) are still allowed.

ξ_{td}, ξ_{ts}, and ξ_{tb}. We collect the naive constraints on ξ_{td}, ξ_{ts}, and ξ_{tb} in, respectively, the top-left, top-right, and bottom panels of figure 9. The figure shows that all the top-row elements are strongly constrained by $\Delta B = 1$ observables. In particular, ξ_{td} is constrained by $B \to X_d\gamma$, while for $\xi_{ts,tb}$ stringent limits arise from $B \to X_s\gamma$.[4] A comparable limit on $\mathrm{Im}\,\xi_{tb}$ comes from EDMs, while for ξ_{td} the EDM limits are stronger than the $\Delta B = 1$ constraints by an order of magnitude. Due to the imaginary part of V_{td}, EDMs constrain the real part of ξ_{td} as well. In contrast, due to the poorly known matrix element related to $\tilde{c}_{\gamma d}^{(ss)}$, there are no EDM constraints on ξ_{ts}. Finally, ξ_{td} (ξ_{ts}) also contributes to $K_L \to \pi^0 e^+ e^-$, but the bounds are weaker by roughly a factor 10 (100). For all ξ_{tj} elements the indirect bounds are stronger than the direct collider bounds, by at least an order of magnitude.

8.1 Summary

We summarize the strongest constraints on the real and imaginary parts in the left and right panels of figure 10, respectively. The solid bars depict the constraints derived using the Rfit approach for the EDM uncertainties as outlined at the end of section 5. Instead, the dashed bars indicate the 'central' case, in which we set the theory errors in d_n and

[4] It should be noted that, apart from the allowed range given in eq. (8.1), the flavor and low-energy observables allow for larger negative values of $\mathrm{Re}\,\xi_{tb}$ namely, $\mathrm{Re}\,\xi_{tb} \in [-0.034, -0.031]$. However, this possibility is excluded by LHC constraints on $h \to b\bar{b}$.

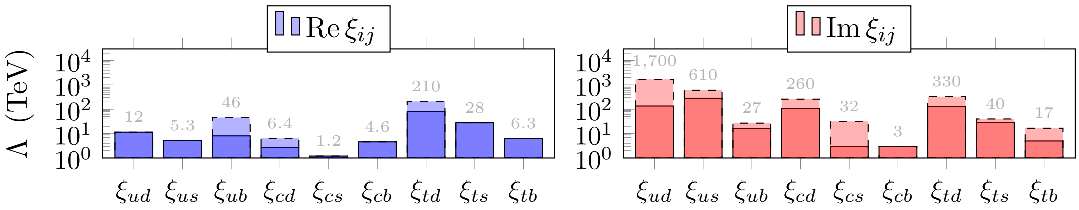

Figure 10. The figure summarizes the most stringent naive constraints on ξ_{ij}. The dashed bars show the naive constraints in the case that we do not take into account the theory errors that appear in the EDM expressions eqs. (5.3) and (5.4). Notation is the same as in figure 6.

$d_{\rm Hg}$ to zero. The difference in the strengths of the constraints illustrates the impact of the hadronic and nuclear uncertainties.

The real parts of ξ_{td} and ξ_{ts} are the most stringently constrained elements (by $b \to q\gamma$), while the weakest constraints are obtained in the case of $\xi_{cd,cs}$. In the latter case, the precision of the semileptonic decays and the corresponding lattice input is at the percent level, thus allowing for couplings of order $\mathcal{O}(10^{-2})$. The remaining real parts are constrained at the sub-percent level. Furthermore, as can be seen from the dashed bars, most of the real parts are unaffected by the theory uncertainties related to EDMs. The exceptions are ξ_{ub}, ξ_{cd}, and ξ_{td}, which contribute to EDMs as their corresponding CKM elements have sizable imaginary parts. The main effect of neglecting the theoretical errors is that cancellations in the neutron and mercury EDMs are no longer possible. As a result, the mercury EDM provides the most stringent limit on the real parts of $\xi_{ub,cd,td}$ in the 'central' case. Although the mercury EDM also constrains ξ_{ts} in the 'central' scenario it does not overtake the $b \to s\gamma$ limits.

Moving on to the imaginary parts, one can compare the left and right panels of figure 10 to see that, even when using the Rfit approach, the limits on the imaginary parts are generally better than those on the real parts. All constraints are well below the percent level, apart from those on ξ_{cb} and ξ_{cs}. The weak bounds on the cb and cs elements result partially due to suppressed contributions to d_n: the ξ_{cs} contribution depends on the poorly known strange-EDM matrix element, while the ξ_{cb} contributions only arise at the two-loop level. Among the stronger constraints are those on $\xi_{td,ts}$ (from $b \to q\gamma$ and EDMs), however the most impressive limits are set on ξ_{ud} and ξ_{us} and arise from the neutron EDM and ϵ'/ϵ which probe effective scales around $\mathcal{O}(100\,\text{TeV})$.

As seen from the dashed bars, most constraints on the imaginary parts are at least somewhat affected when moving from the Rfit approach to the 'central' case. For most couplings this results in an improvement of the EDM limit by a factor of a few to $\mathcal{O}(10)$. More drastic changes occur for $\xi_{cs,ts}$, ξ_{ud}, and ξ_{us}. In case of ξ_{cs} this is due to the poorly known strange-EDM matrix element resulting in a vanishing EDM constraint in the Rfit approach, whereas the neutron EDM strongly constraints $\text{Im}\,\xi_{cs}$ in the central case. The situation is similar for ξ_{ts}, although less clear from figure 10 as the improved EDM limits do not overtake the $b \to s\gamma$ constraints. For ξ_{ud} and ξ_{us} the EDM limits improve by factors of $\mathcal{O}(300)$ and $\mathcal{O}(100)$, respectively. These large factors arise due to the fact that the

JHEP05(2017)086

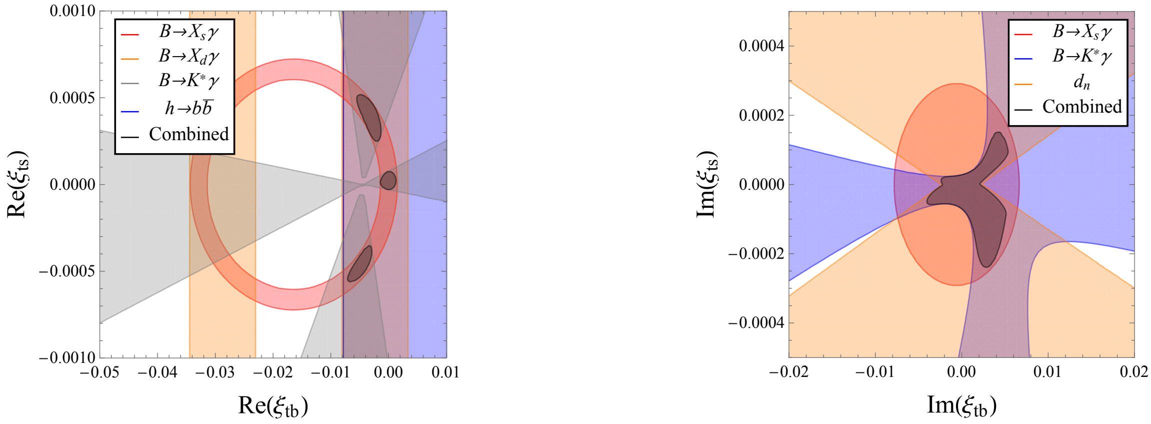

Figure 11. The left (right) panel shows the constraints on the real (imaginary) parts of ξ_{tb} and ξ_{ts}. These limits assume that only the real or imaginary parts of ξ_{tb} and ξ_{ts} are generated at the scale Λ.

four-quark operators $O_{i\,LR}^{udud}$ and $O_{i\,LR}^{usus}$ induce a large pion-nucleon coupling $\bar{g}_1$, to which the mercury EDM has an increased sensitivity compared to d_n. The resulting limits then overtake the ϵ'/ϵ constraints and naively reach scales up to $\mathcal{O}(10^3)$ TeV.

As the above discussion shows, in some cases the uncertainties related to the matrix elements can mean the difference between a stringent limit or no bound at all. For example, although the neutron and mercury EDMs are in principle sensitive to the right-handed couplings to strange quarks, the poor knowledge of the strange matrix elements does not allow us to set EDM bounds on ξ_{cs} and ξ_{ts}. This also holds true for the nuclear matrix elements related to the pion-nucleon couplings $\bar{g}_{0,1}$. These matrix elements allow the mercury EDM to vanish for all ξ_{ij} elements, even though the 'central' limits on ξ_{ud} and ξ_{us} show that $d_{\rm Hg}$ could potentially probe scales up to 10^3 TeV. These observations are similar to those discussed in ref. [181] in the context of CPV Higgs-quark interactions, and further motivate studies of hadronic and nuclear matrix elements with lattice QCD and modern nuclear many-body methods.

Finally, it is interesting to see whether the limits given in eq. (8.1) and (8.2) are stable against turning on several ξ_{ij} couplings at the same time. Here we do not commit to a global analysis involving all the ξ_{ij} couplings. Instead, as an example, we briefly discuss the resulting limits when turning on one row of the ξ_{ij} matrix at a time. In this scenario the real parts of the first two rows remain largely unaffected.[5]

The imaginary parts are more sensitive to the effect of turning on additional couplings, as this allows for cancellations in d_n and ϵ'/ϵ. As a result, the limit on the imaginary part of ξ_{ud} is now determined by the D_n coefficient, giving constraints at the $\mathcal{O}(10^{-4})$ level. In turn, this leaves room for an imaginary part of ξ_{us} up to $\mathcal{O}(10^{-3})$. The limit on $\mathrm{Im}\,\xi_{cd}$ is

[5]The only exception is ξ_{ub} for which nonzero values, $|\mathrm{Re}\,\xi_{ub}| \approx 2 \cdot 10^{-3}$, are preferred due to the discrepancy between inclusive and exclusive semileptonic decays. Given that our determination of the inclusive decay is not entirely consistent, see section 4, these nonzero values should not be taken too seriously. The reason that ξ_{ub} is consistent with zero in the single-coupling analysis, eq. (8.1), is that nonzero values are disfavored by the neutron EDM. When several couplings can be nonzero at once, however, the neutron EDM limit can be canceled by $\mathrm{Im}\,\xi_{ud}$ and $\mathrm{Im}\,\xi_{us}$ contributions.

weakened by roughly two orders of magnitude due to similar cancellations in d_n. Instead, the constraints on the imaginary parts of $\xi_{ub,cb}$ and ξ_{cs} do not change much since they are mainly determined by the semileptonic decays and $K_L \to \pi^0 e^+ e^-$, respectively.

For the third row, the limits on both the real and imaginary parts are weakened by factors of a few for $\xi_{td,ts}$, while those on ξ_{tb} deteriorate by an order of magnitude. As an example of the interplay between the different ξ_{tq} elements, we show the $\xi_{tb} - \xi_{ts}$ plane for the real (imaginary) parts in the left (right) panel of figure 11. The constraints shown in the left (right) panel assume that only the real (imaginary) parts ξ_{tb} and ξ_{ts} are present at the scale Λ.

9 Identifying right-handed currents at low and high energy

In section 8 we showed that, under the assumption that the SM is modified dominantly by a RHCC at high energy, low-energy bounds from leptonic and semileptonic charged-current decays, $B \to X_{s,d}\gamma$, ϵ'/ϵ, and EDMs are significantly stronger than collider bounds. On the other hand, in explicit models of new physics the low-energy observables unavoidably involve some degeneracy [182]. In this section we therefore study more general scenarios in which other operators apart from a RHCC are induced at high energy and how to unambiguously identify RHCCs both at high and low energy. In sections 9.1 and 9.2 we focus on the couplings of the W to ud and us quarks, while in section 9.3 we examine the Wtb coupling.

9.1 Low-energy probes

In section 8 we used superallowed β decays, and leptonic and semileptonic pion and kaon decays to put stringent bounds on RHCC involving the u and d, and the u and s quarks. The processes we used to constrain $\mathrm{Re}\,\xi_{ud}$ and $\mathrm{Re}\,\xi_{us}$ are, however, sensitive not only to RHCC, but can be affected by additional contributions. These can be studied by considering the most general semileptonic dimension-six Lagrangian at low energy [183, 184, 186]

$$\mathcal{L} = -\frac{4G_F}{\sqrt{2}} V_{ud}\bigg[(1+\delta V_{ud} + (\varepsilon_L)_{ud})\, \bar{u}\gamma^\mu P_L d\, \bar{l}\gamma_\mu P_L \nu + \frac{\xi_{ud}}{V_{ud}}\, \bar{u}\gamma^\mu P_R d\, \bar{l}\gamma_\mu P_L \nu \\ + \frac{1}{2}(\varepsilon_S)_{ud}\, \bar{u}d\, \bar{l}P_L\nu - \frac{1}{2}(\varepsilon_P)_{ud}\, \bar{u}\gamma_5 d\, \bar{l}P_L\nu + (\varepsilon_T)_{ud}\, \bar{u}\sigma^{\mu\nu}P_L d\, \bar{l}\sigma_{\mu\nu}P_L\nu + \text{h.c.}\bigg], \tag{9.1}$$

and analogous contributions for the us couplings. In eq. (9.1), we separated the contribution to left-handed currents coming from corrections to the W couplings to left-handed quark or leptons, δV_{ud}, from a semileptonic four-fermion operator, ε_L. While these operators are degenerate at low energy, they have different manifestations at collider experiments [183, 184, 186]. The operators in eq. (9.1) are in direct correspondence with gauge-invariant operators in the basis of ref. [6], and the mapping is discussed in refs. [183, 184]. Semileptonic operators arising from vertex corrections, δV_{ud} and ξ_{ud}, are automatically lepton-flavor universal. For the four-fermion operators, $\varepsilon_{L,P,S,T}$, we assumed the couplings to be diagonal in lepton flavor.

JHEP05(2017)086

The operators in eq. (9.1) affect all the observables introduced in section 4, which we used to bound ξ_{ud} and ξ_{us} (see ref. [187] for a comprehensive analysis). For example, superallowed β decays receive corrections from the scalar coupling ε_S, which shifts V_{ud} into [184, 186, 188]

$$|V_{ud}(0^+ \to 0^+)|_{\rm exp} = |V_{ud}| \left| 1 + \delta V_{ud} + (\varepsilon_L)_{ud} + \frac{\xi_{ud}}{V_{ud}} + \frac{g_S}{2} c^S_{0^+}(Z)(\varepsilon_S)_{ud} \right| , \tag{9.2}$$

where g_S is the nucleon matrix element of the scalar current, and $c^S_{0^+}(Z)$ is a function which depends on the individual nuclear transition. The expression for $\pi^\pm \to \mu^\pm \nu_\mu$ is modified into

$$|V_{ud}(\pi \to \mu\nu) f_\pi|_{\rm exp} = |V_{ud}| \left| 1 + \delta V_{ud} + (\varepsilon_L)_{ud} - \frac{\xi_{ud}}{V_{ud}} - (\varepsilon_P)_{ud} \frac{m_\pi^2}{m_\mu(m_d + m_u)} \right| f_\pi , \tag{9.3}$$

and, similarly, the ratio of pion and kaon decays

$$\left(\left| \frac{V_{us}}{V_{ud}} \right| \frac{f_K}{f_\pi} \right)_{\rm exp} = \frac{\left| 1 + \delta V_{us} + (\varepsilon_L)_{us} - \frac{\xi_{us}}{V_{us}} - (\varepsilon_P)_{us} \frac{m_K^2}{m_\mu(m_s+m_u)} \right| |V_{us}| \, f_K}{\left| 1 + \delta V_{ud} + (\varepsilon_L)_{ud} - \frac{\xi_{ud}}{V_{ud}} - (\varepsilon_P)_{ud} \frac{m_\pi^2}{m_\mu(m_d+m_u)} \right| |V_{ud}| \, f_\pi} . \tag{9.4}$$

Analogously, the semileptonic decay $K^0 \to \pi^+ l \nu_l$ receives contributions from δV_{us}, $(\varepsilon_S)_{us}$, and $(\varepsilon_T)_{us}$.

The difficulty in identifying a right-handed current at low energies can be illustrated by looking at the degeneracy with anomalous left-handed currents. By setting the four-fermion couplings to zero but allowing for nonzero values of δV_{ud} and δV_{us}, we obtain significantly weaker constraints on, for example, ξ_{ud}

$$\mathrm{Re}\, \xi_{ud} \in [-1.0, 0.7] \cdot 10^{-2} , \tag{9.5}$$

which is in reach of future collider searches. The bound is determined by the theoretical uncertainty of f_π, which is at the percent level [93]. If we only allow BSM effects in the left- and right-handed currents, ξ_{ud} and δV_{ud} are completely anticorrelated, since the vector combination $|V_{ud} + \xi_{ud}|$ has to satisfy the stringent constraints from superallowed β decays. Introducing additional operators further weakens the bounds on ξ_{ud} and ξ_{us} [187]. Still, in order to not disrupt the agreement between the SM and the data for leptonic and semileptonic decays, strong correlations between the operators in eq. (9.1) must exist, posing non-trivial constraints on models of new physics.

In light of the intrinsic degeneracy of the observables used in section 4, one might ask if there is a more direct way to access RHCCs at low energy. Decay correlations in the neutron and hyperon β decays are particularly sensitive to the Lorentz structure of the quark and lepton coupling [184, 186–189]. For example, the β and neutrino asymmetry in neutron β decay can be expressed as [184, 186]

$$A(E_e) = \frac{2\lambda(1-\lambda)}{1+3\lambda^2} , \qquad B(E_e) = \frac{2\lambda(1+\lambda)}{1+3\lambda^2} . \tag{9.6}$$

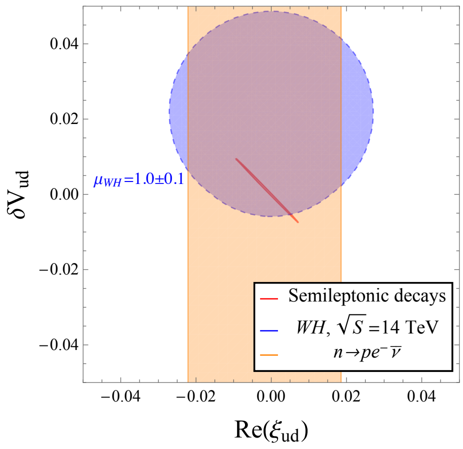

Figure 12. The figure shows the constraints in the $\xi_{ud} - \delta V_{ud}$ plane, after marginalizing over ξ_{us} and δV_{us}. The blue line depicts the constraint from WH production, while the red line indicates the limits from superallowed β decay and leptonic pion decay. The vertical orange band results from the experimental determination of λ, from neutron decay correlations, in combination with an assumed lattice determination of $g_A = 1.27 \pm 0.05$.

In the presence of the most general modification of the semi-leptonic dimension-six Lagrangian [188, 190], we have

$$\lambda = \frac{g_A}{g_V} \left| \frac{1 + \delta V_{ud} + (\varepsilon_L)_{ud} - \frac{\xi_{ud}}{V_{ud}}}{1 + \delta V_{ud} + (\varepsilon_L)_{ud} + \frac{\xi_{ud}}{V_{ud}}} \right| = \frac{g_A}{g_V} \left(1 - 2\mathrm{Re}\left(\frac{\xi_{ud}}{V_{ud}} \right) \right) + \mathcal{O}\left(\frac{v^4}{\Lambda^4} \right), \tag{9.7}$$

where g_V and g_A are the nucleon matrix elements of the vector and axial-vector currents. Experimentally, the ratio g_A/g_V is determined with per mil uncertainties, $\lambda = 1.2723 \pm 0.0023$. In order to constrain ξ_{ud} one needs precise information on g_A. While this is the subject of intense research in LQCD, current determinations of g_A have about a 4-5% uncertainty [140, 185], which allows for percent-level right-handed contributions, as first discussed in ref. [187] . Setting the central value of g_A to 1.27, and assigning a 4% theoretical error, $g_A = 1.27 \pm 0.05$, would result in $\mathrm{Re}\,\xi_{ud} \in [-2.1, 2.0] \cdot 10^{-2}$, in the same range as the values probed by WH production. To illustrate the interplay between the different low-energy and collider constraints, we show in figure 12 the limits in the $\xi_{ud} - \delta V_{ud}$ plane, after marginalizing over ξ_{us} and δV_{us}. As can be seen from the figure, superallowed β decay and $\pi \to \mu\nu$ currently provide the strongest limits. However, as mentioned, these observables get additional contributions from scalar and pseudo-scalar interactions (ε_S and ε_P), and do not uniquely probe RHCCs. The experimental determination of λ combined with lattice calculation of g_A provides a direct low-energy probe of right-handed currents in the ud sector. Currently this leads to a constraint that is comparable to future collider limits.

9.2 Collider probes

In similar fashion we can ask whether a discrepancy in a collider setting could be unambiguously attributed to a RHCC. In this section we focus on observables related to WH productions as this process, as discussed in section 2.2, is particular sensitive to

JHEP05(2017)086

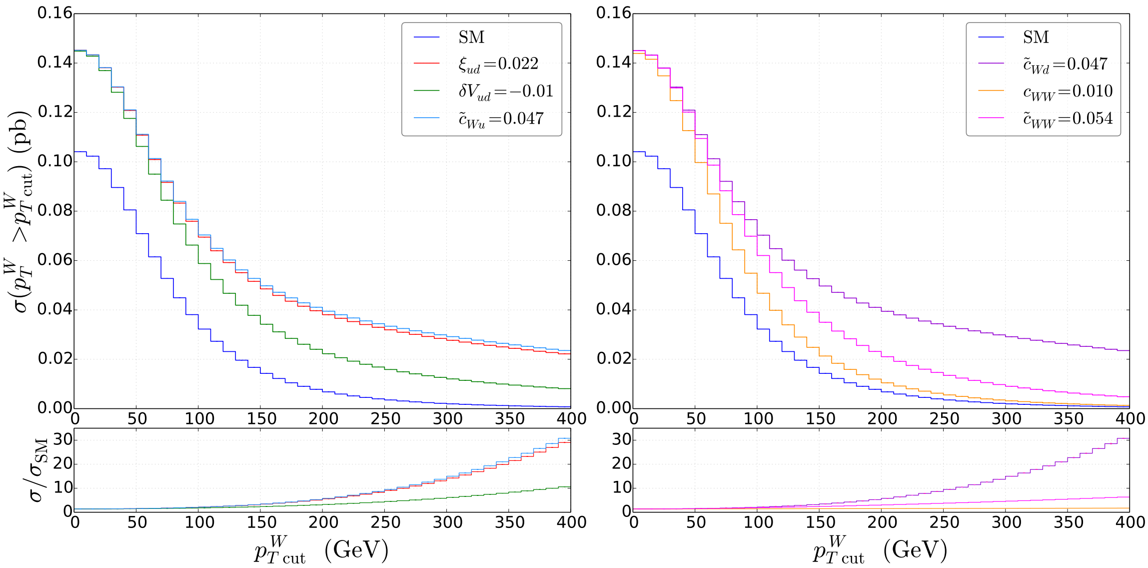

Figure 13. W^+H cross section for $p_T^W > p_{T\,\mathrm{cut}}^W$, at $\sqrt{S} = 14\,\mathrm{TeV}$. The blue line denotes the SM cross section, the remaining lines include the contributions of the operators in eq. (9.10).

right-handed interactions. To address the issue of identifying the ξ operator, we explore observables that could disentangle RHCCs from other BSM contributions. We consider the full set of dimension-six operators that modifies WH production using the basis of ref. [6]

$$\begin{aligned}\mathcal{L}_6 = & \, C_{\varphi W}\varphi^\dagger\varphi W_{\mu\nu}W^{\mu\nu} + C_{\varphi\tilde{W}}\varphi^\dagger\varphi\tilde{W}_{\mu\nu}W^{\mu\nu} \\ & + \varphi^\dagger\tau^I i\overleftrightarrow{D}_\mu\varphi\,\bar{q}_L\tau^I\gamma^\mu c_{Q\varphi}^{(3)}q_L + \varphi^\dagger i\overleftrightarrow{D}_\mu\varphi\,\bar{q}_L\gamma^\mu c_{Q\varphi}^{(1)}q_L \\ & - \frac{g}{\sqrt{2}}\bar{q}_L\sigma^{\mu\nu}\Gamma_W^u\tau^I W_{\mu\nu}^I\tilde{\varphi}\,u_R - \frac{g}{\sqrt{2}}\bar{q}_L\sigma^{\mu\nu}\Gamma_W^d\tau^I W_{\mu\nu}^I\varphi\,d_R \\ & + \frac{2}{v^2}i\tilde{\varphi}^\dagger D_\mu\varphi\,\bar{u}_R\gamma^\mu\,\xi d_R + \text{h.c.}\,, \end{aligned} \tag{9.8}$$

where φ is the Higgs doublet, τ^I are Pauli matrices, $\tilde{\varphi} = i\tau_2\varphi^*$, $W_{\mu\nu}^I$ denotes the SU(2) field strengths, and $\tilde{W}^{\mu\nu} = \varepsilon^{\mu\nu\alpha\beta}W_{\alpha\beta}/2$. The Higgs covariant derivatives are given by

$$\varphi^\dagger i\overleftrightarrow{D}_\mu\varphi = i\varphi^\dagger(D_\mu - \overleftarrow{D}_\mu)\varphi\,, \qquad \varphi^\dagger\tau^I i\overleftrightarrow{D}_\mu\varphi = i\varphi^\dagger(\tau^I D_\mu - \overleftarrow{D}_\mu\tau^I)\varphi\,. \tag{9.9}$$

For fermionic operators we consider couplings to the u and d quarks (the us couplings can be studied in analogous fashion), which, in the mass basis, can be written as

$$\begin{aligned}\mathcal{L} = & \frac{h}{v}\left(c_{WW}W^{\mu\nu}W_{\mu\nu} + \tilde{c}_{WW}\tilde{W}^{\mu\nu}W_{\mu\nu}\right) + \frac{g}{\sqrt{2}}V_{ud}\left(1 + \delta V_{ud}\left(1+\frac{h}{v}\right)^2\right)\bar{u}_L\gamma^\mu d_L W_\mu^+ \\ & + \frac{g}{\sqrt{2}}\xi_{ud}\left(1+\frac{h}{v}\right)^2\bar{u}_R\gamma^\mu d_R W_\mu^+ \\ & - \frac{gV_{ud}}{\sqrt{2}v}\left(1+\frac{h}{v}\right)\left(c_{Wd}\bar{u}_L\sigma^{\mu\nu}d_R + c_{Wu}\bar{u}_R\sigma^{\mu\nu}d_L\right)W_{\mu\nu}^+ + \text{h.c.} \end{aligned} \tag{9.10}$$

The CKM factors in the previous expressions arise from rotating to the mass basis. In order to avoid flavor-changing neutral currents at tree level, we impose that the matrices

JHEP05(2017)086

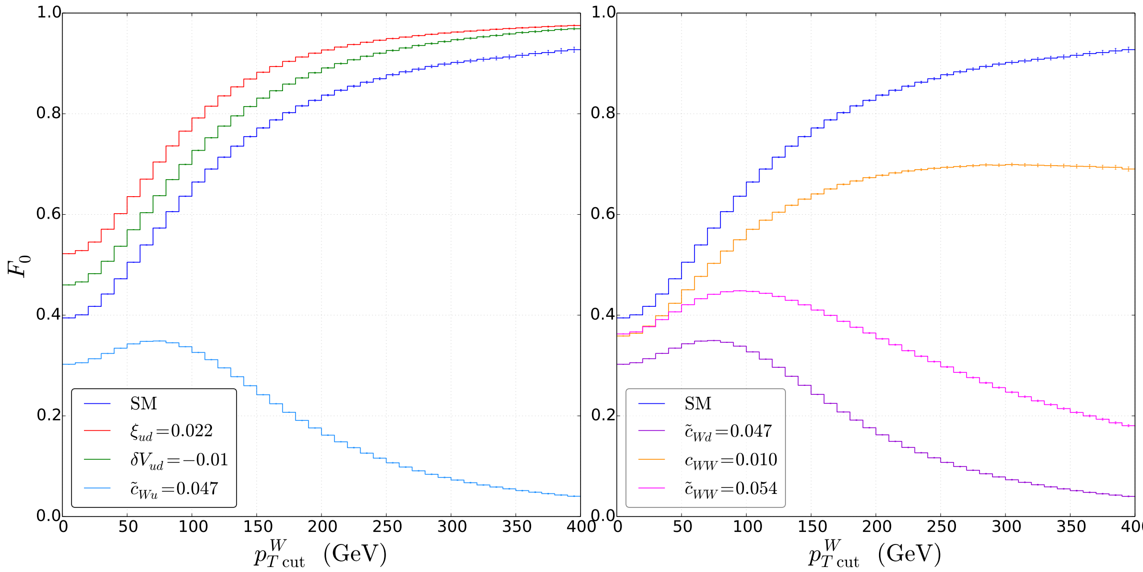

Figure 14. Longitudinal polarization of the W^+ boson in W^+H production as a function of $p^W_{T\,\rm cut}$, at $\sqrt{S} = 14\,\text{TeV}$.

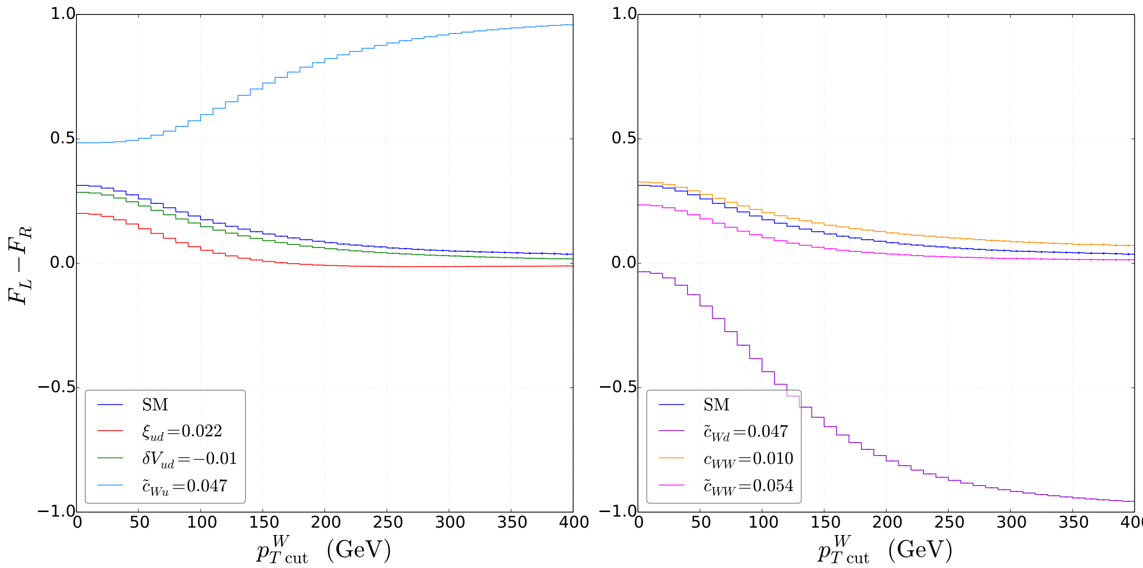

Figure 15. Difference of left and right-handed polarizations of the W^+ boson in W^+H production as a function of $p^W_{T\,\rm cut}$, at $\sqrt{S} = 14\,\text{TeV}$.

Γ^u_W, Γ^d_W, $c^{(1)}_{Q\varphi}$, and $c^{(3)}_{Q\varphi}$ are diagonal in the mass basis. In addition to ξ_{ud} we then need to consider the dimensionless couplings

$$c_{WW} = v^2 C_{\varphi W}\,, \qquad \tilde{c}_{WW} = v^2 C_{\varphi \tilde{W}}\,,$$
$$\delta V_{ud} = \left(v^2 c^{(3)}_{Q\varphi}\right)_{11}, \qquad \tilde{c}_{Wd} = \left(v^2 \Gamma^d_W\right)_{11}, \qquad \tilde{c}_{Wu} = \left(v^2 \Gamma^u_W\right)_{11}. \tag{9.11}$$

These couplings scale as v^2/Λ^2. Hermiticity implies that c_{WW}, $\tilde{c}_{WW}$, and δV_{ud} are real, whereas ξ_{ud}, $\tilde{c}_{Wu}$, and $\tilde{c}_{Wd}$ in general have real and imaginary parts. Since we are neglecting

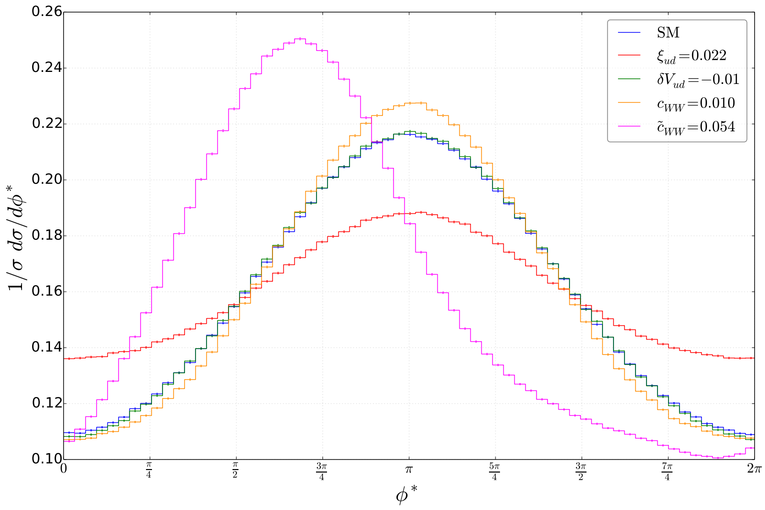

Figure 16. W^+H differential cross section with respect to ϕ^* at $\sqrt{S} = 14\,\text{TeV}$, in the SM (blue line), and in the presence of dimension-six operators.

interference terms proportional to the light quark masses, the cross section only depends on the absolute values of these couplings.

To illustrate the diagnostic power of collider measurements, we set $\xi_{ud} = 0.022$. This value is still allowed by the 8 and 13 TeV data and produces a 40% modification of the signal strength at 14 TeV. We then proceed by turning on one of the couplings in eq. (9.10) at a time, and tune them such that they give the same signal-strength modification as ξ_{ud}. In figure 13 we show the effect of the different couplings on the cumulative W^+H cross section for $p_T^W > p_{T\,\text{cut}}^W$, where p_T^W is the transverse momentum of the W boson. In general this observable receives different corrections from different operators. However, as can be seen from the figure, this observable is not sufficient to lift the degeneracy. In particular, ξ_{ud} and the dipole operators, $\tilde{c}_{Wu}$ and $\tilde{c}_{Wd}$, induce very similar corrections.

A more suitable observable to disentangle the effects of the various BSM contributions is the angular distributions of the charged lepton coming from the decay of the W boson. We work in the W-boson rest frame, with the direction of the z-axis along the momentum of the W boson in the lab frame. θ^* is the polar angle of the charged lepton in this frame. The x-axis is in the direction orthogonal to the Higgs and W momenta $\hat{x} \sim (\vec{p}_W \times \vec{p}_H)$. In this frame, we define the azimuthal angle ϕ^* as the angle between the plane containing the W and the Higgs bosons, and the plane containing the W and its charged decay product. That is

$$\cos\phi^* = \frac{(\vec{p}_W \times \vec{p}_H) \cdot (\vec{p}_W \times \vec{p}_e)}{|\vec{p}_W \times \vec{p}_H|\,|\vec{p}_W \times \vec{p}_e|}\,, \tag{9.12}$$

and we note that ϕ^* is invariant under boosts along the W momentum $\vec{p}_W$.

The angular distribution of the W boson in this frame is parameterized by 8 coefficients, which completely characterize the W-boson spin-density matrix

$$\frac{1}{\sigma}\frac{d\sigma}{d\cos\theta^*\,d\phi^*} = \frac{3}{16\pi}\left[1 + \cos^2\theta^* + \frac{A_0}{2}(1 - 3\cos^2\theta^*)\right.$$

$$+A_1 \sin 2\theta^* \cos\phi^* + \frac{A_2}{2}\sin^2\theta^* \cos 2\phi^*$$
$$+A_3 \sin\theta^* \cos\phi^* + A_4 \cos\theta^* + A_5 \sin\theta^* \sin\phi^*$$
$$+A_6 \sin 2\theta^* \sin\phi^* + A_7 \sin^2\theta^* \sin 2\phi^* \Big] . \quad (9.13)$$

The differential distributions with respect to θ^* and ϕ^* are obtained by integrating eq. (9.13), and are given by

$$\frac{1}{\sigma}\frac{d\sigma}{d\cos\theta^*} = \frac{3}{8}\left[1+\cos^2\theta^* + \frac{A_0}{2}(1-3\cos^2\theta^*) + A_4\cos\theta^*\right], \quad (9.14)$$

$$\frac{1}{\sigma}\frac{d\sigma}{d\phi^*} = \frac{1}{2\pi}\left[1+\frac{3\pi}{16}(A_3\cos\phi^*+A_5\sin\phi^*)+\frac{1}{4}(A_2\cos 2\phi^*+A_7\sin 2\phi^*)\right]. \quad (9.15)$$

The coefficients A_0 and A_4 are related to the W-boson helicity fractions [35],

$$F_0 = \frac{A_0}{2}\,, \qquad F_L = \frac{1}{4}(2-A_0 \mp A_4)\,, \qquad F_R = \frac{1}{4}(2-A_0 \pm A_4)\,, \quad (9.16)$$

for $W^\pm$, respectively.

In figures 14 and 15 we plot the longitudinal, and the difference of the left- and right-handed polarization fractions of the W^+ boson, for $p_T^W > p_{T\,\mathrm{cut}}^W$. We show these quantities for the pure SM and for the SM modified by one of the dimension-six operators in eq. (9.10). For the Wilson coefficients we use the same values as used in figure 13 such that the signal strength at 14 TeV is modified by 40%. As can be glimpsed from the figures, within the SM the W-boson becomes increasingly polarized in the longitudinal direction as the cut on the W transverse momentum increases [191]. This behavior is not significantly affected by a right-handed current, ξ_{ud}, or a gauge-invariant correction to the left-handed current, δV_{ud}. The operator c_{WW} would also preferentially induce a longitudinally polarized W at large $p_{T\,\mathrm{cut}}^W$, but with a smaller fraction.

On the other hand, dipole couplings of the W boson to the up and down quarks would greatly reduce the longitudinal fraction at large p_T. In figure 15 we show that $\tilde{c}_{Wu}$ and $\tilde{c}_{Wd}$ induce, respectively, a left- and right-handed polarized W. Finally, a nonzero value of $\tilde{c}_{WW}$ would also reduce the longitudinal fraction and produce equal amount of left- and right-polarized W bosons at large p_T. The W-boson helicity fractions would therefore make it possible to identify the effects of the dipole interactions, or perhaps of $\tilde{c}_{WW}$, but they would not clearly identify a right-handed current.

We now turn to the azimuthal-angle distribution which does turn out to be sensitive to RHCC. In figure 16 we show the normalized differential cross section with respect to ϕ^*, with no cut on p_T^W, for the SM, and for the operators ξ_{ud}, δV_{ud}, c_{WW}, and $\tilde{c}_{WW}$. In the SM, the cross section is well described by the $\cos\phi^*$ term, with a smaller component proportional to $\cos 2\phi^*$. We observe that the left-handed current, δV_{ud}, does not significantly affect the shape of the ϕ^* distribution. c_{WW} induces a slightly larger $\cos 2\phi^*$ component which only mildly modifies the distribution. ξ_{ud} does not modify the functional form of the distribution, which is proportional to $\cos\phi^*$, but significantly affects the amplitude. This is captured by the coefficient A_3, which we show in the left-panel of figure 17 as a function

JHEP05(2017)086

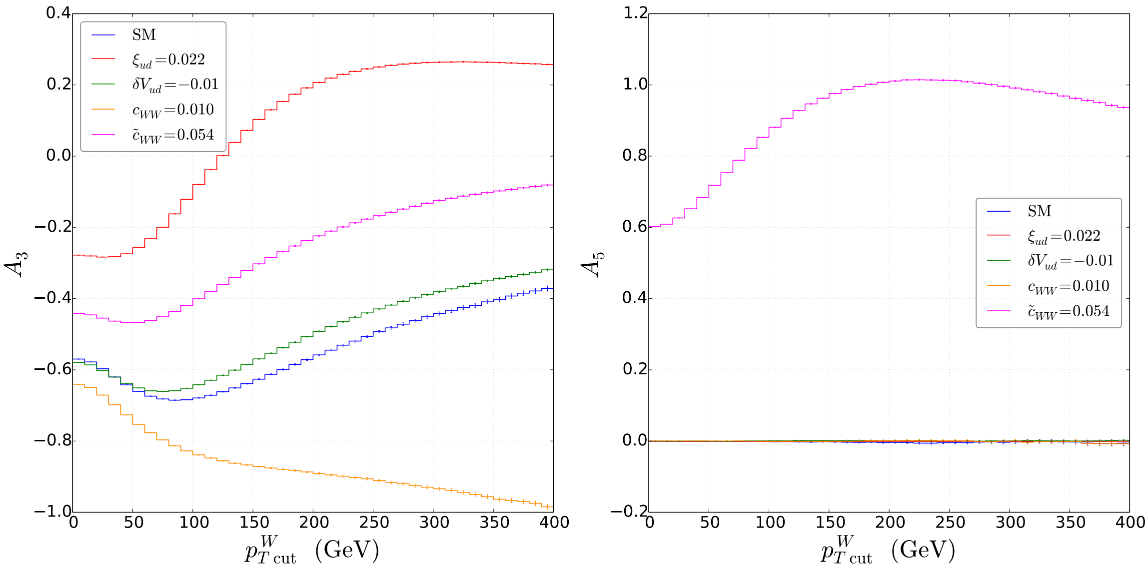

Figure 17. A_3 and A_5 coefficients in W^+H production as a function of $p^W_{T\,\mathrm{cut}}$, at $\sqrt{S} = 14\,\mathrm{TeV}$.

of $p^W_{T\,\mathrm{cut}}$. A_3 vanishes if parity is conserved in the production of the W boson, and, for the chosen value of ξ_{ud}, this effectively occurs at $p^W_{T\,\mathrm{cut}} = 120\,\mathrm{GeV}$. For larger cuts, ξ_{ud} overtakes the SM contribution and the sign of A_3 flips.

Figure 16 shows another interesting feature, namely that $\tilde{c}_{WW}$ induces a $\sin\phi^*$ dependence of the cross section. Differently from all other operators in eq. (9.10), for $\tilde{c}_{WW}$ a CPV interference term with the SM survives. This term does not induce any corrections to the total cross section, but it does induce a large A_5 coefficient as shown in the right-panel of figure 17. Such a signature is a distinctive feature of a $\varphi^\dagger\varphi\tilde{W}W$ operator at the LHC.

This discussion shows that, in the presence of a deviation of the total WH cross section from the SM prediction, a study of the p^W_T spectrum and of angular distributions of the charged lepton produced by W decay, would provide important information in identifying the origin of the discrepancy. We should point out that our preliminary study did not include detector effects, background estimates, nor reconstruction efficiencies and a more careful investigation is warranted. Such an investigation would be better performed within the framework of an experimental collaboration.

9.3 Anomalous Wtb couplings

Analogously to the *ud*-*us* sector it is interesting to see to what extent the constraints in the *tb* sector are affected by turning on additional operators. To explore this, we extend our Lagrangian, involving right-handed (*tb*) currents, with the following set of operators,

$$O_{LL} = \frac{gv^2}{2}\left[\frac{1}{\sqrt{2}}\bar{t}_L\gamma^\mu b'_L W^+_\mu + \frac{1}{\sqrt{2}}\bar{b}'_L\gamma^\mu t_L W^-_\mu + \frac{1}{c_W}Z_\mu \bar{t}_L\gamma^\mu t_L\right]\left(1+\frac{h}{v}\right)^2, \quad (9.17a)$$

$$O_{Wt} = -gm_t\left[\frac{1}{\sqrt{2}}\bar{b}'_L\sigma^{\mu\nu}t_R W^-_{\mu\nu} + \bar{t}_L\sigma^{\mu\nu}t_R\left(\frac{1}{2c_W}Z_{\mu\nu} + igW^-_\mu W^+_\nu\right)\right]\left(1+\frac{h}{v}\right), \quad (9.17b)$$

Real	**Individual**	**Marginalized**	Imaginary	**Individual**	**Marginalized**
ξ_{tb}	$[-1.4, 1.5] \cdot 10^{-3}$	$[-0.01, 0.12]$	ξ_{tb}	$[-2.4, 2.4] \cdot 10^{-3}$	$[-0.16, 0.13]$
δ_{LL}	$[-0.03, 0.04]$	$[-0.03, 0.04]$	–		
$v^2\,C_{Wt}$	$[-0.09, 0.05]$	$[-0.10, 0.04]$	$v^2\,C_{Wt}$	$[-6.0, 6.0] \cdot 10^{-4}$	$[-1.0, 0.9] \cdot 10^{-3}$
$v^2\,C_{Wb}$	$[-0.04, 0.05]$	$[-3.5, 0.4]$	$v^2\,C_{Wb}$	$[-3.5, 3.5] \cdot 10^{-2}$	$[-1.9, 2.2]$

Table 12. Allowed regions (90% C.L.) for the Wtb couplings at the scale $\Lambda = 1\,\text{TeV}$. The second and fifth columns show the constraints under the assumption that only a single coupling is generated at the high scale. In the third and sixth columns we assume that all Wtb couplings in eq. (9.17) are present at the scale of new physics and we marginalize over all couplings.

$$O_{Wb} = -gm_b\left[\frac{1}{\sqrt{2}}\bar{t}'_L\sigma^{\mu\nu}b_R W^+_{\mu\nu} - \bar{b}_L\sigma^{\mu\nu}b_R\left(\frac{1}{2c_W}Z_{\mu\nu} + igW^-_\mu W^+_\nu\right)\right]\left(1+\frac{h}{v}\right), \quad (9.17c)$$

which appear in the Lagrangian with couplings $C_{LL,Wt,Wb}$, respectively. Here, $b' = V_{tb}b + V_{ts}s + V_{td}d$, $t' = V^*_{tb}t + V^*_{cb}c + V^*_{ub}u$, and $c_W = \cos\theta_W$, with θ_W the Weinberg angle. In total, the effective Wtb vertex can then be written as

$$\mathcal{L}_{tb} = \frac{g}{\sqrt{2}}\bar{t}\left[\gamma^\mu\left(V_{tb}(1+\delta_{LL})\,P_L + \xi_{tb}\,P_R\right)W^+_\mu - \sigma^{\mu\nu}W^+_{\mu\nu}\left(m_t C^*_{Wt}P_L + m_b C_{Wb}P_R\right)\right]b + \text{h.c.}\,, \quad (9.18)$$

where[6] $\delta_{LL} = \frac{v^2}{2}C_{LL}$. Eq. (9.18) provides a general parametrization of the Wtb vertex [193] and these couplings have been studied in many previous works [79, 192–205]. Most of these studies constrain the Wtb vertex by looking at collider processes or flavor constraints (in particular $\Delta B = 1$ processes). Here we study the effect of turning on ξ_{tb} and $C_{LL,Wt,Wb}$ simultaneously, while taking into account both collider and low-energy constraints including those from EDM experiments which are usually not considered.

To derive the resulting constraints we require several additions to the expressions discussed in previous sections. In particular, for the $C_{LL,Wb,Wt}$ contributions to the helicity fractions discussed in section 2.4, we employ the expressions given in ref. [79]. We take into account δ_{LL} contributions to single-top production by replacing $V_{tq} \to V_{tq}(1+\delta_{LL})$, where $q \in (d, s, b)$. For the running and matching of $C_{LL,Wt,Wb}$ onto the $C_{7,8}$ operators relevant for $b \to q\gamma$, we use the expressions in refs. [192, 206]. Finally, for the contributions of C_{Wt} and C_{Wb} to EDMs we follow the analysis of refs. [207, 208]. With this combined input we turn on δ_{LL}, ξ_{tb}, and $C_{Wt,Wb}$ simultaneously, while setting $V_{tb} = 1$. The resulting constraints are shown in table 12, together with the bounds that result from a single-coupling analysis.

The constraints on δ_{LL} and C_{Wt} are the least affected by the presence of the other operators, and the marginalized bounds are fairly close to the single-coupling analysis. This can be understood by noticing that δ_{LL} is stringently constrained by single-top production, which does not allow for cancellations against the other couplings. Similarly, $\text{Im}\,C_{Wt}$

[6]Within the framework of the SMEFT, O_{LL} arises from the operators $Q^{(1)}_{Hq}$ and $Q^{(3)}_{Hq}$ in the notation of [42, 43, 80]. We follow ref. [192] and assume no flavor-changing neutral currents at tree level, the Wtb coupling is then hermitian and C_{LL} is forced to be real.

JHEP05(2017)086

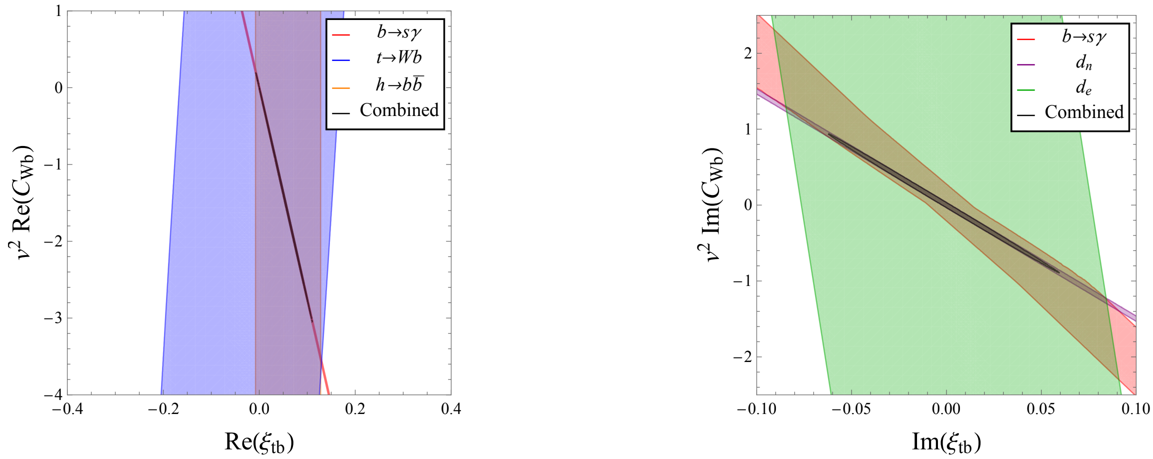

Figure 18. The figure shows the constraints in the $\xi_{tb} - v^2\, C_{Wb}$ plane, illustrating the significant cancellations that can occur between the two couplings. The real (imaginary) couplings are shown in the left (right) panel. The exclusion bands (at 90% C.L.) assume that only C_{Wb} and ξ_{tb} are generated at the scale Λ.

provides the dominant contribution to the electron EDM such that its constraint survives to large extent the global analysis as well. $\mathrm{Re}\, C_{Wt}$ is constrained by several observables with similar strength (electroweak precision tests, W helicity fractions, and $b \to s\gamma$, see ref. [208]) such that the marginalized constraint is not too different from the individual one.

The situation is significantly different for C_{Wb} and ξ_{tb}. In the single-coupling analysis the real parts of these couplings are mainly constrained by $b \to s\gamma$, while their imaginary parts are constrained by the neutron EDM. When both operators are present the constraints on the real and imaginary parts can be weakened significantly by mutual cancellations in $\mathrm{BR}(b \to s\gamma)$ and d_n, respectively. In fact, comparing the second (fifth) and third (sixth) columns of table 12 we see that the limits on the real (imaginary) part of ξ_{tb} deteriorate by roughly two orders of magnitude. The bounds are similarly weakened for C_{Wb}.

This effect is illustrated in figure 18, where we show the constraints in the $\xi_{tb} - C_{Wb}$ plane for the real and imaginary parts. The results in this figure assumes only ξ_{tb} and C_{Wb} to be present at the scale Λ, but this is sufficient to see that significant cancellations can occur between these two couplings. The left-panel shows that the CP-even $b \to s\gamma$ observables allow for a free direction, and the much weaker limits from the helicity fractions and $h \to b\bar{b}$ are needed to obtain a constraint. In the case of the imaginary parts, shown in the right panel, the neutron EDM allows for a free direction and the electron EDM is needed to obtain a bound. As can be seen from table 12, including C_{Wt} and δ_{LL} hardly affects the bounds on the real parts of ξ_{tb} and C_{Wb} compared to figure 18. The limits on the imaginary parts are weakened by a minor factor compared to figure 18, confirming that the major deterioration between the single-coupling and global constraints are indeed due to cancellations between ξ_{tb} and C_{Wb}. A comparison of the single-coupling and global constraints for the $\mathrm{Re}\, \xi_{tb}$–$\mathrm{Im}\, \xi_{tb}$ plane is shown in figure 19. Again, it is clear that turning on several couplings can severely weaken the various constraints.

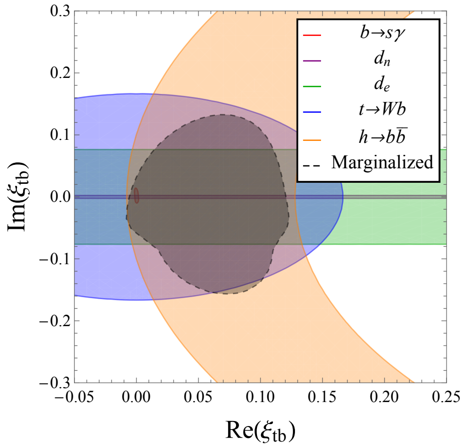

Figure 19. The figure shows the constraints in the $\mathrm{Re}\,\xi_{tb} - \mathrm{Im}\,\xi_{tb}$ plane. The constraints from $b \to s\gamma$, d_n, d_e, the helicity fractions, and $h \to b\bar{b}$ are shown in red, purple, green, blue, and orange, respectively, and assume that only ξ_{tb} is generated at the scale Λ. The dashed black line is the resulting constraint when marginalizing over the other tb couplings.

In summary, in the tb sector isolating the right-handed current is complicated by the degeneracy with the C_{Wb} dipole operator. Nevertheless, as shown in table 9.3, the marginalized constraints on most of the anomalous Wtb operators are very stringent.

10 Conclusion

Motivated by the attractive possibility of parity restoration at high energies, we investigated possible footprints left behind by a right-handed extension of the SM. We studied in detail the right-handed charged-current couplings ξ_{ij} defined in eq. (1.1), looking at their manifestations in collider experiments, flavor physics, and low-energy precision tests.

Our work provides a case study of the complementarity of low-energy and collider experiments in probing heavy new physics which is not within direct reach of the LHC, and therefore can be analyzed in the framework of the SMEFT.

In a first major thrust of our work, assuming that at the scale Λ the SM is modified dominantly by the RHCC operator, we have worked out the bounds on the ξ_{ij} from a broad range of probes. The resulting 90% C.L. limits are summarized in eqs. (2.27) (collider) and (8.1), (8.2) (global fit). A graphical summary is presented in figure 10. Note that in this setup one can straightforwardly compare the sensitivity of various direct and indirect probes both at high and low energy. Such a comparison reveals that low-energy probes provide the strongest constraints, putting most of the ξ_{ij} out of LHC sensitivity reach.

The above results, however, should be put in a broader context. Since most explicit models of new physics generate more than one class of operators at the UV-matching scale Λ, many of the observables used in our analysis would receive contributions form several other dimension-six operators in the SMEFT. Therefore, in a more general setting, the low-energy constraints require that certain linear combinations of dimension-six Wilson coefficients (including the ξ_{ij}) be highly constrained, which in turn imposes non-trivial constraints on new physics scenarios. Realizing this, in a second thrust of our work we have explored: (i) the impact of degeneracies on the ξ_{ij}, finding that the low-energy bounds can be weakened to a level comparable to the collider sensitivity by turning on additional operators; (ii) ways to remove this degeneracy, identifying observables that would uniquely point to RHCC, both at collider and low-energy. Details can be found in section 9, with focus on the couplings ξ_{ud}, ξ_{us}, and ξ_{tb}. Our analysis shows the importance of pursuing improved searches of ξ_{ij} manifestations at both the energy and precision frontiers, and suggests new handles on RHCC at colliders.

We conclude by listing the main highlights of our analysis:

- Keeping in mind the significant theoretical uncertainties, we note that the introduction of appropriate ξ_{ij} elements can help resolve some tensions between data and SM predictions in flavor physics, such as ϵ'/ϵ [11] and the inclusive-exclusive discrepancy in V_{ub} and V_{cb} [209, 210].

- In the framework of the linearly realized SMEFT, the most stringent collider constraint on the light elements ξ_{ij}, with $i \in \{u, c\}$ and $j \in \{d, s, b\}$, come from the associated production of a Higgs and a W boson, followed by W production and Higgs production via vector boson fusion. The right-handed charged-current operator ξ also affects WZ production, which, at the moment, provides somewhat weaker bounds.

- Nucleon beta decay, and leptonic and semileptonic decays of pion, kaons, and D mesons allow one to obtain strong bounds on the elements ξ_{ud}, ξ_{us}, ξ_{cd}, and ξ_{cs}. Under the assumption that the SM is modified solely by the RHCC operator ξ, the low-energy bounds put on ξ_{ud} and ξ_{us} are out of the collider reach, while in the case of ξ_{cd} and ξ_{cs} improved constraints from the LHC Run II can compete with low-energy bounds. If we allow for modifications to the couplings of left-handed quarks to the W boson, or for additional semileptonic operators, the single coupling bounds on ξ_{ud} can be weakened to the percent level, see figure 12, making it important to look for collider constraints on this coupling.

- To this end, we identified differential distributions in WH production which are very sensitive to the Lorentz structure of the coupling of the light quarks to the W boson. In the presence of a deviation from the SM expectations, these distributions could help identify the possible origin of the correction, disentangling RHCC interactions from other possible modifications of the WH process (see for example figure 16).

- At colliders, it is hard to probe ξ_{ub} and ξ_{cb} at a level comparable to the one achievable in exclusive and inclusive B decays. Possible strategies might involve tagging b jets in WH and VBF, but in both cases it would remain hard to access values of ξ_{ub} and ξ_{cb} smaller than the corresponding CKM elements. We observe that, even including flavor observables, the bounds on ξ_{ub} and ξ_{cb} are not extremely strong. In light of this, a more detailed study of RH contributions to inclusive B-meson decays might be appropriate. Such a study might also resolve whether RHCCs can explain the current tension between the determinations from exclusive and inclusive B decays.

JHEP05(2017)086

- The collider observables that are needed to constrain the third row of the ξ matrix are single-top production, top decays, with particular attention to the W polarization in the decay, and $h \to b\bar{b}$. It is quite interesting that the loop process $h \to b\bar{b}$ already probes ξ_{tb} at a level comparable to top decays.

- Right-handed currents in the top sector are, however, severely constrained by $B \to X_{s,d}\gamma$ and EDMs. In a single-coupling analysis, the limits are two to three orders of magnitude stronger than collider limits, and are not severely weakened by turning on ξ_{td}, ξ_{ts}, and ξ_{tb} at the same time. The collider limits become relevant only if we allow for more general modifications of the Wtb vertex. In section 9.3 we therefore performed a global analysis, including all relevant low- and high-energy experiments, of the most general modification of the Wtb interactions. In such a scenario, ξ_{tb} and C_{Wb} are strongly correlated (see figure 18) and the resulting limits are significantly softened. Our analysis extends those based on subsets of the available data, see e.g. refs. [196, 197, 205], and reflects the relevance of low-energy precision experiments.

- Despite the large theoretical uncertainties, limits on EDMs provide strong constraints on the imaginary parts of many ξ elements and even on some of the real parts because of the interplay with imaginary parts of certain CKM elements. Improvements of hadronic and nuclear theory could further strengthen the constraining power of EDM experiments as can be seen from figure 10. In the ideal case of negligible theoretical uncertainties, EDM experiments would set the strongest constraints on all imaginary parts (except for $\mathrm{Im}\,\xi_{bc}$), reaching the $\mathcal{O}(10^3\,\mathrm{TeV})$ scale for $\mathrm{Im}\,\xi_{ud}$, and the real parts of ξ_{ub}, ξ_{cd}, and ξ_{td}.

Acknowledgments

SA acknowledges support by the COFUND Fellowship under grant agreement PCOFUND-GA-2012-600377. VC and EM acknowledge support by the US DOE Office of Nuclear Physics and by the LDRD program at Los Alamos National Laboratory. WD and JdV acknowledge support by the Dutch Organization for Scientific Research (NWO) through a RUBICON and VENI grant, respectively. We thank Paolo Gambino for discussion on the inclusive decays $B \to X_c l\nu$ and for providing us his code for the evaluation of the leptonic moments of the inclusive decay distribution. We thank Mikolaj Misiak for providing us the generalization of the anomalous dimension (3.10) to generic values of the charges Q_u and Q_d. We acknowledge several useful discussions with Zoltan Ligeti, Giuseppe Cerati, Andreas Crivellin, Ivo van Vulpen, and Marc de Beurs. We thank U. Egede, M. González-Alonso, and N. Yamanaka for comments on the manuscript.

A Additional input for CKM fits

In this appendix we discuss several processes that get small contributions from RHCCs, but that were used in the fits discussed in section 8 to constrain the SM CKM elements. In appendix A.1 we discuss $B \to J/\psi K$, which determines the CKM angle β. RHCC in the

Wbc vertex contribute to this observable at tree level, but, as we will argue, the contribution is suppressed with respect to the SM. The remaining elements of the ξ_{ij} matrix generate no or small contributions, after taking into account the limits from other observables.

In appendix A.2 we discuss the FCNC decays $B_q \to \mu^+\mu^-$, $K_L \to \pi^0\nu\nu$, and the penguin contributions to $K_L \to \pi^0 e^+e^-$. These contributions are quadratic in ξ and necessarily involve two different ξ elements. Thus, they do not play any role in a single coupling analysis. Finally, in appendix A.3 we discuss $\Delta F = 2$ processes. Also in this case, contributions are quadratic in ξ. Both types of processes might play a more important role in a global analysis involving all ξ_{ij} couplings, as possible cancellations may allow for larger values of the ξ_{ij} couplings. However, this is beyond the scope of the current work, and we neglect all dimension-eight effects discussed in these appendices.

A.1 $B \to J/\psi K$

The CKM angle $\beta = \arg\big(-\frac{V_{cd}V_{cb}^*}{V_{td}V_{tb}^*}\big)$ is determined from $S_{J/\psi K}$ which appears in the CP asymmetry,

$$\frac{\Gamma(\bar{B} \to J/\psi K) - \Gamma(B \to J/\psi K)}{\Gamma(\bar{B} \to J/\psi K) + \Gamma(B \to J/\psi K)} = S_{J/\psi K}\sin(\Delta m_d t) + C_{J/\psi K}\cos(\Delta m_d t)\,. \tag{A.1}$$

Here

$$S_{J/\psi K} = \frac{2\mathrm{Im}\lambda_{J/\psi K}}{1+|\lambda_{J/\psi K}|^2}, \qquad \lambda_{J/\psi K} = \frac{q}{p}\frac{\bar{A}_{J/\psi K}}{A_{J/\psi K}} = \frac{V_{tb}^* V_{td}}{V_{tb}V_{td}^*}\frac{\bar{A}_{J/\psi K}}{A_{J/\psi K}}\,, \tag{A.2}$$

where the ratio $\frac{q}{p} = \frac{V_{tb}^* V_{td}}{V_{tb}V_{td}^*}$ is due to the $\bar{B}-B$ mixing and $A_{J/\psi K}$ ($\bar{A}_{J/\psi K}$) is the amplitude for the decay $B \to J/\psi K$ ($\bar{B} \to J/\psi K$). In the SM, this amplitude is due to a tree-level decay (proportional to $V_{cb}V_{cs}^*$) followed by $\bar{K}-K$ mixing (the real part of which is dominated by a term proportional to $V_{cs}V_{cd}^*$), such that to good approximation we have,

$$\frac{\bar{A}_{J/\psi K}}{A_{J/\psi K}} = \frac{V_{cb}V_{cd}^*}{V_{cb}^* V_{cd}}\,, \qquad S_{J/\psi K} = \sin 2\beta\,. \tag{A.3}$$

The experimental value is given by [71],

$$S_{J/\psi K} = 0.682 \pm 0.019\,. \tag{A.4}$$

RHCCs can contribute to this observable through the amplitude, $A_{J/\psi K}$, or through B or K mixing. As discussed in appendix A.3, the RHCC contributions to meson mixing are quadratic in ξ, and we neglect them here. The RHCC contributions to the amplitude can arise from ξ_{cs} and ξ_{cb}. The constraints on ξ_{cs} from semileptonic D and D_s decays imply that the contribution to $S_{J/\psi K}$ is at the percent level and therefore negligible. As for ξ_{cb}, the corrections to $S_{J/\psi K}$ are proportional to ξ_{cb}/V_{cb} and to ratios of the matrix elements of the left-right and SM operators, $\mathcal{O}^{cb\,cs}_{1,2\,LR}$ and $\mathcal{O}^{cb\,cs}_{1,2\,LL}$. In this case, inclusive and exclusive B decays into charmed final states and $B_q-\bar{B}_q$ oscillations allow for relatively large values of $\mathrm{Im}(\xi_{cb})/V_{cb}$, $\mathrm{Im}(\xi_{cb})/V_{cb} \sim 0.3$. For exclusive B decays into s-wave charmonia, it was shown that the matrix elements factorize [211–213]. In particular, in the case of the left-right operators, one has to estimate the matrix element $\langle J/\psi|\bar{c}_L c_R|0\rangle$. While a precise evaluation

JHEP05(2017)086

is difficult, we notice that both in the nonrelativistic and in the $m_c \to 0$ limit, the matrix element vanishes at leading order. We therefore expect the corrections to $A_{J/\psi K}$ to be relatively small. Since the suppression factors in the two limits, the relative velocity of the charm quarks in the J/ψ or the ratio $m_{J/\psi}/m_B$, are not extremely small, it might nonetheless be worthwhile to more rigorously investigate RHCC contributions to $B \to J/\psi K$.

A.2 $\Delta F = 1$ neutral current decays

The effective Hamiltonian for $B^0_{s,d} \to \mu^+\mu^-$, $K_L \to \mu^+\mu^-$, $K_L \to \pi^0 e^+e^-$ and $K_L \to \pi^0\nu\nu$ contains the semileptonic operators

$$\mathcal{H} = -\frac{G_F^2 m_W^2}{16\pi^2}\Big\{C^{ij}_{LV}\,\bar{d}^j\gamma^\mu P_L d^i\,\bar{l}\gamma_\mu l + C^{ij}_{RV}\,\bar{d}^j\gamma^\mu P_R d^i\,\bar{l}\gamma_\mu l + C^{ij}_{Lll}\,\bar{d}^j\gamma^\mu P_L d^i\,\bar{l}\gamma_\mu P_L l \tag{A.5}$$
$$+C^{ij}_{Rll}\,\bar{d}^j\gamma^\mu P_R d^i\,\bar{l}\gamma_\mu P_L l + C^{ij}_{L\nu\nu}\,\bar{d}^j\gamma^\mu P_L d^i\,\bar{\nu}\gamma_\mu P_L\nu + C^{ij}_{R\nu\nu}\,\bar{d}^j\gamma^\mu P_R d^i\,\bar{\nu}\gamma_\mu P_L\nu\Big\}.$$

The matching coefficients at the scale $\mu = m_W$ are obtained by computing penguin and box diagrams, and, for $i \neq j$, we find in the $\overline{\text{MS}}$ scheme

$$\begin{aligned}
C^{ij}_{LV} &= V^*_{tj}V_{ti}s_w^2\left\{\frac{8(8-50x_t+63x_t^2+6x_t^3-24x_t^4)}{9(x_t-1)^4}\log x_t\right.\\
&\qquad\left.+\frac{4x_t(108-259x_t+163x_t^2-18x_t^3)}{9(x_t-1)^3}\right\},\\
C^{ij}_{RV} &= \xi^*_{tj}\xi_{ti}s_w^2\left\{\frac{32}{3}(2-3x_t)\log\frac{\mu^2}{m_W^2}+\frac{8(8-14x_t-81x_t^2+222x_t^3-168x_t^4+36x_t^5)}{9(x_t-1)^4}\log x_t\right.\\
&\qquad\left.-\frac{4(-320+528x_t+141x_t^2-493x_t^3+162x_t^4)}{27(x_t-1)^3}\right\}\\
&\quad-\left(\frac{1472}{27}-\frac{256}{9}\log\frac{\mu^2}{m_W^2}\right)s_w^2(\xi^*_{cj}\xi_{ci}+\xi^*_{uj}\xi_{ui}),\\
C^{ij}_{Lll} &= V^*_{tj}V_{ti}\left\{\frac{12x_t^2}{(x_t-1)^2}\log x_t+\frac{4x_t(x_t-4)}{x_t-1}\right\},\\
C^{ij}_{Rll} &= \xi^*_{tj}\xi_{ti}\left\{4(-3+4x_t)\log\frac{\mu^2}{m_W^2}-\frac{4x_t(10-11x_t+4x_t^2)}{(x_t-1)^2}\log x_t+4\frac{4-4x_t+3x_t^2}{x_t-1}\right\}\\
&\quad-\left(16+12\log\frac{\mu^2}{m_W^2}\right)(\xi^*_{cj}\xi_{ci}+\xi^*_{uj}\xi_{ui}),\\
C^{ij}_{L\nu\nu} &= V^*_{tj}V_{ti}\left\{-12\frac{x_t(x_t-2)}{(1-x_t)^2}\log x_t-4x_t\frac{2+x_t}{x_t-1}\right\},\\
C^{ij}_{R\nu\nu} &= \xi^*_{tj}\xi_{ti}\left\{4(3-4x_t)\log\frac{\mu^2}{m_W^2}+4x_t\frac{4-11x_t+4x_t^2}{(1-x_t)^2}\log x_t+4\frac{2+4x_t-3x_t^2}{x_t-1}\right\}\\
&\quad-\left(8-12\log\frac{\mu^2}{m_W^2}\right)(\xi^*_{cj}\xi_{ci}+\xi^*_{uj}\xi_{ui}),
\end{aligned}\tag{A.6}$$

where we neglected powers of x_c and x_u and we used unitarity for the SM contributions.

Of the above operators, C^{bq}_{Lll} and C^{bq}_{Rll} contribute to $B^0_{s,d} \to l^+l^-$ and $K_L \to \mu^+\mu^-$. The photon penguins C^{ij}_{LV} and C^{ij}_{RV} do not contribute due to vector current conservation.

JHEP05(2017)086

The decay rate is

$$\Gamma(B_q^0 \to l^+ l^-) = \frac{1}{32\pi}\sqrt{1-\frac{4m_l^2}{m_{B_q}^2}}\, m_{B_q} f_{B_q}^2 m_l^2 \left(\frac{G_F^2 m_W^2}{16\pi^2}\right)^2 \left|C^{bq}_{L\,ll} - C^{bq}_{R\,ll}\right|^2 , \tag{A.7}$$

where the minus sign between the Wilson coefficients is due to the fact that only the axial part of the quark current contributes. The observed branching ratios for $B_{d,s} \to \mu^+\mu^-$ are [101]

$$\mathrm{BR}(B_d^0 \to \mu^+\mu^-) = \left(3.9^{+1.6}_{-1.4}\right)\cdot 10^{-10}, \qquad \mathrm{BR}(B_s \to \mu^+\mu^-) = \left(2.8^{+0.7}_{-0.6}\right)\cdot 10^{-9}. \tag{A.8}$$

From eq. (A.6) one sees that RHCC contributions to these processes are relevant if $\xi^*_{tb}\xi_{tq} \sim V^*_{tb}V_{tq}$. As discussed in section 8, this possibility is ruled out by $B \to X_{s,d}\gamma$, even when all ξ_{tj} are turned on at the same time. Similarly, the RHCC contributions to $K_L \to \mu^+\mu^-$ are small after taking into account limits from semileptonic decays and $B \to X_q\gamma$. In our analysis we therefore only use $\mathrm{BR}(B^0_{s,d} \to \mu^+\mu^-)$ to constrain the CKM elements V_{ts} and V_{td}.

$C^{sd}_{L\,\nu\nu}$ and $C^{sd}_{R\,\nu\nu}$ contribute to the decay $K_L \to \pi^0\nu\bar{\nu}$. The contributions of the SM and RHCC are of similar size if $\mathrm{Im}\,(\xi^*_{ts}\xi_{td}) \sim \mathrm{Im}(V^*_{ts}V_{td}) \sim 10^{-4}$, which is ruled out by EDMs, and by the branching ratio and CP asymmetry in $B \to X_{s,d}\gamma$. Therefore, this channel might become interesting only in scenarios in which multiple operators are turned on at the same time.

The operators C^{sd}_{LV} and $C^{sd}_{L\,\mu\mu}$ give the leading SM contribution to $K_L \to \pi^0 e^+ e^-$. They are related to the operators C_{7V} and C_{7A} defined in ref. [85] by

$$C_{7V} = \frac{\alpha_{\rm em}}{32\pi s_w^2}\left(C^{ds}_{LV} + \frac{C^{ds}_{L\,\mu\mu}}{2}\right), \qquad C_{7A} = -\frac{\alpha_{\rm em}}{64\pi s_w^2}\, C^{ds}_{L\,\mu\mu}\,. \tag{A.9}$$

C_{7A} does not run, while C_{7V} mixes with tree-level charged currents. Factoring out a factor of $\alpha_{\rm em}/2\pi$, the authors of ref. [85] define the couplings

$$\tilde{y}_{7V}(\mu) = P_0(\mu) - 4\left(C_0(x_t) + \frac{1}{4}D_0(x_t)\right) + \frac{Y_0(x_t)}{s_w^2}, \qquad \tilde{y}_{7A} = -\frac{Y_0(x_t)}{s_w^2}\,, \tag{A.10}$$

with

$$\begin{aligned} Y_0(x_t) &= \frac{x_t}{8}\left(\frac{4-x_t}{1-x_t} + \frac{3x_t}{(1-x_t)^2}\log x_t\right), \\ C_0(x_t) &= \frac{x_t}{8}\left(\frac{x_t-6}{x_t-1} + \frac{3x_t+2}{(1-x_t)^2}\log x_t\right), \\ D_0(x_t) &= -\frac{4}{9}\log x_t + \frac{-19x_t^3+25x_t^2}{36(x_t-1)^3} + \frac{x_t^2(5x_t^2-2x_t-6)}{18(1-x_t)^4}\log x_t\,, \end{aligned} \tag{A.11}$$

where $x_t = m_t^2/m_W^2$. Without resummation, $P_0 = -4/9\log x_c$. The value of $P_0(\mu)$ at different scales is given in ref. [85].

A.3 $\Delta F = 2$ processes

The effective Hamiltonian for $\Delta S = 2$ processes in the presence of a RHCC is given by [214]

$$\mathcal{H}^{\text{eff}} = \frac{G_F^2 m_W^2}{16\pi^2} \sum C_i(\mu)\mathcal{O}_i(\mu), \tag{A.12}$$

with

$$\begin{aligned}
\mathcal{O}_1^{\text{VLL}} &= (\bar{s}\gamma_\mu\, P_L d)\,(\bar{s}\gamma^\mu\, P_L d), & \mathcal{O}_1^{\text{VRR}} &= (\bar{s}\gamma_\mu\, P_R d)\,(\bar{s}\gamma^\mu\, P_R d),\\
\mathcal{O}_1^{\text{LR}} &= (\bar{s}\gamma_\mu\, P_L d)\,(\bar{s}\gamma^\mu\, P_R d), & \mathcal{O}_2^{\text{LR}} &= (\bar{s}P_L d)\,(\bar{s}P_R d),\\
\mathcal{O}_1^{\text{SLL}} &= (\bar{s}P_L d)\,(\bar{s}P_L d), & \mathcal{O}_1^{\text{SRR}} &= (\bar{s}P_R d)\,(\bar{s}P_R d),\\
\mathcal{O}_2^{\text{SLL}} &= (\bar{s}\sigma^{\mu\nu}P_L d)\,(\bar{s}\sigma_{\mu\nu}P_L d) & \mathcal{O}_2^{\text{SRR}} &= (\bar{s}\sigma^{\mu\nu}P_R d)\,(\bar{s}\sigma_{\mu\nu}P_R d)\,.
\end{aligned} \tag{A.13}$$

An analogous Hamiltonian can be written for $\Delta B = 2$ and $\Delta C = 2$ processes.

The coefficients C_i are obtained by computing the box diagrams with two W exchanges, for which we find in the $\overline{\text{MS}}$ scheme

$$\begin{aligned}
C_1^{\text{VLL}} &= V_{is}^* V_{id} V_{js}^* V_{jd} \left((6 - x_i - x_j) \log \frac{\mu^2}{m_W^2} + f_1(x_i, x_j) \right),\\
C_1^{\text{LR}} &= 2 V_{is}^* V_{id} \xi_{js}^* \xi_{jd} \left((6 - x_i - x_j) \log \frac{\mu^2}{m_W^2} + f_2(x_i, x_j) \right),\\
C_2^{\text{LR}} &= 2 \frac{m_i m_j}{m_W^2}\, \xi_{is}^* V_{id} V_{js}^* \xi_{jd} \left(-4 \log \frac{\mu^2}{m_W^2} + f_3(x_i, x_j) - 4\delta_{u,c}^i \delta_{u,c}^j\, g(x_i, x_j) \right),\\
C_1^{\text{SLL}} &= \frac{m_i m_j}{m_W^2}\, \xi_{is}^* V_{id} \xi_{js}^* V_{jd} \left(-4 \log \frac{\mu^2}{m_W^2} + f_3(x_i, x_j) - 4\delta_{u,c}^i \delta_{u,c}^j\, g(x_i, x_j) \right),\\
C_1^{\text{SRR}} &= \frac{m_i m_j}{m_W^2}\, V_{is}^* \xi_{id} V_{js}^* \xi_{jd} \left(-4 \log \frac{\mu^2}{m_W^2} + f_3(x_i, x_j) - 4\delta_{u,c}^i \delta_{u,c}^j\, g(x_i, x_j) \right),\\
C_2^{\text{SLL}} &= \frac{m_i m_j}{m_W^2}\, \xi_{is}^* V_{id} \xi_{js}^* V_{jd} \left(f_4(x_i, x_j) - \delta_{u,c}^i \delta_{u,c}^j\, g(x_i, x_j) \right),\\
C_2^{\text{SRR}} &= \frac{m_i m_j}{m_W^2}\, V_{is}^* \xi_{id} V_{js}^* \xi_{jd} \left(f_4(x_i, x_j) - \delta_{u,c}^i \delta_{u,c}^j\, g(x_i, x_j) \right),
\end{aligned} \tag{A.14}$$

where $i = u, c, t$ and $j = u, c, t$ label the internal up-type quark, and a summation over i, j is understood. m_i, m_j are the masses of the internal up-type quarks, and $x_i = m_i^2/m_W^2$. The loop functions are

$$\begin{aligned}
f_1(x_i, x_j) &= -\frac{x_j^2(4 - 8x_j + x_j^2)}{(x_i - x_j)(-1 + x_j)^2} \log(x_j) + \frac{x_i^2(4 - 8x_i + x_i^2)}{(-1 + x_i)^2(x_i - x_j)} \log x_i\\
&\quad +2 - \frac{3}{2}(x_i + x_j) - \frac{3(x_i + x_j - x_i x_j)}{(1 - x_i)(1 - x_j)},\\
f_2(x_i, x_j) &= -\frac{(-4 + x_j)^2 x_j^2}{(x_i - x_j)(x_j - 1)^2} \log(x_j) - \frac{(-4 + x_i)^2 x_i^2}{(-1 + x_i)^2(-x_i + x_j)} \log x_i\\
&\quad +14 - \frac{3}{2}(x_i + x_j) + 9 \frac{x_i + x_j - x_i x_j}{(1 - x_i)(1 - x_j)},
\end{aligned}$$

$$
\begin{aligned}
f_3(x_i,x_j) &= -\frac{4x_j(4-2x_j+x_j^2)}{(x_i-x_j)(-1+x_j)^2}\log x_j + \frac{4x_i(4-2x_i+x_i^2)}{(-1+x_i)^2(x_i-x_j)}\log x_i, \\
&\quad +\frac{4(2+x_i+x_j-x_ix_j)}{(-1+x_i)(-1+x_j)}, \\
f_4(x_i,x_j) &= \frac{2(-2+x_j)x_j}{(x_i-x_j)(-1+x_j)^2}\log x_j + \frac{2(-2+x_i)x_i}{(-1+x_i)^2(-x_i+x_j)}\log x_i \\
&\quad +\frac{2}{(-1+x_i)(-1+x_j)}\,.
\end{aligned} \tag{A.15}
$$

The remaining function, $g(x_i, x_j)$, arises from the matching contributions in the theory below $\mu = m_W$, which is why it does not receive contributions from diagrams involving the top quark. Up to $\mathcal{O}(x_u, x_c)$ corrections, it is given by,

$$
g(x_i,x_j) = -4\left(1+\log\frac{\mu^2}{m_W^2} - \frac{x_i\log x_i - x_j\log x_j}{x_i-x_j}\right)\,. \tag{A.16}
$$

We verified that the expressions in eq. (A.14) are gauge independent. Our results are in agreement with ref. [215], except that we find matching contributions to $C_2^{\rm LR}$, $C_2^{\rm SLL}$ and $C_2^{\rm SRR}$, which are not given in ref. [215], and we do not assume unitarity of the ξ_{ij} matrix. Most expressions in eq. (A.14) are UV divergent. For the SM coefficient $C_1^{\rm VLL}$ the unitarity of the CKM guarantees that after summing over i, j the divergence cancels. In all other cases, the divergence indicates mixing of two insertions of RHCC onto $\Delta F = 2$ four-fermion operators between the high-energy scale, Λ, and m_W. The QCD running of the operators in eq. (A.13) below the scale m_W is discussed in detail in ref. [214].

A.3.1 $B - \bar{B}$ oscillations

The Hamiltonian in eq. (A.12) can be used to compute the mass difference between mass eigenstates in the $B^0_{d,s}$-$\overline{B}^0_{d,s}$ systems

$$
\Delta m_q = 2|M_{12}^{(q)}| = \frac{|\langle \bar{B}^0_q|\mathcal{H}^{\rm eff}|B^0_q\rangle|}{m_{B_q}} = \left(\frac{G_F^2 m_W^2}{16\pi^2}\right)\frac{1}{m_{B_q}}\left|\sum_i C_i(\mu)\,\langle \bar{B}^0_q|\mathcal{O}_i|B^0_q\rangle\right|. \tag{A.17}
$$

The matrix elements for the operators in the basis (A.13) have been computed on the lattice in ref. [216], and we have

$$
\langle \bar{B}^0_q|\mathcal{O}_1^{\rm VLL}|B^0_q\rangle = \langle \bar{B}^0_q|\mathcal{O}_1^{\rm VRR}|B^0_q\rangle = \frac{8}{3}B_1^q(\mu) m_{B_q}^2 f_{B_q}^2\,, \tag{A.18}
$$

$$
\langle \bar{B}^0_q|\mathcal{O}_1^{\rm SLL}|B^0_q\rangle = \langle \bar{B}^0_q|\mathcal{O}_1^{\rm SRR}|B^0_q\rangle = -\frac{5}{12}B_2^q(\mu) R(\mu)\, m_{B_q}^2 f_{B_q}^2\,, \tag{A.19}
$$

$$
\langle \bar{B}^0_q|\mathcal{O}_2^{\rm SLL}|B^0_q\rangle = \langle \bar{B}^0_q|\mathcal{O}_2^{\rm SRR}|B^0_q\rangle = \left(\frac{5}{3}B_2^q(\mu) - \frac{2}{3}B_3^q\right) R(\mu) m_{B_q}^2 f_{B_q}^2\,, \tag{A.20}
$$

$$
\langle \bar{B}^0_q|\mathcal{O}_1^{\rm LR}|B^0_q\rangle = -\frac{1}{3}B_5^q(\mu)\, R(\mu) m_{B_q}^2 f_{B_q}^2\,, \tag{A.21}
$$

$$
\langle \bar{B}^0_q|\mathcal{O}_2^{\rm LR}|B^0_q\rangle = \frac{1}{2}B_4^q(\mu)\, R(\mu) m_{B_q}^2 f_{B_q}^2\,, \tag{A.22}
$$

where $R(\mu) = m_{B_q}^2/(m_b(\mu)+m_q(\mu))^2$. The bag parameters, in the $\overline{\rm MS}$ scheme at the scale $\mu = m_b = 4.2\,\text{GeV}$ are summarized in table 13. The FLAG average for the B_d and B_s

	B_1	B_2	B_3	B_4	B_5
$B_d^0 - \bar{B}_d^0$ [216]	0.85 ± 0.04	0.72 ± 0.03	0.88 ± 0.13	0.95 ± 0.05	1.47 ± 0.12
$B_s^0 - \bar{B}_s^0$ [216]	0.86 ± 0.03	0.73 ± 0.03	0.89 ± 0.12	0.93 ± 0.04	1.57 ± 0.11
$K^0 - \bar{K}^0$ [93]	0.56 ± 0.01	0.50 ± 0.01	0.77 ± 0.03	0.93 ± 0.02	0.72 ± 0.04

Table 13. Bag parameters for $B_q - \bar{B}_q$ and $K^0 - \bar{K}^0$ oscillations, in the $\overline{\text{MS}}$ scheme. For $B_q - \bar{B}_q$ oscillations, we use the results of ref. [216], and the bags parameters are given at the renormalization scale $\mu = m_b$. For $K^0 - \bar{K}^0$ oscillation, we quote the FLAG averages of simulations performed with $n_f = 2+1$ flavors [93]. In this case, $B_1 = B_K$ is given at the renormalization scale $\mu = 2\,\text{GeV}$, while $B_{2,\ldots,5}$ are given at $\mu = 3\,\text{GeV}$.

decay constants is given in table 8. The RGE factors to run the coefficients in eq. (A.14) to the scale $\mu = m_t$ to $\mu = m_b$ are given in ref. [214].

Neglecting the RHCC contributions which are quadratic in ξ, one has to good approximation in the SM,

$$\Delta m_q = 2|M_{12}^{(q)}| = \frac{G_F^2 m_W^2}{6\pi^2}|V_{tq}V_{tb}^*|^2 f_{B_q}^2 \hat{B}_{B_q}\eta_B S_0(x_t, x_t)\,, \tag{A.23}$$

in which x_t should be evaluated at $\mu = m_t$ and $\eta_B = 0.55 \pm 0.01$ [217], $S_0(x_i, x_j) = \frac{1}{4}(f_1(x_i,x_j) - f_1(0,x_j) - f_1(x_i,0) + f_1(0,0))$. In place of $B_1^{s,d}$, it is convenient to introduce the renormalization-group-independent bag parameters $\hat{B}_{B_{d,s}}$, for which we use [93]

$$f_{B_d}\sqrt{\hat{B}_{B_d}} = 219 \pm 14\,\text{MeV}\,, \qquad f_{B_s}\sqrt{\hat{B}_{B_s}} = 270 \pm 16\,\text{MeV}\,. \tag{A.24}$$

The experimental values of Δm_s and Δm_d are

$$\Delta m_d = (0.5064 \pm 0.0019)\ \text{ps}^{-1}\,, \qquad \Delta m_s = (17.757 \pm 0.021)\ \text{ps}^{-1}\,. \tag{A.25}$$

A.3.2 ε_K

In the case of $K^0 - \bar{K}^0$ oscillations, the mass difference $\Delta m_K = m_{K_L} - m_{K_S}$ receives sizable long-distance contributions [85], whose uncertainties prevent the use of Δm_K for a precise extraction of the CKM elements. On the other hand, CPV in $K_0 - \bar{K}_0$ mixing is dominated by short-distance effects. The indirect CP violation in $K \to \pi\pi$ decays is parametrized by the parameter ε_K, which, up to $\mathcal{O}(\xi^2)$ corrections, is given by [176]

$$\varepsilon_K = \frac{G_F^2 m_W^2}{12\pi^2}\frac{m_K f_K^2 \hat{B}_K}{\sqrt{2}\Delta m_K}\kappa_\varepsilon \text{Im}\Big(\eta_{cc}(V_{cs}^* V_{cd})^2 S_0(x_c) + 2\eta_{ct}V_{cs}^* V_{cd} V_{ts}^* V_{td} S_0(x_c, x_t) + \eta_{tt}(V_{ts}^* V_{td})^2 S_0(x_t)\Big)\,.$$

Here x_t should be evaluated at $\mu = m_t$ and x_c at $\mu = m_c$, furthermore from FLAG and ref. [217]

$$\hat{B}_K = 0.717 \pm 0.018 \pm 0.016\,, \qquad \kappa_\varepsilon = 0.94 \pm 0.02\,,$$
$$\eta_{cc} = 1.87 \pm 0.76, \qquad \eta_{ct} = 0.496 \pm 0.047\,, \qquad \eta_{tt} = 0.5765 \pm 0.065\,. \tag{A.26}$$

$\hat{B}_K$ is the renormalization-group-invariant bag factor. In ref. [11], we considered long-range contributions to ε_K, linear in ξ_{us} and ξ_{ud}. Since the ensuing constraints on these couplings are much weaker than the one from ϵ'/ϵ, we do not include these corrections here.

B Two-loop contributions to the electron EDM

As the ξ operator only couples the W boson to quarks it mainly induces hadronic EDMs. However, the ξ_{tb} coupling also generates a (fairly small) electron EDM at the two-loop level. Here we briefly describe this contribution.

In the relevant diagram two W bosons connect an electron line with a top-bottom loop which emits a photon. Neglecting the lepton masses, this produces the following contribution to the electron EDM,

$$v^2\,\tilde{c}_{\gamma l}^{(ee)}|_{\rm 2loop} = -16 N_c \frac{y_t y_b}{(4\pi)^4} {\rm Im}\left(\xi_{tb} V_{tb}^*\right) \left[\frac{Q_t}{Q_e} F(x_t, x_b) + (t \leftrightarrow b)\right], \tag{B.1}$$

where $x_i \equiv m_i^2/m_W^2$, and

$$F(x_i, x_j) = \frac{1}{2}\int_0^1 dx \frac{x-1}{x^2 + x(x_j - x_i - 1) + x_i} \ln \frac{x(1-x)}{x(x_j - x_i) + x_i}\,. \tag{B.2}$$

In the approximation of small x_b, the loop function becomes,

$$\begin{aligned} F(x_t, 0) &= \frac{1}{2}\left[{\rm Li}_2(1 - 1/x_t) - \frac{\pi^2}{6}\right], \\ F(x_b, x_t) &\simeq \frac{1}{2}\frac{1}{x_t - 1}\left[\ln x_t \ln \frac{x_b}{x_t} - (x_t + 1){\rm Li}_2(1 - 1/x_t)\right] + \frac{\pi^2}{12}\,. \end{aligned} \tag{B.3}$$

Below the scale $\mu = m_W$, a second matching contribution arises from an operator of the form, $\mathcal{L} = C^{(b,e)} \bar{b} \sigma^{\mu\nu} b\, \bar{e}\, i\sigma_{\mu\nu}\gamma_5 e$. This operator is generated at one loop and, in turn, induces the electron EDM through an additional loop. All combined, the matching conditions at the scales $\mu = m_W$ and $\mu = m_b$ become

$$\begin{aligned} v^2\, C^{(b,e)}(\mu_W) &= \frac{y_t y_e}{(4\pi)^2}\frac{\ln x_t}{1 - x_t} {\rm Im}\left(\xi_{tb} V_{tb}^*\right), \\ \tilde{c}_{\gamma l}^{(ee)}(\mu_W) &= \tilde{c}_{\gamma l}^{(ee)}|_{\rm 2loop} - \frac{8 N_c}{(4\pi)^2}\frac{m_b Q_b}{m_e Q_e} \ln \frac{m_b^2}{\mu_W^2}\, C^{(b,e)}(\mu_W), \\ \tilde{c}_{\gamma l}^{(ee)}(\mu_b^-) &= \tilde{c}_{\gamma l}^{(ee)}(\mu_b^+) + \frac{8 N_c}{(4\pi)^2}\frac{m_b Q_b}{m_e Q_e} \ln \frac{m_b^2}{\mu_b^2}\, C^{(b,e)}(\mu_b), \end{aligned} \tag{B.4}$$

where $\mu_W \simeq m_W$ indicates a scale around $\mu = m_W$, while μ_b^+ (μ_b^-) refers to a scale just above (below) the b-quark threshold. Finally, the RG evolution between m_W and m_b, which determines $C^{(b,e)}(\mu_b^+)$ and $\tilde{c}_{\gamma l}^{(ee)}(\mu_b^+)$, is given by

$$\frac{d}{d\ln\mu}\tilde{c}_{\gamma l}^{(ee)}(\mu) = 16 N_c \frac{1}{(4\pi)^2}\frac{m_b Q_b}{m_e Q_e} C^{(b,e)}(\mu)\,, \qquad \frac{d}{d\ln\mu} C^{(b,e)}(\mu) = 2 C_F \frac{\alpha_s}{4\pi} C^{(b,e)}(\mu)\,. \tag{B.5}$$

The electron EDM does not evolve under RG $\mu = m_b$ (apart from small QED corrections), we use $\tilde{c}_{\gamma l}^{(ee)}(2\,{\rm GeV}) = \tilde{c}_{\gamma l}^{(ee)}(\mu_b^-)$ which is given in table 7.

JHEP05(2017)086

References

[1] R.N. Mohapatra and J.C. Pati, *Left-right gauge symmetry and an isoconjugate model of CP-violation*, Phys. Rev. **D 11** (1975) 566 [INSPIRE].

[2] G. Senjanović and R.N. Mohapatra, *Exact left-right symmetry and spontaneous violation of parity*, Phys. Rev. **D 12** (1975) 1502 [INSPIRE].

[3] G. Senjanović, *Spontaneous breakdown of parity in a class of gauge theories*, Nucl. Phys. **B 153** (1979) 334 [INSPIRE].

[4] R.N. Mohapatra and G. Senjanović, *Neutrino mass and spontaneous parity violation*, Phys. Rev. Lett. **44** (1980) 912 [INSPIRE].

[5] W. Buchmüller and D. Wyler, *Effective Lagrangian analysis of new interactions and flavor conservation*, Nucl. Phys. **B 268** (1986) 621 [INSPIRE].

[6] B. Grzadkowski, M. Iskrzynski, M. Misiak and J. Rosiek, *Dimension-six terms in the Standard Model Lagrangian*, JHEP **10** (2010) 085 [arXiv:1008.4884] [INSPIRE].

[7] Y. Zhang, H. An, X. Ji and R.N. Mohapatra, *General CP-violation in minimal left-right symmetric model and constraints on the right-handed scale*, Nucl. Phys. **B 802** (2008) 247 [arXiv:0712.4218] [INSPIRE].

[8] A. Maiezza, M. Nemevšek, F. Nesti and G. Senjanović, *Left-right symmetry at LHC*, Phys. Rev. **D 82** (2010) 055022 [arXiv:1005.5160] [INSPIRE].

[9] G. Senjanović and V. Tello, *Right handed quark mixing in left-right symmetric theory*, Phys. Rev. Lett. **114** (2015) 071801 [arXiv:1408.3835] [INSPIRE].

[10] G. Senjanović and V. Tello, *Restoration of parity and the right-handed analog of the CKM matrix*, Phys. Rev. **D 94** (2016) 095023 [arXiv:1502.05704] [INSPIRE].

[11] V. Cirigliano, W. Dekens, J. de Vries and E. Mereghetti, *An ϵ' improvement from right-handed currents*, Phys. Lett. **B 767** (2017) 1 [arXiv:1612.03914] [INSPIRE].

[12] P. Nason, *A new method for combining NLO QCD with shower Monte Carlo algorithms*, JHEP **11** (2004) 040 [hep-ph/0409146] [INSPIRE].

[13] S. Frixione, P. Nason and C. Oleari, *Matching NLO QCD computations with parton shower simulations: the POWHEG method*, JHEP **11** (2007) 070 [arXiv:0709.2092] [INSPIRE].

[14] S. Alioli, P. Nason, C. Oleari and E. Re, *A general framework for implementing NLO calculations in shower Monte Carlo programs: the POWHEG BOX*, JHEP **06** (2010) 043 [arXiv:1002.2581] [INSPIRE].

[15] ATLAS collaboration, *Measurement of W boson angular distributions in events with high transverse momentum jets at $\sqrt{s} = 8$ TeV using the ATLAS detector*, Phys. Lett. **B 765** (2017) 132 [arXiv:1609.07045] [INSPIRE].

[16] ATLAS collaboration, *Measurement of $W^{\pm}$ and Z-boson production cross sections in pp collisions at $\sqrt{s} = 13$ TeV with the ATLAS detector*, Phys. Lett. **B 759** (2016) 601 [arXiv:1603.09222] [INSPIRE].

JHEP05(2017)086

[17] ATLAS collaboration, *Measurement of k_T splitting scales in $W \to \ell\nu$ events at $\sqrt{s} = 7$ TeV with the ATLAS detector*, *Eur. Phys. J.* **C 73** (2013) 2432 [arXiv:1302.1415] [INSPIRE].

[18] ATLAS collaboration, *Measurement of the polarisation of W bosons produced with large transverse momentum in pp collisions at $\sqrt{s} = 7$ TeV with the ATLAS experiment*, *Eur. Phys. J.* **C 72** (2012) 2001 [arXiv:1203.2165] [INSPIRE].

[19] ATLAS collaboration, *Measurement of the transverse momentum distribution of W bosons in pp collisions at $\sqrt{s} = 7$ TeV with the ATLAS detector*, *Phys. Rev.* **D 85** (2012) 012005 [arXiv:1108.6308] [INSPIRE].

[20] CMS collaboration, *Measurement of the transverse momentum spectra of weak vector bosons produced in proton-proton collisions at $\sqrt{s} = 8$ TeV*, *JHEP* **02** (2017) 096 [arXiv:1606.05864] [INSPIRE].

[21] CMS collaboration, *Measurement of the differential cross section and charge asymmetry for inclusive $pp \to W^{\pm} + X$ production at $\sqrt{s} = 8$ TeV*, *Eur. Phys. J.* **C 76** (2016) 469 [arXiv:1603.01803] [INSPIRE].

[22] CMS collaboration, *Measurement of inclusive W and Z boson production cross sections in pp collisions at $\sqrt{s} = 8$ TeV*, *Phys. Rev. Lett.* **112** (2014) 191802 [arXiv:1402.0923] [INSPIRE].

[23] CMS collaboration, *Measurement of the inclusive W and Z production cross sections in pp collisions at $\sqrt{s} = 7$ TeV*, *JHEP* **10** (2011) 132 [arXiv:1107.4789] [INSPIRE].

[24] CMS collaboration, *Measurement of the lepton charge asymmetry in inclusive W production in pp collisions at $\sqrt{s} = 7$ TeV*, *JHEP* **04** (2011) 050 [arXiv:1103.3470] [INSPIRE].

[25] CMS collaboration, *Measurements of inclusive W and Z cross sections in pp collisions at $\sqrt{s} = 7$ TeV*, *JHEP* **01** (2011) 080 [arXiv:1012.2466] [INSPIRE].

[26] C. Anastasiou, L.J. Dixon, K. Melnikov and F. Petriello, *Dilepton rapidity distribution in the Drell-Yan process at NNLO in QCD*, *Phys. Rev. Lett.* **91** (2003) 182002 [hep-ph/0306192] [INSPIRE].

[27] K. Melnikov and F. Petriello, *Electroweak gauge boson production at hadron colliders through $O(\alpha_s^2)$*, *Phys. Rev.* **D 74** (2006) 114017 [hep-ph/0609070] [INSPIRE].

[28] S. Catani, L. Cieri, G. Ferrera, D. de Florian and M. Grazzini, *Vector boson production at hadron colliders: a fully exclusive QCD calculation at NNLO*, *Phys. Rev. Lett.* **103** (2009) 082001 [arXiv:0903.2120] [INSPIRE].

[29] G. Bozzi, S. Catani, G. Ferrera, D. de Florian and M. Grazzini, *Production of Drell-Yan lepton pairs in hadron collisions: transverse-momentum resummation at next-to-next-to-leading logarithmic accuracy*, *Phys. Lett.* **B 696** (2011) 207 [arXiv:1007.2351] [INSPIRE].

[30] S. Catani, D. de Florian, G. Ferrera and M. Grazzini, *Vector boson production at hadron colliders: transverse-momentum resummation and leptonic decay*, *JHEP* **12** (2015) 047 [arXiv:1507.06937] [INSPIRE].

[31] A. Karlberg, E. Re and G. Zanderighi, *NNLOPS accurate Drell-Yan production*, *JHEP* **09** (2014) 134 [arXiv:1407.2940] [INSPIRE].

[32] S. Alioli et al., *Precision studies of observables in $pp \to W \to \ell\nu$ and $pp \to \gamma, Z \to \ell^+\ell^-$ processes at the LHC*, submitted to *Working Group Report* (2016) [arXiv:1606.02330] [INSPIRE].

[33] S. Alioli, P. Nason, C. Oleari and E. Re, *NLO vector-boson production matched with shower in POWHEG*, JHEP **07** (2008) 060 [arXiv:0805.4802] [INSPIRE].

[34] R.K. Ellis, W.J. Stirling and B.R. Webber, *QCD and collider physics*, *Camb. Monogr. Part. Phys. Nucl. Phys. Cosmol.* **8** (1996) 1 [INSPIRE].

[35] Z. Bern et al., *Left-handed W bosons at the LHC*, Phys. Rev. **D 84** (2011) 034008 [arXiv:1103.5445] [INSPIRE].

[36] G. Ferrera, M. Grazzini and F. Tramontano, *Associated WH production at hadron colliders: a fully exclusive QCD calculation at NNLO*, Phys. Rev. Lett. **107** (2011) 152003 [arXiv:1107.1164] [INSPIRE].

[37] G. Ferrera, M. Grazzini and F. Tramontano, *Higher-order QCD effects for associated WH production and decay at the LHC*, JHEP **04** (2014) 039 [arXiv:1312.1669] [INSPIRE].

[38] J.M. Campbell, R.K. Ellis and C. Williams, *Associated production of a Higgs boson at NNLO*, JHEP **06** (2016) 179 [arXiv:1601.00658] [INSPIRE].

[39] W. Astill, W. Bizon, E. Re and G. Zanderighi, *NNLOPS accurate associated HW production*, JHEP **06** (2016) 154 [arXiv:1603.01620] [INSPIRE].

[40] G. Luisoni, P. Nason, C. Oleari and F. Tramontano, *$HW^{\pm}/HZ + 0$ and 1 jet at NLO with the POWHEG BOX interfaced to GoSam and their merging within MiNLO*, JHEP **10** (2013) 083 [arXiv:1306.2542] [INSPIRE].

[41] ATLAS and CMS collaborations, *Measurements of the Higgs boson production and decay rates and constraints on its couplings from a combined ATLAS and CMS analysis of the LHC pp collision data at $\sqrt{s} = 7$ and 8 TeV*, JHEP **08** (2016) 045 [arXiv:1606.02266] [INSPIRE].

[42] E.E. Jenkins, A.V. Manohar and M. Trott, *Renormalization group evolution of the Standard Model dimension six operators II: Yukawa dependence*, JHEP **01** (2014) 035 [arXiv:1310.4838] [INSPIRE].

[43] R. Alonso, E.E. Jenkins, A.V. Manohar and M. Trott, *Renormalization group evolution of the Standard Model dimension six operators III: gauge coupling dependence and phenomenology*, JHEP **04** (2014) 159 [arXiv:1312.2014] [INSPIRE].

[44] ATLAS collaboration, *Search for the Standard Model Higgs boson produced in association with a vector boson and decaying to a $b\bar{b}$ pair in pp collisions at 13 TeV using the ATLAS detector*, ATLAS-CONF-2016-091, CERN, Geneva Switzerland, (2016).

[45] F.A. Dreyer and A. Karlberg, *Vector-boson fusion Higgs production at three loops in QCD*, Phys. Rev. Lett. **117** (2016) 072001 [arXiv:1606.00840] [INSPIRE].

[46] M. Cacciari, F.A. Dreyer, A. Karlberg, G.P. Salam and G. Zanderighi, *Fully differential vector-boson-fusion Higgs production at next-to-next-to-leading order*, Phys. Rev. Lett. **115** (2015) 082002 [arXiv:1506.02660] [INSPIRE].

[47] P. Nason and C. Oleari, *NLO Higgs boson production via vector-boson fusion matched with shower in POWHEG*, JHEP **02** (2010) 037 [arXiv:0911.5299] [INSPIRE].

[48] ATLAS collaboration, *Comprehensive measurements of t-channel single top-quark production cross sections at $\sqrt{s} = 7$ TeV with the ATLAS detector*, Phys. Rev. **D 90** (2014) 112006 [arXiv:1406.7844] [INSPIRE].

[49] CMS collaboration, *Measurement of the single-top-quark t-channel cross section in pp collisions at $\sqrt{s} = 7$ TeV*, JHEP **12** (2012) 035 [arXiv:1209.4533] [INSPIRE].

[50] ATLAS collaboration, *Fiducial, total and differential cross-section measurements of t-channel single top-quark production in pp collisions at 8 TeV using data collected by the ATLAS detector*, arXiv:1702.02859 [INSPIRE].

[51] CMS collaboration, *Measurement of the t-channel single-top-quark production cross section and of the $|V_{tb}|$ CKM matrix element in pp collisions at $\sqrt{s} = 8$ TeV*, JHEP **06** (2014) 090 [arXiv:1403.7366] [INSPIRE].

[52] ATLAS collaboration, *Measurement of the inclusive cross-sections of single top-quark and top-antiquark t-channel production in pp collisions at $\sqrt{s} = 13$ TeV with the ATLAS detector*, JHEP **04** (2017) 086 [arXiv:1609.03920] [INSPIRE].

[53] CMS collaboration, *Cross section measurement of t-channel single top quark production in pp collisions at $\sqrt{s} = 13$ TeV*, submitted to *Phys. Lett.* **B** (2016) [arXiv:1610.00678] [INSPIRE].

[54] ATLAS collaboration, *Measurement of the production cross-section of a single top quark in association with a W boson at 8 TeV with the ATLAS experiment*, JHEP **01** (2016) 064 [arXiv:1510.03752] [INSPIRE].

[55] CMS collaboration, *Observation of the associated production of a single top quark and a W boson in pp collisions at $\sqrt{s} = 8$ TeV*, Phys. Rev. Lett. **112** (2014) 231802 [arXiv:1401.2942] [INSPIRE].

[56] CDF and D0 collaborations, T.A. Aaltonen et al., *Observation of s-channel production of single top quarks at the Tevatron*, Phys. Rev. Lett. **112** (2014) 231803 [arXiv:1402.5126] [INSPIRE].

[57] M. Brucherseifer, F. Caola and K. Melnikov, *On the NNLO QCD corrections to single-top production at the LHC*, Phys. Lett. **B 736** (2014) 58 [arXiv:1404.7116] [INSPIRE].

[58] M. Brucherseifer, F. Caola and K. Melnikov, *$O(\alpha_s^2)$ corrections to fully-differential top quark decays*, JHEP **04** (2013) 059 [arXiv:1301.7133] [INSPIRE].

[59] J. Gao, C.S. Li and H.X. Zhu, *Top quark decay at next-to-next-to leading order in QCD*, Phys. Rev. Lett. **110** (2013) 042001 [arXiv:1210.2808] [INSPIRE].

[60] E.L. Berger, J. Gao, C.P. Yuan and H.X. Zhu, *NNLO QCD corrections to t-channel single top-quark production and decay*, Phys. Rev. **D 94** (2016) 071501 [arXiv:1606.08463] [INSPIRE].

[61] J.M. Campbell, R. Frederix, F. Maltoni and F. Tramontano, *Next-to-leading-order predictions for t-channel single-top production at hadron colliders*, Phys. Rev. Lett. **102** (2009) 182003 [arXiv:0903.0005] [INSPIRE].

[62] R. Frederix, E. Re and P. Torrielli, *Single-top t-channel hadroproduction in the four-flavour scheme with POWHEG and aMC@NLO*, JHEP **09** (2012) 130 [arXiv:1207.5391] [INSPIRE].

[63] T. Ježo and P. Nason, *On the treatment of resonances in next-to-leading order calculations matched to a parton shower*, JHEP **12** (2015) 065 [arXiv:1509.09071] [INSPIRE].

[64] A.S. Papanastasiou, R. Frederix, S. Frixione, V. Hirschi and F. Maltoni, *Single-top t-channel production with off-shell and non-resonant effects*, Phys. Lett. **B 726** (2013) 223 [arXiv:1305.7088] [INSPIRE].

JHEP05(2017)086

[65] R. Frederix, S. Frixione, A.S. Papanastasiou, S. Prestel and P. Torrielli, *Off-shell single-top production at NLO matched to parton showers*, *JHEP* **06** (2016) 027 [arXiv:1603.01178] [INSPIRE].

[66] S. Alioli, P. Nason, C. Oleari and E. Re, *NLO single-top production matched with shower in POWHEG: s- and t-channel contributions*, *JHEP* **09** (2009) 111 [*Erratum ibid.* **02** (2010) 011] [arXiv:0907.4076] [INSPIRE].

[67] S. Alekhin et al., *The PDF4LHC working group interim report*, arXiv:1101.0536 [INSPIRE].

[68] H.-L. Lai et al., *New parton distributions for collider physics*, *Phys. Rev.* **D 82** (2010) 074024 [arXiv:1007.2241] [INSPIRE].

[69] A.D. Martin, W.J. Stirling, R.S. Thorne and G. Watt, *Parton distributions for the LHC*, *Eur. Phys. J.* **C 63** (2009) 189 [arXiv:0901.0002] [INSPIRE].

[70] R.D. Ball et al., *Parton distributions with LHC data*, *Nucl. Phys.* **B 867** (2013) 244 [arXiv:1207.1303] [INSPIRE].

[71] Particle Data Group collaboration, C. Patrignani et al., *Review of particle physics*, *Chin. Phys.* **C 40** (2016) 100001 [INSPIRE].

[72] CDF and D0 collaboration, T. Aaltonen et al., *Combination of CDF and D0 measurements of the W boson helicity in top quark decays*, *Phys. Rev.* **D 85** (2012) 071106 [arXiv:1202.5272] [INSPIRE].

[73] ATLAS collaboration, *Measurement of the W boson polarization in top quark decays with the ATLAS detector*, *JHEP* **06** (2012) 088 [arXiv:1205.2484] [INSPIRE].

[74] CMS collaboration, *Measurement of the W-boson helicity in top-quark decays from $t\bar{t}$ production in lepton+jets events in pp collisions at $\sqrt{s} = 7$ TeV*, *JHEP* **10** (2013) 167 [arXiv:1308.3879] [INSPIRE].

[75] ATLAS collaboration, *Search for anomalous couplings in the Wtb vertex from the measurement of double differential angular decay rates of single top quarks produced in the t-channel with the ATLAS detector*, *JHEP* **04** (2016) 023 [arXiv:1510.03764] [INSPIRE].

[76] CMS collaboration, *Measurement of the W boson helicity in events with a single reconstructed top quark in pp collisions at $\sqrt{s} = 8$ TeV*, *JHEP* **01** (2015) 053 [arXiv:1410.1154] [INSPIRE].

[77] ATLAS collaboration, *Measurement of the W boson polarisation in $t\bar{t}$ events from pp collisions at $\sqrt{s} = 8$ TeV in the lepton+jets channel with ATLAS*, arXiv:1612.02577 [INSPIRE].

[78] A. Czarnecki, J.G. Korner and J.H. Piclum, *Helicity fractions of W bosons from top quark decays at NNLO in QCD*, *Phys. Rev.* **D 81** (2010) 111503 [arXiv:1005.2625] [INSPIRE].

[79] J. Drobnak, S. Fajfer and J.F. Kamenik, *New physics in $t \to bW$ decay at next-to-leading order in QCD*, *Phys. Rev.* **D 82** (2010) 114008 [arXiv:1010.2402] [INSPIRE].

[80] E.E. Jenkins, A.V. Manohar and M. Trott, *Renormalization group evolution of the Standard Model dimension six operators I: formalism and λ dependence*, *JHEP* **10** (2013) 087 [arXiv:1308.2627] [INSPIRE].

[81] M. Spira, *QCD effects in Higgs physics*, *Fortsch. Phys.* **46** (1998) 203 [hep-ph/9705337] [INSPIRE].

[82] G. Perez, Y. Soreq, E. Stamou and K. Tobioka, *Constraining the charm Yukawa and Higgs-quark coupling universality*, *Phys. Rev.* **D 92** (2015) 033016 [arXiv:1503.00290] [INSPIRE].

[83] Y. Soreq, H.X. Zhu and J. Zupan, *Light quark Yukawa couplings from Higgs kinematics*, *JHEP* **12** (2016) 045 [arXiv:1606.09621] [INSPIRE].

[84] C. Bobeth, A.J. Buras, A. Celis and M. Jung, *Yukawa enhancement of Z-mediated new physics in $\Delta S = 2$ and $\Delta B = 2$ processes*, arXiv:1703.04753 [INSPIRE].

[85] G. Buchalla, A.J. Buras and M.E. Lautenbacher, *Weak decays beyond leading logarithms*, *Rev. Mod. Phys.* **68** (1996) 1125 [hep-ph/9512380] [INSPIRE].

[86] W. Dekens and J. de Vries, *Renormalization group running of dimension-six sources of parity and time-reversal violation*, *JHEP* **05** (2013) 149 [arXiv:1303.3156] [INSPIRE].

[87] S. Weinberg, *Larger Higgs exchange terms in the neutron electric dipole moment*, *Phys. Rev. Lett.* **63** (1989) 2333 [INSPIRE].

[88] F. Wilczek and A. Zee, *$\Delta I = 1/2$ rule and right-handed currents: heavy quark expansion and limitation on Zweig's rule*, *Phys. Rev.* **D 15** (1977) 2660 [INSPIRE].

[89] E. Braaten, C.-S. Li and T.-C. Yuan, *The evolution of Weinberg's gluonic CP violation operator*, *Phys. Rev. Lett.* **64** (1990) 1709 [INSPIRE].

[90] P.L. Cho and M. Misiak, *$b \to s\gamma$ decay in $\mathrm{SU}(2)_L \times \mathrm{SU}(2)_R \times \mathrm{U}(1)$ extensions of the Standard Model*, *Phys. Rev.* **D 49** (1994) 5894 [hep-ph/9310332] [INSPIRE].

[91] M. Misiak, private communication, (2016).

[92] D. Chang, C.S. Li and T.C. Yuan, *Larger neutron electric dipole moment in left-right symmetric models*, *Phys. Rev.* **D 42** (1990) 867 [INSPIRE].

[93] S. Aoki et al., *Review of lattice results concerning low-energy particle physics*, *Eur. Phys. J.* **C 77** (2017) 112 [arXiv:1607.00299] [INSPIRE].

[94] J.C. Hardy and I.S. Towner, *Superallowed $0^+ \to 0^+$ nuclear β decays: 2014 critical survey, with precise results for V_{ud} and CKM unitarity*, *Phys. Rev.* **C 91** (2015) 025501 [arXiv:1411.5987] [INSPIRE].

[95] S. Aoki et al., *Review of lattice results concerning low-energy particle physics*, *Eur. Phys. J.* **C 74** (2014) 2890 [arXiv:1310.8555] [INSPIRE].

[96] FlaviaNet Working Group on Kaon Decays collaboration, M. Antonelli et al., *An evaluation of $|V_{us}|$ and precise tests of the Standard Model from world data on leptonic and semileptonic kaon decays*, *Eur. Phys. J.* **C 69** (2010) 399 [arXiv:1005.2323] [INSPIRE].

[97] H.P. Mumm et al., *A new limit on time-reversal violation in beta decay*, *Phys. Rev. Lett.* **107** (2011) 102301 [arXiv:1104.2778] [INSPIRE].

[98] K.K. Vos, H.W. Wilschut and R.G.E. Timmermans, *Symmetry violations in nuclear and neutron beta decay*, *Rev. Mod. Phys.* **87** (2015) 1483 [arXiv:1509.04007] [INSPIRE].

[99] J.D. Jackson, S.B. Treiman and H.W. Wyld, *Possible tests of time reversal invariance in beta decay*, *Phys. Rev.* **106** (1957) 517 [INSPIRE].

[100] A.V. Manohar and M.B. Wise, *Heavy quark physics*, *Camb. Monogr. Part. Phys. Nucl. Phys. Cosmol.* **10** (2000) 1 [INSPIRE].

[101] Y. Amhis et al., *Averages of b-hadron, c-hadron and τ-lepton properties as of summer* 2016, arXiv:1612.07233 [INSPIRE].

[102] D. Becirevic, S. Fajfer, I. Nisandzic and A. Tayduganov, *Angular distributions of $\bar{B} \to D^{(*)}\ell\bar{\nu}_\ell$ decays and search of new physics*, arXiv:1602.03030 [INSPIRE].

[103] C.W. Bauer, Z. Ligeti, M. Luke and A.V. Manohar, *B decay shape variables and the precision determination of $|V_{cb}|$ and m_b*, Phys. Rev. **D 67** (2003) 054012 [hep-ph/0210027] [INSPIRE].

[104] P. Gambino, *B semileptonic moments at NNLO*, JHEP **09** (2011) 055 [arXiv:1107.3100] [INSPIRE].

[105] P. Gambino and C. Schwanda, *Inclusive semileptonic fits, heavy quark masses and V_{cb}*, Phys. Rev. **D 89** (2014) 014022 [arXiv:1307.4551] [INSPIRE].

[106] A. Alberti, P. Gambino, K.J. Healey and S. Nandi, *Precision determination of the Cabibbo-Kobayashi-Maskawa element V_{cb}*, Phys. Rev. Lett. **114** (2015) 061802 [arXiv:1411.6560] [INSPIRE].

[107] B. Dassinger, R. Feger and T. Mannel, *Complete Michel parameter analysis of inclusive semileptonic $b \to c$ transition*, Phys. Rev. **D 79** (2009) 075015 [arXiv:0803.3561] [INSPIRE].

[108] R. Feger, T. Mannel, V. Klose, H. Lacker and T. Luck, *Limit on a right-handed admixture to the weak $b \to c$ current from semileptonic decays*, Phys. Rev. **D 82** (2010) 073002 [arXiv:1003.4022] [INSPIRE].

[109] A. Crivellin and S. Pokorski, *Can the differences in the determinations of V_{ub} and V_{cb} be explained by new physics?*, Phys. Rev. Lett. **114** (2015) 011802 [arXiv:1407.1320] [INSPIRE].

[110] F.U. Bernlochner, Z. Ligeti and S. Turczyk, *New ways to search for right-handed current in $B \to \rho\ell\bar{\nu}$ decay*, Phys. Rev. **D 90** (2014) 094003 [arXiv:1408.2516] [INSPIRE].

[111] C.W. Bauer, Z. Ligeti and M.E. Luke, *Precision determination of $|V_{ub}|$ from inclusive decays*, Phys. Rev. **D 64** (2001) 113004 [hep-ph/0107074] [INSPIRE].

[112] B.O. Lange, M. Neubert and G. Paz, *Theory of charmless inclusive B decays and the extraction of V_{ub}*, Phys. Rev. **D 72** (2005) 073006 [hep-ph/0504071] [INSPIRE].

[113] W. Detmold, C. Lehner and S. Meinel, *$\Lambda_b \to p\ell^-\bar{\nu}_\ell$ and $\Lambda_b \to \Lambda_c\ell^-\bar{\nu}_\ell$ form factors from lattice QCD with relativistic heavy quarks*, Phys. Rev. **D 92** (2015) 034503 [arXiv:1503.01421] [INSPIRE].

[114] LHCb collaboration, *Determination of the quark coupling strength $|V_{ub}|$ using baryonic decays*, Nature Phys. **11** (2015) 743 [arXiv:1504.01568] [INSPIRE].

[115] A.V. Manohar and M.B. Wise, *Inclusive semileptonic B and polarized Λ_b decays from QCD*, Phys. Rev. **D 49** (1994) 1310 [hep-ph/9308246] [INSPIRE].

[116] ACME collaboration, J. Baron et al., *Order of magnitude smaller limit on the electric dipole moment of the electron*, Science **343** (2014) 269 [arXiv:1310.7534] [INSPIRE].

[117] C.A. Baker et al., *An improved experimental limit on the electric dipole moment of the neutron*, Phys. Rev. Lett. **97** (2006) 131801 [hep-ex/0602020] [INSPIRE].

[118] J.M. Pendlebury et al., *Revised experimental upper limit on the electric dipole moment of the neutron*, Phys. Rev. **D 92** (2015) 092003 [arXiv:1509.04411] [INSPIRE].

[119] W.C. Griffith, M.D. Swallows, T.H. Loftus, M.V. Romalis, B.R. Heckel and E.N. Fortson, *Improved limit on the permanent electric dipole moment of* ^{199}*Hg*, *Phys. Rev. Lett.* **102** (2009) 101601 [INSPIRE].

[120] B. Graner, Y. Chen, E.G. Lindahl and B.R. Heckel, *Reduced limit on the permanent electric dipole moment of* ^{199}*Hg*, *Phys. Rev. Lett.* **116** (2016) 161601 [arXiv:1601.04339] [INSPIRE].

[121] M.A. Rosenberry and T.E. Chupp, *Atomic electric dipole moment measurement using spin exchange pumped masers of* ^{129}*Xe and* ^{3}*He*, *Phys. Rev. Lett.* **86** (2001) 22.

[122] M. Bishof et al., *Improved limit on the* ^{225}*Ra electric dipole moment*, *Phys. Rev.* **C 94** (2016) 025501 [arXiv:1606.04931] [INSPIRE].

[123] R.H. Parker et al., *First measurement of the atomic electric dipole moment of* ^{225}*Ra*, *Phys. Rev. Lett.* **114** (2015) 233002 [arXiv:1504.07477] [INSPIRE].

[124] K. Kumar, Z.-T. Lu and M.J. Ramsey-Musolf, *Working group report: nucleons, nuclei and atoms*, in *Community Summer Study* 2013*: Snowmass on the Mississippi (CSS*2013*)*, Minneapolis MN U.S.A., 29 July–6 August 2013 [arXiv:1312.5416] [INSPIRE].

[125] T. Chupp and M. Ramsey-Musolf, *Electric dipole moments: a global analysis*, *Phys. Rev.* **C 91** (2015) 035502 [arXiv:1407.1064] [INSPIRE].

[126] J. de Vries, E. Mereghetti, R.G.E. Timmermans and U. van Kolck, *The effective chiral Lagrangian from dimension-six parity and time-reversal violation*, *Annals Phys.* **338** (2013) 50 [arXiv:1212.0990] [INSPIRE].

[127] J. Bsaisou, U.-G. Meißner, A. Nogga and A. Wirzba, *P- and T-violating Lagrangians in chiral effective field theory and nuclear electric dipole moments*, *Annals Phys.* **359** (2015) 317 [arXiv:1412.5471] [INSPIRE].

[128] T. Blum et al., *Lattice determination of the* $K \to (\pi\pi)_{I=2}$ *decay amplitude* A_2, *Phys. Rev.* **D 86** (2012) 074513 [arXiv:1206.5142] [INSPIRE].

[129] T. Blum et al., $K \to \pi\pi$ $\Delta I = 3/2$ *decay amplitude in the continuum limit*, *Phys. Rev.* **D 91** (2015) 074502 [arXiv:1502.00263] [INSPIRE].

[130] J. de Vries, E. Mereghetti, C.-Y. Seng and A. Walker-Loud, *Lattice QCD spectroscopy for hadronic CP-violation*, *Phys. Lett.* **B 766** (2017) 254 [arXiv:1612.01567] [INSPIRE].

[131] M. Pospelov and A. Ritz, *Neutron EDM from electric and chromoelectric dipole moments of quarks*, *Phys. Rev.* **D 63** (2001) 073015 [hep-ph/0010037] [INSPIRE].

[132] O. Lebedev, K.A. Olive, M. Pospelov and A. Ritz, *Probing CP-violation with the deuteron electric dipole moment*, *Phys. Rev.* **D 70** (2004) 016003 [hep-ph/0402023] [INSPIRE].

[133] M. Pospelov and A. Ritz, *Electric dipole moments as probes of new physics*, *Annals Phys.* **318** (2005) 119 [hep-ph/0504231] [INSPIRE].

[134] J. Hisano, J.Y. Lee, N. Nagata and Y. Shimizu, *Reevaluation of neutron electric dipole moment with QCD sum rules*, *Phys. Rev.* **D 85** (2012) 114044 [arXiv:1204.2653] [INSPIRE].

[135] R.D. Peccei and H.R. Quinn, *CP conservation in the presence of instantons*, *Phys. Rev. Lett.* **38** (1977) 1440 [INSPIRE].

[136] C.-Y. Seng, J. de Vries, E. Mereghetti, H.H. Patel and M. Ramsey-Musolf, *Nucleon electric dipole moments and the isovector parity- and time-reversal-odd pion-nucleon coupling*, *Phys. Lett.* **B 736** (2014) 147 [arXiv:1401.5366] [INSPIRE].

[137] A. Maiezza and M. Nemevšek, *Strong P invariance, neutron electric dipole moment and minimal left-right parity at LHC*, Phys. Rev. **D 90** (2014) 095002 [arXiv:1407.3678] [INSPIRE].

[138] T. Bhattacharya, V. Cirigliano, R. Gupta, H.-W. Lin and B. Yoon, *Neutron electric dipole moment and tensor charges from lattice QCD*, Phys. Rev. Lett. **115** (2015) 212002 [arXiv:1506.04196] [INSPIRE].

[139] PNDME collaboration, T. Bhattacharya et al., *Iso-vector and iso-scalar tensor charges of the nucleon from lattice QCD*, Phys. Rev. **D 92** (2015) 094511 [arXiv:1506.06411] [INSPIRE].

[140] T. Bhattacharya, V. Cirigliano, S. Cohen, R. Gupta, H.-W. Lin and B. Yoon, *Axial, scalar and tensor charges of the nucleon from* $2+1+1$*-flavor lattice QCD*, Phys. Rev. **D 94** (2016) 054508 [arXiv:1606.07049] [INSPIRE].

[141] T. Bhattacharya, V. Cirigliano, R. Gupta, E. Mereghetti and B. Yoon, *Neutron electric dipole moment from quark chromoelectric dipole moment*, PoS(LATTICE 2015)238 [arXiv:1601.02264] [INSPIRE].

[142] T. Bhattacharya, V. Cirigliano, R. Gupta and B. Yoon, *Quark chromoelectric dipole moment contribution to the neutron electric dipole moment*, in Proceedings, 34^{th} *International Symposium on Lattice Field Theory (Lattice* 2016*)*, Southampton U.K., 24–30 July 2016 [PoS(LATTICE2016)225] [arXiv:1612.08438] [INSPIRE].

[143] M. Abramczyk, S. Aoki, T. Blum, T. Izubuchi, H. Ohki and S. Syritsyn, *On lattice calculation of electric dipole moments and form factors of the nucleon*, arXiv:1701.07792 [INSPIRE].

[144] D.A. Demir, M. Pospelov and A. Ritz, *Hadronic EDMs, the Weinberg operator and light gluinos*, Phys. Rev. **D 67** (2003) 015007 [hep-ph/0208257] [INSPIRE].

[145] J.H. de Jesus and J. Engel, *Time-reversal-violating Schiff moment of* ^{199}Hg, Phys. Rev. **C 72** (2005) 045503 [nucl-th/0507031] [INSPIRE].

[146] J. Dobaczewski and J. Engel, *Nuclear time-reversal violation and the Schiff moment of* ^{225}Ra, Phys. Rev. Lett. **94** (2005) 232502 [nucl-th/0503057] [INSPIRE].

[147] S. Ban, J. Dobaczewski, J. Engel and A. Shukla, *Fully self-consistent calculations of nuclear Schiff moments*, Phys. Rev. **C 82** (2010) 015501 [arXiv:1003.2598] [INSPIRE].

[148] V.A. Dzuba, V.V. Flambaum and S.G. Porsev, *Calculation of* (P,T)*-odd electric dipole moments for diamagnetic atoms* ^{129}Xe, ^{171}Yb, ^{199}Hg, ^{211}Rn *and* ^{225}Ra, Phys. Rev. **A 80** (2009) 032120 [arXiv:0906.5437] [INSPIRE].

[149] J. Engel, M.J. Ramsey-Musolf and U. van Kolck, *Electric dipole moments of nucleons, nuclei and atoms: the Standard Model and beyond*, Prog. Part. Nucl. Phys. **71** (2013) 21 [arXiv:1303.2371] [INSPIRE].

[150] J. de Vries et al., *Electric dipole moments of light nuclei from chiral effective field theory*, Phys. Rev. **C 84** (2011) 065501 [arXiv:1109.3604] [INSPIRE].

[151] Y. Singh and B.K. Sahoo, *Rigorous limits for hadronic and semi-leptonic CP-violating coupling constants from the electric dipole moment of* ^{199}Hg, Phys. Rev. **A 91** (2015) 030501 [arXiv:1408.4337] [INSPIRE].

[152] Y. Singh and B.K. Sahoo, *Electric dipole moment of ^{225}Ra due to P- and T-violating weak interactions*, Phys. Rev. **A 92** (2015) 022502 [arXiv:1504.00269] [INSPIRE].

[153] N. Yamanaka and E. Hiyama, *Enhancement of the CP-odd effect in the nuclear electric dipole moment of ^{6}Li*, Phys. Rev. **C 91** (2015) 054005 [arXiv:1503.04446] [INSPIRE].

[154] N. Yamanaka, B.K. Sahoo, N. Yoshinaga, T. Sato, K. Asahi and B.P. Das, *Probing exotic phenomena at the interface of nuclear and particle physics with the electric dipole moments of diamagnetic atoms: a unique window to hadronic and semi-leptonic CP-violation*, Eur. Phys. J. **A 53** (2017) 54 [arXiv:1703.01570] [INSPIRE].

[155] N. Yoshinaga, K. Higashiyama and R. Arai, *Shell model estimate of nuclear electric dipole moments*, Prog. Theor. Phys. **124** (2010) 1115.

[156] CKMfitter Group collaboration, J. Charles et al., *CP violation and the CKM matrix: assessing the impact of the asymmetric B factories*, Eur. Phys. J. **C 41** (2005) 1 [hep-ph/0406184] [INSPIRE].

[157] M. Ciuchini, E. Franco, G. Martinelli and L. Reina, *ϵ'/ϵ at the next-to-leading order in QCD and QED*, Phys. Lett. **B 301** (1993) 263 [hep-ph/9212203] [INSPIRE].

[158] A.J. Buras, M. Jamin and M.E. Lautenbacher, *The anatomy of ϵ'/ϵ beyond leading logarithms with improved hadronic matrix elements*, Nucl. Phys. **B 408** (1993) 209 [hep-ph/9303284] [INSPIRE].

[159] M. Ciuchini, E. Franco, G. Martinelli, L. Reina and L. Silvestrini, *An upgraded analysis of ϵ'/ϵ at the next-to-leading order*, Z. Phys. **C 68** (1995) 239 [hep-ph/9501265] [INSPIRE].

[160] RBC and UKQCD collaborations, Z. Bai et al., *Standard Model prediction for direct CP-violation in $K \to \pi\pi$ decay*, Phys. Rev. Lett. **115** (2015) 212001 [arXiv:1505.07863] [INSPIRE].

[161] P. Chen, H. Ke and X. Ji, *Direct CP-violation in K-decay and minimal left-right symmetry scale*, Phys. Lett. **B 677** (2009) 157 [arXiv:0810.2576] [INSPIRE].

[162] S. Bertolini, A. Maiezza and F. Nesti, *$K \to \pi\pi$ hadronic matrix elements of left-right current-current operators*, Phys. Rev. **D 88** (2013) 034014 [arXiv:1305.5739] [INSPIRE].

[163] I. Baum, V. Lubicz, G. Martinelli, L. Orifici and S. Simula, *Matrix elements of the electromagnetic operator between kaon and pion states*, Phys. Rev. **D 84** (2011) 074503 [arXiv:1108.1021] [INSPIRE].

[164] T. Hurth, E. Lunghi and W. Porod, *Untagged $\bar{B} \to X_{s+d}\gamma$ CP asymmetry as a probe for new physics*, Nucl. Phys. **B 704** (2005) 56 [hep-ph/0312260] [INSPIRE].

[165] M. Misiak et al., *Estimate of $B(\bar{B} \to X_s\gamma)$ at $O(\alpha_s^2)$*, Phys. Rev. Lett. **98** (2007) 022002 [hep-ph/0609232] [INSPIRE].

[166] M. Misiak et al., *Updated NNLO QCD predictions for the weak radiative B-meson decays*, Phys. Rev. Lett. **114** (2015) 221801 [arXiv:1503.01789] [INSPIRE].

[167] M. Czakon, P. Fiedler, T. Huber, M. Misiak, T. Schutzmeier and M. Steinhauser, *The $(Q_7, Q_{1,2})$ contribution to $\bar{B} \to X_s\gamma$ at $O(\alpha_s^2)$*, JHEP **04** (2015) 168 [arXiv:1503.01791] [INSPIRE].

[168] W. Altmannshofer and D.M. Straub, *Cornering new physics in $b \to s$ transitions*, JHEP **08** (2012) 121 [arXiv:1206.0273] [INSPIRE].

JHEP05(2017)086

[169] W. Altmannshofer, P. Paradisi and D.M. Straub, *Model-independent constraints on new physics in $b \to s$ transitions*, JHEP **04** (2012) 008 [arXiv:1111.1257] [INSPIRE].

[170] M. Benzke, S.J. Lee, M. Neubert and G. Paz, *Long-distance dominance of the CP asymmetry in $B \to X_{s,d} + \gamma$ decays*, Phys. Rev. Lett. **106** (2011) 141801 [arXiv:1012.3167] [INSPIRE].

[171] A. Paul and D.M. Straub, *Constraints on new physics from radiative B decays*, JHEP **04** (2017) 027 [arXiv:1608.02556] [INSPIRE].

[172] P. Ball and R. Zwicky, *Time-dependent CP asymmetry in $B \to K^*\gamma$ as a (quasi) null test of the Standard Model*, Phys. Lett. **B 642** (2006) 478 [hep-ph/0609037] [INSPIRE].

[173] P. Ball, G.W. Jones and R. Zwicky, *$B \to V\gamma$ beyond QCD factorisation*, Phys. Rev. **D 75** (2007) 054004 [hep-ph/0612081] [INSPIRE].

[174] A.J. Buras and R. Fleischer, *Quark mixing, CP-violation and rare decays after the top quark discovery*, Adv. Ser. Direct. High Energy Phys. **15** (1998) 65 [hep-ph/9704376] [INSPIRE].

[175] M. Artuso, G. Borissov and A. Lenz, *CP violation in the B_s^0 system*, Rev. Mod. Phys. **88** (2016) 045002 [arXiv:1511.09466] [INSPIRE].

[176] A.J. Buras, *Weak Hamiltonian, CP-violation and rare decays*, in *Probing the Standard Model of particle interactions. Proceedings, Summer School in Theoretical Physics, NATO Advanced Study Institute,* 68th *session*, Les Houches France, 28 July–5 September 1997 [hep-ph/9806471] [INSPIRE].

[177] A.J. Buras, M. Gorbahn, S. Jäger and M. Jamin, *Improved anatomy of ϵ'/ϵ in the Standard Model*, JHEP **11** (2015) 202 [arXiv:1507.06345] [INSPIRE].

[178] A.J. Buras and J.-M. Gérard, *Upper bounds on ϵ'/ϵ parameters $B_6^{(1/2)}$ and $B_8^{(3/2)}$ from large-N QCD and other news*, JHEP **12** (2015) 008 [arXiv:1507.06326] [INSPIRE].

[179] T. Kitahara, U. Nierste and P. Tremper, *Singularity-free next-to-leading order $\Delta S = 1$ renormalization group evolution and ϵ'_K/ϵ_K in the Standard Model and beyond*, JHEP **12** (2016) 078 [arXiv:1607.06727] [INSPIRE].

[180] A.J. Buras and J.-M. Gerard, *Final state interactions in $K \to \pi\pi$ decays: $\Delta I = 1/2$ rule vs. ϵ'/ϵ*, Eur. Phys. J. **C 77** (2017) 10 [arXiv:1603.05686] [INSPIRE].

[181] Y.T. Chien, V. Cirigliano, W. Dekens, J. de Vries and E. Mereghetti, *Direct and indirect constraints on CP-violating Higgs-quark and Higgs-gluon interactions*, JHEP **02** (2016) 011 [arXiv:1510.00725] [INSPIRE].

[182] Y. Jiang and M. Trott, *On the non-minimal character of the SMEFT*, arXiv:1612.02040 [INSPIRE].

[183] V. Cirigliano, J. Jenkins and M. Gonzalez-Alonso, *Semileptonic decays of light quarks beyond the Standard Model*, Nucl. Phys. **B 830** (2010) 95 [arXiv:0908.1754] [INSPIRE].

[184] V. Cirigliano, M. González-Alonso and M.L. Graesser, *Non-standard charged current interactions: beta decays versus the LHC*, JHEP **02** (2013) 046 [arXiv:1210.4553] [INSPIRE].

[185] E. Berkowitz et al., *An accurate calculation of the nucleon axial charge with lattice QCD*, arXiv:1704.01114 [INSPIRE].

[186] V. Cirigliano, S. Gardner and B. Holstein, *Beta decays and non-standard interactions in the LHC era*, Prog. Part. Nucl. Phys. **71** (2013) 93 [arXiv:1303.6953] [INSPIRE].

[187] M. González-Alonso and J. Martin Camalich, *Global effective-field-theory analysis of new-physics effects in (semi)leptonic kaon decays*, JHEP **12** (2016) 052 [arXiv:1605.07114] [INSPIRE].

[188] T. Bhattacharya et al., *Probing novel scalar and tensor interactions from (ultra)cold neutrons to the LHC*, Phys. Rev. **D 85** (2012) 054512 [arXiv:1110.6448] [INSPIRE].

[189] O. Naviliat-Cuncic and M. González-Alonso, *Prospects for precision measurements in nuclear β decay at the LHC era*, Annalen Phys. **525** (2013) 600 [arXiv:1304.1759] [INSPIRE].

[190] V. Bernard, M. Oertel, E. Passemar and J. Stern, *Tests of non-standard electroweak couplings of right-handed quarks*, JHEP **01** (2008) 015 [arXiv:0707.4194] [INSPIRE].

[191] W.J. Stirling and E. Vryonidou, *Electroweak gauge boson polarisation at the LHC*, JHEP **07** (2012) 124 [arXiv:1204.6427] [INSPIRE].

[192] B. Grzadkowski and M. Misiak, *Anomalous Wtb coupling effects in the weak radiative B-meson decay*, Phys. Rev. **D 78** (2008) 077501 [*Erratum ibid.* **D 84** (2011) 059903] [arXiv:0802.1413] [INSPIRE].

[193] J.A. Aguilar-Saavedra, *A minimal set of top anomalous couplings*, Nucl. Phys. **B 812** (2009) 181 [arXiv:0811.3842] [INSPIRE].

[194] G.A. Gonzalez-Sprinberg, R. Martinez and J. Vidal, *Top quark tensor couplings*, JHEP **07** (2011) 094 [*Erratum ibid.* **05** (2013) 117] [arXiv:1105.5601] [INSPIRE].

[195] J. Drobnak, S. Fajfer and J.F. Kamenik, *Probing anomalous tWb interactions with rare B decays*, Nucl. Phys. **B 855** (2012) 82 [arXiv:1109.2357] [INSPIRE].

[196] Q.-H. Cao, B. Yan, J.-H. Yu and C. Zhang, *A general analysis of Wtb anomalous couplings*, arXiv:1504.03785 [INSPIRE].

[197] Z. Hioki and K. Ohkuma, *Full analysis of general non-standard tbW couplings*, Phys. Lett. **B 752** (2016) 128 [arXiv:1511.03437] [INSPIRE].

[198] M. Schulze and Y. Soreq, *Pinning down electroweak dipole operators of the top quark*, Eur. Phys. J. **C 76** (2016) 466 [arXiv:1603.08911] [INSPIRE].

[199] J.F. Kamenik, M. Papucci and A. Weiler, *Constraining the dipole moments of the top quark*, Phys. Rev. **D 85** (2012) 071501 [arXiv:1107.3143] [INSPIRE].

[200] C. Zhang, N. Greiner and S. Willenbrock, *Constraints on non-standard top quark couplings*, Phys. Rev. **D 86** (2012) 014024 [arXiv:1201.6670] [INSPIRE].

[201] J. de Blas, M. Chala and J. Santiago, *Renormalization group constraints on new top interactions from electroweak precision data*, JHEP **09** (2015) 189 [arXiv:1507.00757] [INSPIRE].

[202] A. Buckley et al., *Global fit of top quark effective theory to data*, Phys. Rev. **D 92** (2015) 091501 [arXiv:1506.08845] [INSPIRE].

[203] A. Buckley et al., *Constraining top quark effective theory in the LHC run II era*, JHEP **04** (2016) 015 [arXiv:1512.03360] [INSPIRE].

[204] O. Bessidskaia Bylund, F. Maltoni, I. Tsinikos, E. Vryonidou and C. Zhang, *Probing top quark neutral couplings in the Standard Model effective field theory at NLO in QCD*, JHEP **05** (2016) 052 [arXiv:1601.08193] [INSPIRE].

[205] N. Castro, J. Erdmann, C. Grunwald, K. Kröninger and N.-A. Rosien, *EFTfitter — a tool for interpreting measurements in the context of effective field theories*, Eur. Phys. J. **C 76** (2016) 432 [arXiv:1605.05585] [INSPIRE].

[206] J. Aebischer, A. Crivellin, M. Fael and C. Greub, *Matching of gauge invariant dimension-six operators for $b \to s$ and $b \to c$ transitions*, JHEP **05** (2016) 037 [arXiv:1512.02830] [INSPIRE].

[207] V. Cirigliano, W. Dekens, J. de Vries and E. Mereghetti, *Constraining the top-Higgs sector of the Standard Model effective field theory*, Phys. Rev. **D 94** (2016) 034031 [arXiv:1605.04311] [INSPIRE].

[208] V. Cirigliano, W. Dekens, J. de Vries and E. Mereghetti, *Is there room for CP-violation in the top-Higgs sector?*, Phys. Rev. **D 94** (2016) 016002 [arXiv:1603.03049] [INSPIRE].

[209] A. Crivellin, *Effects of right-handed charged currents on the determinations of $|V_{ub}|$ and $|V_{cb}|$*, Phys. Rev. **D 81** (2010) 031301 [arXiv:0907.2461] [INSPIRE].

[210] A.J. Buras, K. Gemmler and G. Isidori, *Quark flavour mixing with right-handed currents: an effective theory approach*, Nucl. Phys. **B 843** (2011) 107 [arXiv:1007.1993] [INSPIRE].

[211] M. Beneke, G. Buchalla, M. Neubert and C.T. Sachrajda, *QCD factorization for exclusive, nonleptonic B meson decays: general arguments and the case of heavy light final states*, Nucl. Phys. **B 591** (2000) 313 [hep-ph/0006124] [INSPIRE].

[212] J. Chay and C. Kim, *Analysis of the QCD improved factorization in $B \to J/\psi K$*, hep-ph/0009244 [INSPIRE].

[213] M. Beneke, *Soft-collinear factorization in B decays*, Nucl. Part. Phys. Proc. **261-262** (2015) 311 [arXiv:1501.07374] [INSPIRE].

[214] A.J. Buras, S. Jager and J. Urban, *Master formulae for $\Delta F = 2$ NLO QCD factors in the Standard Model and beyond*, Nucl. Phys. **B 605** (2001) 600 [hep-ph/0102316] [INSPIRE].

[215] X.-G. He, J. Tandean and G. Valencia, *Penguin and box diagrams in unitary gauge*, Eur. Phys. J. **C 64** (2009) 681 [arXiv:0909.3638] [INSPIRE].

[216] ETM collaboration, N. Carrasco et al., *B-physics from $N_f = 2$ tmQCD: the Standard Model and beyond*, JHEP **03** (2014) 016 [arXiv:1308.1851] [INSPIRE].

[217] A.J. Buras and J. Girrbach, *Towards the identification of new physics through quark flavour violating processes*, Rept. Prog. Phys. **77** (2014) 086201 [arXiv:1306.3775] [INSPIRE].

JHEP05(2017)086